Polarization and Spin Effects in Production and Decay of Charginos and Neutralinos at a Muon Collider

Dissertation zur Erlangung des
naturwissenschaftlichen Doktorgrades
der Bayerischen Julius-Maximilians-Universität
Würzburg

vorgelegt von

Federico von der Pahlen

aus Buenos Aires

Würzburg 2005

Eingereicht am: 12.10.2005
bei der Fakultät für Physik und Astronomie

1. Gutachter: Prof. Dr. H. Fraas
2. Gutachter: Prof. Dr. R. Rückl
der Dissertation.

1. Prüfer: Prof. Dr. H. Fraas
2. Prüfer: Prof. Dr. R. Rückl
3. Prüfer: Prof. Dr. E. Umbach
im Promotionskolloquium.

Tag des Promotionskolloquiums: 14.06.2006

Doktorurkunde ausgehändigt am: .....

Contents

Chapter 1

Introduction

1.1 Motivation

The ultimate goal of elementary particle physics is to gain insight of the basic principles in nature. In the past century we have been able to understand the underlying structure of the electroweak and strong interactions as quantum gauge field theories with three chiral fermion families. The Glashow-Weinberg-Salam model [1] successfully unifies the electromagnetic and weak interactions while quantum chromodynamics (QCD) [2] describes the strong interactions as an asymptotic free $SU(3)$ gauge theory. There is hope to describe all interactions as a unified gauge theory.

The Standard Model (SM) of strong and electroweak interactions, despite its impressive success in describing particle physics phenomena, has not yet been completely verified. The spontaneous symmetry breaking mechanism predicts the existence of a massive scalar, the Higgs boson [3], which has still to be experimentally discovered. Indirectly, however, there are strong indications from precision measurements at lower energies that the Higgs boson, and thus the mechanism of spontaneous symmetry breaking which generates masses for the weak gauge bosons and the fermions, will be discovered in the next generation of colliders.

The SM is believed to be an effective theory valid only at the present energies of a more fundamental Grand Unified Theory (GUT) which describes the three fundamental forces through a single gauge group. One of the most attractive candidates for a more fundamental theory is supersymmetry (SUSY) [4], a symmetry which relates fermions and bosons and thus predicts a partner to every known particle which differs in spin by $\frac{1}{2}$. Since no partners have been observed so far, SUSY must be broken. Phenomenologically, the most attractive features of low-energy SUSY theories are:

- The new supersymmetric particles contribute to the evolution of the couplings with the renormalization group equation. Therefore, unification of

couplings at a mass scale below the Plank mass is achieved automatically [5].

– One can postulate a new discrete symmetry, R parity [6], with the consequence that the lightest supersymmetric particle is stable. SUSY thus provides a suitable dark matter candidate.

– The quadratic divergences to scalar masses from fermion and boson loops cancel out. SUSY thus stabilizes the hierarchy between the GUT scale and solves the naturalness and hierarchy problems which are encountered in renormalizable theories with scalars [7].

The most economical low-energy supersymmetric extension of the SM, the Minimal Supersymmetric Standard Model (MSSM) [8], has the SM gauge group and minimal particle content. The Higgs sector, however, requires two isodoublets of complex scalar fields, leading to three neutral Higgs bosons, the scalars h and H and the pseudoscalar A, and a pair of charged ones, $H^{\pm}$. Although the Higgs phenomenology in the MSSM is richer than in the SM, it is strongly constrained by SUSY. A determination of the Higgs parameters is thus an essential test of the theory.

After the potential discovery of Higgs bosons at hadron colliders, lepton colliders are necessary to perform precision measurements. A linear e^+e^- collider will be an ideal instrument to search for MSSM Higgs bosons [9]. However, there are a few key issues for which an e^+e^- machine is not satisfactory and the production of Higgs bosons as s-channel resonances is needed. These issues can best be investigated at $\gamma\gamma$ and $\mu^+\mu^-$ colliders.

At a $\gamma\gamma$ collider [10, 11] neutral Higgs bosons are resonantly produced mainly through loops of fermions and sfermions of the third generation, which couple to the photons electromagnetically and to the Higgs bosons with large Yukawa couplings. It has the possibility to obtain large photon polarizations. At a $\mu^+\mu^-$ collider [12–16] the small Yukawa coupling of the muons is compensated by the resonant enhancement of the Higgs exchange channels, which is possible since the energy of the muon beams, can be precisely tuned. Therefore, both machines are ideal for precision studies of the Higgs sector.

A unique possibility for a $\mu^+\mu^-$ collider as a Higgs factory are measurements of the Higgs line-shape. These measurements allow to determine the widths of the Higgs bosons, to separate the resonant and non-resonant contributions and, eventually, to separate overlapping resonances. A requirement is here a good energy resolution of the beams, whose energy spread should be smaller than the widths of the resonances.

The decays of the Higgs bosons into SUSY particles may be possible if the latter are light. A muon collider provides a clean environment to study these interactions since no additional particles need to be produced. For charginos and neutralinos, the charged and neutral SUSY partners, respectively, of the

electroweak gauge and Higgs bosons, their parameters will then have been determined at the ILC [9, 17]. Therefore a measurement of their couplings to the Higgs bosons can focus on their interaction to the Higgs sector. In the MSSM the mass of the lightest Higgs boson is constrained by the gauge couplings, with current limits from two-loop calculations setting the upper bound $m_h < 140$ GeV [18]. Therefore charginos are too heavy to be directly produced at the h resonance, since from LEP exclusion limits $m_{\chi_1^\pm} > 104$ GeV [19]. The lightest neutralino pairs may be eventually produced at this resonance. However, due to R parity conservation, this channel is invisible.

The neutral Higgs bosons H and A, on the other hand, may be significantly heavier, and their decays into charginos and neutralinos open the possibility to directly probe the interaction structure of the Higgs boson to the supersymmetric particles.

In order to obtain as much information as possible from these processes the dependence on the polarizations of the beams and of the charginos or neutralinos needs to be analyzed, both for the resonant channels as for the non-resonant contributions. Polarization effects in chargino and neutralino production have been shown to be great interest at e^+e^- colliders [20–22]. At a $\mu^+\mu^-$ collider the dependence on the initial and final polarizations are sensitive to the Higgs couplings to the initial and final particles and, for overlapping Higgs boson resonances, to their interference [23–25]. It is thus necessary to classify the polarization dependent observables and assess the possibility of measuring them at a muon collider.

The luminosity of a muon collider strongly depends on the center of mass energy $\sqrt{s}$ and on the required energy resolution of the beams. For $\sqrt{s} = 400$ GeV a luminosity $\mathcal{L} = 10^{33}$ cm^{-2}s^{-1} is proposed [12], which for a collider-year $= 10^7$ s corresponds to 10 fb^{-1}/year. Therefore, we consider effective luminosities of $\mathcal{O}(1\text{fb}^{-1})$.

1.2 Fermion pair production at a muon collider

Since we study the production of charginos and neutralinos in $\mu^+\mu^-$ annihilation around the energies of the heavy neutral Higgs resonances H and A it is important to discuss the general features of fermion pair production.

The muon-Higgs Yukawa couplings, see Appendix B, are of order gm_μ/m_W, where g is the weak coupling constant and m_μ and m_W are the masses of the muon and W boson. These couplings are thus three orders of magnitude smaller that the Z couplings to the Higgs bosons. Therefore, unless an enhancement mechanism takes place the Higgs exchange amplitudes can safely be neglected with respect to the non-Higgs channels. At center of mass energy $\sqrt{s} = m_\phi$, where m_ϕ is the mass of a Higgs boson ϕ, the resonant amplitudes are roughly

enhanced by a factor m_ϕ/Γ_ϕ, with Γ_ϕ the width of the Higgs boson ϕ, resulting from the Breit-Wigner propagator on top of the resonance.

For the heavier Higgs bosons H and A the widths are expected to be of $\mathcal{O}$(GeV) [26]. Therefore, the contributions to the amplitudes from Higgs exchange and from the continuum of gauge boson and slepton exchange are expected to be of the same order. At energies around the resonances of H and A we then neglect the contributions of the light Higgs h, suppressed by the factor m_μ/m_W with respect to the non-Higgs channels.

We analyze separately the cases of longitudinally and transversely polarized beams.

While scalars couple left with right chiral fermion fields, gauge bosons couplings conserve chirality. This implies that, for longitudinally polarized as well as for unpolarized beams, the interference of the Higgs and gauge boson exchange channels is suppressed by a factor of order $m_\mu/\sqrt{s}$. The same applies for the interference of the Higgs bosons and the t- and u-channel exchange of a slepton. In fact, the left (right) sleptons couple to left (right) chiral lepton fields, and thus preserve chirality, as the gauge boson interactions.

Therefore we neglect the interference between Higgs and non-Higgs channels.

For transversely polarized beams the interference of the Higgs exchange channels with the continuum does not vanish and is proportional to the transverse polarizations of the beams. These contributions must change sign under a rotation of π around the beam axes, or under a change of sign of the polarizations, and can thus be easily separated from the remaining terms.

1.2.1 CP properties of a two-fermion system

Here we analyze the CP properties of a two-fermion system.

A Dirac $f\bar{f}$ pair with spin S and orbital angular momentum L is in a state with the following charge conjugation C, parity P and CP quantum numbers:

$$C = (-1)^{L+S}, \qquad P = (-1)^{1+L}, \qquad CP = (-1)^{1+2L+S}. \tag{1.1}$$

Since L is an integer, a $f\bar{f}$ system with $S = 0$ ($S = 1$) is in a CP-odd (CP-even) state.

In addition, due to geometrical considerations, the angular orbital momentum along the direction of the beams in the center of mass system always vanishes,

$$L_z = 0. \tag{1.2}$$

This relation implies that $S_z = 0$ for a state with total angular momentum $J = 0$. Therefore, only equal helicities contribute to the Higgs exchange s-channel amplitudes. Analogous conclusions are obtained for the produced charginos, whose longitudinal polarizations are then correlated.

For a pair of neutralinos $\tilde{\chi}_i^0\tilde{\chi}_j^0$ the factor η_{ij}, related to the intrinsic CP quantum number of the neutralino pair, modifies eq. (1.1) and one obtains $CP = \eta_{ij}(-1)^{1+2L+S}$.

Summarizing, to obtain a $\mu^+\mu^-$ state with a definite CP quantum number we need transversely polarized beams with parallel or anti-parallel polarizations, implying $S = 1$ or $S = 0$, respectively. The resulting $\mu^+\mu^-$ states with $|S, S_z >= |0, 0 >$ and $|S, S_z >= |1, 0 >$, interact with the CP-odd and the CP-even scalars, respectively. Analogously, for final fermions produced via scalar s-channel exchange, i.e. with $J = 0$, the correlations of their transverse polarizations can be linked to the CP properties of the exchanged particle.

1.3 Organization of this work

The goal of the thesis is to probe the Higgs couplings to charginos and neutralinos in $\mu^+\mu^-$ annihilation around the resonances of the heavy Higgs bosons in the MSSM. We analyze the polarization effects of the beams and of the charginos and neutralinos. The idea is to obtain observables which allow to separate the pure exchange channels of the Higgs bosons, as well as their interference. Here we study cross sections of chargino and neutralino pair production, as well as energy and angular distributions of the particles of their two-body decays. We define ratios of cross sections as well as charge, polarization and angular asymmetries which allow to probe the Higgs couplings to charginos and neutralinos.

In order to study the dependence on the MSSM parameter space and to assess the feasibility of observing these observables at a muon collider we perform a numerical study for representative scenarios. For the cross sections we analyze the effects of the finite beam energy spread and of the background. We investigate the statistical significances of the asymmetries as a function of the luminosity.

In Chapter 2 we deal with $\tilde{\chi}_i^\mp\tilde{\chi}_j^\pm$ production and decay in $\mu^+\mu^-$ annihilation. In Section 2.1 we briefly discuss the process of chargino pair production. In Sections 2.2 and 2.3 we discuss the production of $\tilde{\chi}_j^+\tilde{\chi}_j^-$, $j = 1, 2$, and $\tilde{\chi}_1^\mp\tilde{\chi}_2^\pm$, respectively. In Section 2.4 we discuss chargino pair production with subsequent two-body decay of one of the charginos: $\tilde{\chi}_j^\pm \to \ell^\pm\tilde{\nu}$, for $\ell = e, \mu, \tau$, and $\tilde{\chi}_j^\pm \to W^\pm\tilde{\chi}_k^0$. In Section 2.5 we discuss the subsequent two-body decay of both charginos and in Section 2.6 we discuss beam transverse polarization effects.

In Chapter 3 we focus on $\tilde{\chi}_i^0\tilde{\chi}_j^0$ production and decay. The organization of this Chapter is analogous to the preceding one. In Section 3.1 we analyze neutralino pair production. In Section 3.2 we discuss the subsequent decay of one of the neutralinos: $\tilde{\chi}_j^0 \to \ell^\pm\tilde{\ell}_{R,L}^\mp$, for $\ell = e, \mu, \tau$. In Section 3.3 we discuss the two-body decays of both neutralinos and in Section 3.4 the beam transverse polarization effects.

Chapter 4 contains summary and conclusions.

In the Appendices we briefly describe the MSSM, with emphasis on the Higgs-

chargino and Higgs-neutralino interactions. We shortly introduce the spin-density matrix formalism and give explicit formulae for chargino and neutralino production. We describe the kinematics. Finally we give useful formulae and definitions.

Chapter 2

Chargino production and decay in $\mu^+\mu^-$-annihilation

In this chapter we study the pair production of charginos in $\mu^+\mu^-$-annihilation for center of mass energies $\sqrt{s}$ around the masses of the heavy neutral Higgs bosons in the CP conserving MSSM,

$$\mu^+\mu^- \to \tilde{\chi}_i^{\mp}\tilde{\chi}_j^{\pm}. \tag{2.1}$$

Our aim is to find appropriate observables with which to probe the Higgs-chargino interactions. Therefore we study the dependence of the process on both the beam and the chargino polarizations.

The pair production of charginos depends mainly on the MSSM parameters that determine the chargino and Higgs sectors, namely the ratio of vacuum expectation values of the Higgs doublets $\tan\beta$, the Higgs sector parameter μ, the gaugino mass parameter M_2 and the mass of the pseudoscalar Higgs m_A.

In Section 2.1 we study the pair production of charginos for longitudinally polarized beams. To determine the couplings we analyze the dependence of the production line-shape on the center of mass energy in order to separate the different contributions from the Higgs resonances and the continuum from the non-resonant γ, Z and $\tilde{\nu}_\mu$ exchange channels.

This is straightforward if the resonances are not degenerate since the interference effects are either negligible or easy to deal with.

In the CP conserving MSSM the heavier Higgs bosons are nearly degenerate in a large region of parameter space [25]. Therefore it may be complicated to separate the resonances from each other. It is thus necessary to analyze the dependence of the production line-shape on the energy spread of the beams. In Section 2.2 we focus on equal chargino pair production and investigate the precision of a determination of couplings on both the effects of the energy spread of the beams and of the background. The latter is due to the continuum contributions, as well as to the standard model processes with similar final states as, e.g., W boson pair production.

A further possibility, if the Higgs resonances overlap, is to gain information from their interference. For resonances with opposite CP quantum numbers, the interference vanishes in production of equal charginos. In Section 2.3 we show that large interference effects can be observed in $\tilde{\chi}_1^\pm \tilde{\chi}_2^\mp$ production for a large range of MSSM scenarios.

The effects of beam and chargino polarization can be analyzed studying the angular or energy distributions of their decay products. In Section 2.4 we analyze the subsequent two-body decay of one of the charginos

$$\tilde{\chi}_j^\pm \to \ell^\pm \tilde{\nu}_\ell, \qquad \ell = e, \mu, \tau \tag{2.2}$$

$$\tilde{\chi}_j^\pm \to W^\pm \tilde{\chi}^0, \tag{2.3}$$

for $j = 1, 2$ [24]. With help of the energy distributions of the charged decay lepton and of the W boson in eqs. (2.2) and (2.3) it is possible to observe the interference of Higgs bosons with different CP quantum numbers, both for equal chargino pairs and for $\tilde{\chi}_1^\pm \tilde{\chi}_2^\mp$ production. We build asymmetries which allow to determine the Higgs chargino couplings, and in particular of their relative phase.

In Section 2.5 we briefly discuss the process of production with subsequent decay of both charginos. While being more complicated to analyze, it provides important new information through the so-called spin-spin terms, i.e. those terms which depend on the correlation of the spins of the charginos. Similar information can be accessed if transverse beam polarization is available. The dependence on the transverse polarization is discussed in Section 2.6.

2.1 Chargino Production

In this section we briefly discuss the process of chargino pair production and give the corresponding spin density matrix for the Higgs exchange channels for longitudinally polarized beams. A more detailed analysis of this process for equal and unequal charginos is presented in the following two sections.

At center of mass energies around the heavy Higgs bosons H and A charginos are produced via the resonant s-channel exchange of the heavy neutral Higgs bosons, shown in Fig. 2.1, as well as via the photon and Z-boson exchange in s-channel and muon-sneutrino exchange in t-channel, shown in Fig. 2.2. The interaction Lagrangians for the Higgs exchange channels are given in Appendix B, eqs. (B.1) and (B.2). The Lagrangians for the non-Higgs exchange channels can be found in [20, 22]. Assuming that the masses and couplings of the muon and electron sneutrino are equal the contributions from the non-Higgs channels to the production process are equivalent to those in e^+e^- collisions.

For the calculation of the cross section for the combined process of chargino production eq. (2.1) and decay, which depends on the chargino $\tilde{\chi}_j^\pm$ polarizations

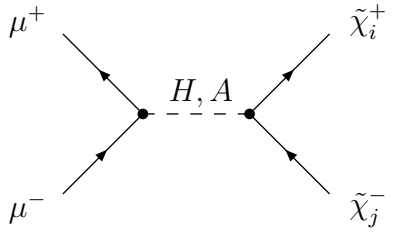

Figure 2.1: Resonant chargino pair production

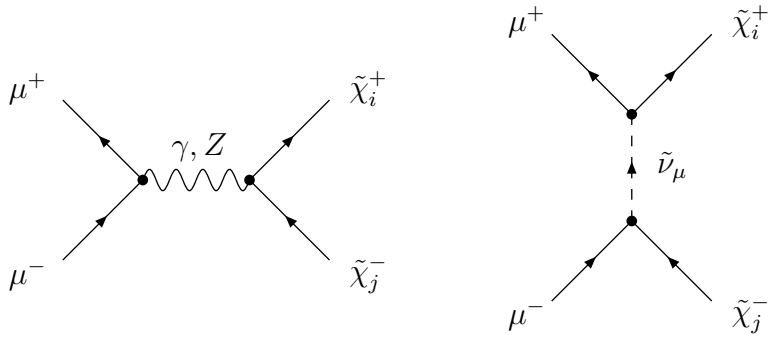

Figure 2.2: Continuum contribution to chargino pair production

λ_j, we use the spin density matrix formalism of [28], see Appendix C. The unnormalized spin density matrix for chargino pair production in $\mu^+\mu^-$-annihilation ρ^P, eq. (C.23), is a function of the polarization degrees of the μ^+ and μ^- beams, denoted with $\mathcal{P}_+^m$ and $\mathcal{P}_-^m$, respectively, for $m = 1, 2, 3$. With our choice of reference system, see Section D.1.3, $\mathcal{P}_\pm^3 \equiv \mathcal{P}_\pm^L$ denote the longitudinal polarization degrees of the beams, i.e. the average helicities of the incoming muons and antimuons, and $\mathcal{P}_\pm^1$ and $\mathcal{P}_\pm^2$ their transverse polarization degrees.

In the following we consider only longitudinally polarized beams. Then, the expansion coefficients of the chargino production matrix, see eqs. (C.25) and (C.39-C.42), subdivide into contributions from the Higgs resonances and the continuum, respectively,

$$P = P_r + P_{cont}, \qquad \Sigma^a_{P_j} = \Sigma^a_{rj} + \Sigma^a_{cont\,j}, \qquad \Sigma^{ab}_P = \Sigma^{ab}_r + \Sigma^{ab}_{cont}\ , \tag{2.4}$$

with $a, b = 1, \ldots, 3$. The continuum contributions P_{cont}, Σ^a_{cont} and Σ^{ab}_{cont} are those from the non-resonant γ, Z and $\tilde{\nu}_\mu$ exchange channels. Explicit expressions can be found in [20, 22]. The coefficients $\Sigma^a_{P_j}$ and Σ^{ab}_P describe the polarization of the charginos and are not further needed in this section.

The resonant contributions, from s-channel exchange of the Higgs bosons H and A, are separated into pure exchange and interference terms,

$$P_r \;=\; \sum_{\phi=H,A} P_r^{(\phi\phi)} + P_r^{(HA)}. \tag{2.5}$$

Evaluating the production amplitudes with the interaction Lagrangians eqs. (B.1) and (B.2) in the center of mass system (CMS) we obtain for $\mu^+\mu^- \to \tilde{\chi}_i^- \tilde{\chi}_j^+$

$$\begin{aligned} P_r^{(\phi\phi)} &= \frac{g^4}{8}(1+\mathcal{P}_+^L\mathcal{P}_-^L)|\Delta(\phi)|^2|c^{(\phi\mu)}|^2 \qquad (2.6)\\ &\quad \Big[(|c_L^{(\phi)}|^2+|c_R^{(\phi)}|^2)(s-m^2_{\chi_i^\pm}-m^2_{\chi_j^\pm})-4\mathrm{Re}\{c_L^{(\phi)}c_R^{(\phi)\,*}\}m_{\chi_i^\pm}m_{\chi_j^\pm}\Big]\,s,\\ P_r^{(HA)} &= -\frac{g^4}{4}(\mathcal{P}_+^L+\mathcal{P}_-^L)\mathrm{Re}\{\Delta(H)\Delta(A)^*\}\mathrm{Im}\{c^{(H\mu)}c^{(A\mu)^*}\}\\ &\quad \Big[\mathrm{Im}\{c_L^{(H)}c_L^{(A)\,*}+c_R^{(H)}c_R^{(A)\,*}\}(s-m^2_{\chi_i^\pm}-m^2_{\chi_j^\pm})\\ &\quad -2\,\mathrm{Im}\{c_L^{(H)}c_R^{(A)\,*}+c_R^{(H)}c_L^{(A)\,*}\}m_{\chi_i^\pm}m_{\chi_j^\pm}\Big]s, \qquad (2.7)\end{aligned}$$

where we used the short-hand notation $c_R^{(\phi)} \equiv c_{Rij}^{(\phi)}$ and $c_L^{(\phi)} \equiv c_{Lij}^{(\phi)}$ for the Higgs-chargino couplings, $\mathcal{P}_+^L$ and $\mathcal{P}_-^L$ denote the longitudinal beam polarizations of μ^+ and μ^-, respectively, and

$$\Delta(\phi) = i[(s-m_\phi^2)+im_\phi\Gamma_\phi]^{-1}, \qquad \phi = H, A, \qquad (2.8)$$

are the Breit-Wigner propagators of the Higgs bosons.

A comment is in place on the chargino masses. In general $m_{\chi_i^\pm}$, $i = 1, 2$, denote the eigenvalues of the diagonalization mass matrix, see Appendix A.2.1, and may differ from the actual masses by a phase. With our choice of diagonalization prescription, however, these phases are zero and $m_{\chi_{1,2}^\pm} > 0$.

Note that $P_r^{(HA)}$ vanishes for production of equal charginos $i = j$ since in this case the Higgs-chargino couplings are parity conserving, with $c_{Lii}^{(\phi)} = c_{Rii}^{(\phi)*}$. This term is thus only present for $\tilde{\chi}_1^\pm\tilde{\chi}_2^\mp$ production.

2.2 Production of equal charginos

Here we discuss pair production of equal charginos at center of masses near the Higgs boson resonances for longitudinally polarized beams. We show that the ratio of H and A couplings to the charginos can be precisely determined for scenarios where the contributions from resonances can be disentangled. We consider both the effects of the background and of the finite energy spread of the beams. Finally we analyze the precision of this determination as a function of the beam energy spread for a set of representative MSSM scenarios in $\tilde{\chi}_1^+\tilde{\chi}_1^-$ production.

For $\tilde{\chi}_i^+\tilde{\chi}_i^-$ production, $i = 1, 2$, the expression for the spin density matrix coefficients, eqs. (2.6) and (2.7), can be further simplified using the relation between the left and right handed Higgs-chargino couplings eq. (B.7). With the shorthand notation $c_{ii}^{(\phi)} = c_{R\,ii}^{(\phi)} = c_{L\,ii}^{(\phi)*}$ for the Higgs-chargino couplings the expansion coefficients of the spin density matrix for pure Higgs exchange, eq. (2.6), can be written as

$$P_r^{(HH)} = \frac{g^4}{4}(1 + \mathcal{P}_+^L\mathcal{P}_-^L)|\Delta(H)|^2|c^{(H\mu)}|^2|c_{ii}^{(H)}|^2 s(s - 4m_{\chi_i^\pm}^2), \tag{2.9}$$

$$P_r^{(AA)} = \frac{g^4}{4}(1 + \mathcal{P}_+^L\mathcal{P}_-^L)|\Delta(A)|^2|c^{(A\mu)}|^2|c_{ii}^{(A)}|^2 s^2, \tag{2.10}$$

while the H-A interference term vanishes due to CP conservation. Furthermore the interference between the Higgs boson exchange and the γ, Z and $\tilde{\nu}_\mu$ channels is strongly suppressed by a factor $m_\mu/\sqrt{s}$, as discussed in the Introduction. Therefore the total production cross section of $\tilde{\chi}_i^+\tilde{\chi}_i^-$ can be separated into the dominating contributions σ_H^{ii} and σ_A^{ii} from H and A exchange, respectively, and the background of non-resonant channels σ_{cont}^{ii} from γ, Z, $\tilde{\nu}_\mu$ and h exchange

$$\sigma^{ii} = \sigma_H^{ii} + \sigma_A^{ii} + \sigma_{cont}^{ii}. \tag{2.11}$$

Chargino production via the γ, Z, $\tilde{\nu}_\mu$ exchange channels will have been thoroughly studied at linear colliders [9]. Here we neglect the contributions from h exchange at the H and A resonances.

At CMS energy $\sqrt{s}$ the cross sections σ_H^{ii} and σ_A^{ii} can be expressed in the form

$$\sigma_\phi^{ii} = \frac{g^4}{4\pi}(1 + \mathcal{P}_+^L\mathcal{P}_-^L)|c^{(\phi\mu)}|^2 \cdot |c_{ii}^{(\phi)}|^2 \cdot B_\phi^{ii}(s)K_\phi(s), \quad \phi = H, A \tag{2.12}$$

with

$$K_\phi(s) = \frac{s}{(s - m_\phi^2)^2 + \Gamma_\phi^2 m_\phi^2}, \tag{2.13}$$

$$B_H^{ii}(s) = \frac{\lambda(s, m_{\chi_i^\pm}^2, m_{\chi_i^\pm}^2)^{3/2}}{s^3}, \tag{2.14}$$

$$B_A^{ii}(s) = \frac{\lambda(s, m_{\chi_i^\pm}^2, m_{\chi_i^\pm}^2)^{1/2}}{s}, \tag{2.15}$$

and the triangle function λ defined in (E.11). Note the different dependence on the center of mass energy of the H and A exchange terms. The CP-even exchange is p-wave suppressed due to the intrinsic negative parity of the chargino pair as well as to angular momentum conservation. This implies that, if the resonances are not much lighter than the production threshold of charginos, the CP-odd resonance is expected to dominate over the CP-even one.

Experimentally, charginos are observed through their decay products. Therefore, precision studies must take these decays into account.

The total cross section $\sigma^{f_+f_-}$ for the pair production $\mu^+\mu^- \to \tilde{\chi}_i^+\tilde{\chi}_i^-$ with subsequent decays $\tilde{\chi}_i^+ \to f_+$ and $\tilde{\chi}_i^- \to f_-$ factorizes into the production cross section σ^{ii} and the branching ratios for the respective decay channels:

$$\sigma^{f_+f_-}(\sqrt{s}) = \sigma^{ii}(\sqrt{s}) \times \mathrm{BR}(\tilde{\chi}_i^+ \to f_+) \times \mathrm{BR}(\tilde{\chi}_i^- \to f_-). \tag{2.16}$$

This result holds for each of the contributions $\sigma_H^{f_+f_-}$ from H exchange, $\sigma_A^{f_+f_-}$ from A exchange and $\sigma_{cont}^{f_+f_-}$ from the background channels in eq. (2.11).

2.2.1 Determination of the Higgs-chargino couplings in production

In order to determine the Higgs-chargino couplings one has to separate the Higgs exchange contributions $\sigma_H^{f_+f_-}+\sigma_A^{f_+f_-}$ from the total measured cross sections $\sigma_{meas}^{f_+f_-}$, at $\sqrt{s} = m_H$ and $\sqrt{s} = m_A$, respectively. Since the interference between the Higgs channels and the background is negligible we can subtract the contributions $\sigma_{cont}^{f_+f_-}$ from the total cross section.

Besides the non-resonant contributions to the chargino pair production one has to consider further background sources from standard model processes. Here W boson pair production and single W boson production constitute the main standard model background, which is in principle rather large [9] but can be strongly reduced by appropriate cuts [29]. Then the resonance peaks remain clearly visible above the smooth standard model background $\sigma_{SM}^{f_+f_-}$ which can therefore be included in the subtraction of the non-resonant contribution from the total cross section.

We determine the total background contribution $\sigma_B^{f_+f_-} = \sigma_{cont}^{f_+f_-} + \sigma_{SM}^{f_+f_-}$ by linear interpolation of $\sigma_{meas}^{f_+f_-}$ far below and above the resonance energies. The precision of this estimate obviously depends on the variation of the background contributions around the heavy Higgs resonances. By this procedure we avoid, however, reference to other experiments at different energy scales as e. g. chargino production at e^+e^- colliders combined with specific model calculations.

Due to their factorization into production and subsequent decay the ratio of the measured minus background contributions from H and A exchange

$$r = \frac{\sigma_{meas}^{f_+f_-}(m_H) - \sigma_B^{f_+f_-}(m_H)}{\sigma_{meas}^{f_+f_-}(m_A) - \sigma_B^{f_+f_-}(m_A)} = \frac{\sigma_H^{ii}(m_H) + \sigma_A^{ii}(m_H)}{\sigma_H^{ii}(m_A) + \sigma_A^{ii}(m_A)} \tag{2.17}$$

is independent of the specific chargino decay channel which may be chosen to give the best experimental signal. Then the measurement of the total cross section for chargino production and decay at the Higgs resonances offers an interesting possibility to determine the ratio of the Higgs-chargino couplings

$$x = \left| \frac{c_{ii}^{(H)}}{c_{ii}^{(A)}} \right|^2 . \tag{2.18}$$

From eqs. (2.12) and (2.17) one obtains

$$x = \frac{r}{C} \cdot \frac{1 - C_1/r}{1 - C_2 r} \cdot \frac{1}{x_\mu}, \tag{2.19}$$

with

$$C = \frac{\beta^3(m_H)}{\beta(m_A)} \frac{\Gamma_A^2}{\Gamma_H^2}, \tag{2.20}$$

$$C_1 = \frac{\beta(m_H)}{\beta(m_A)} K_A(m_H^2)\Gamma_A^2, \tag{2.21}$$

$$C_2 = \left(\frac{\beta(m_A)}{\beta(m_H)} \right)^3 K_H(m_A^2)\Gamma_H^2, \tag{2.22}$$

$$\beta(\sqrt{s}) = \left(\frac{\lambda(s, m_{\chi_i^\pm}^2, m_{\chi_i^\pm}^2)}{s^2} \right)^{1/2} = \left(\frac{s - 4m_{\chi_i^\pm}^2}{s} \right)^{1/2}, \tag{2.23}$$

$$x_\mu = \left| \frac{c^{(H\mu)}}{c^{(A\mu)}} \right|^2 , \tag{2.24}$$

where C, C_1 and C_2 can be determined without model dependent assumptions, and $x_\mu = 1$ in the Higgs decoupling limit [30].

Assuming that the masses of the heavy Higgs bosons and the chargino are precisely known [9, 31] the precision for the determination of x depends on the energy spread of the muon beams, the width of the H and A resonances and on the error in the determination of the background.

Scenarios	**A**	**B**	**C**	**D**	**E**	**F**
M_2[GeV]	188	217.3	154.9	169.5	400	400
μ[GeV]	-188	217.3	-400	400	-154.9	169.5
U_{11}	0.577	-0.632	0.958	-0.943	0.056	-0.184
U_{12}	0.817	0.775	0.288	0.333	0.9984	0.983
V_{11}	0.817	0.775	0.9984	0.983	0.288	0.333
V_{12}	-0.577	-0.632	-0.056	-0.184	-0.958	-0.943
m_H[GeV]	352.1	352.3	351.9	352.3	352.2	352.3
Γ_H[GeV]	0.67	0.58	0.31	0.32	0.32	0.39
Γ_A[GeV]	1.05	1.33	0.43	0.57	0.43	0.64

Table 2.1: Reference scenarios with fixed $m_A = 350$ GeV, $m_{\tilde{\chi}_1^\pm} = 155$ GeV, $\tan\beta = 5$ and $m_{\tilde{\nu}_\mu} = 261.3$ GeV. U_{11} and V_{11} (U_{12} and V_{12}) are the gaugino (higgsino) components of the charginos [33], see Appendix A.

2.2.2 Numerical analysis

In the numerical analysis we study the dependence on the MSSM parameters μ, M_2, $\tan\beta$ and m_A of the production of lighter chargino pairs at center of mass energies around the H and A resonances. We show cross sections for unpolarized beams. Finally we estimate how precisely the ratio of the couplings of the lighter chargino to the heavy Higgs bosons H and A can be measured, as a function of the energy spread of the beams and of the background contributions to the cross section.

In our scenarios the heavier charginos are not light enough to be produced in pairs at the neutral Higgs resonances. This process does not differ qualitatively from the production of lighter charginos. However, the parameter space in which it is kinematically allowed is significantly smaller.

The Higgs sector parameters and the branching ratios for the decays of H and A into charginos are computed with the program HDECAY [32].

2.2.2.1 Scenarios

We choose six representative scenarios **A** – **F** with $m_{\tilde{\chi}_1^\pm} = 155$ GeV, $m_A = 350$ GeV, and $\tan\beta = 5$ which differ by the mixing character of the chargino and by the sign of the higgsino mass parameter μ. The parameters, masses and the gaugino and higgsino contents of $\tilde{\chi}_1^\pm$ are given in Table 2.1. In scenarios **A** with $\mu < 0$ and **B** with $\mu > 0$ the light chargino is a wino-higgsino mixing. In scenarios **C** ($\mu < 0$) and **D** ($\mu > 0$) it has a dominant gaugino character whereas in scenarios **E** ($\mu < 0$) and **F** ($\mu > 0$) it is nearly a pure higgsino. The

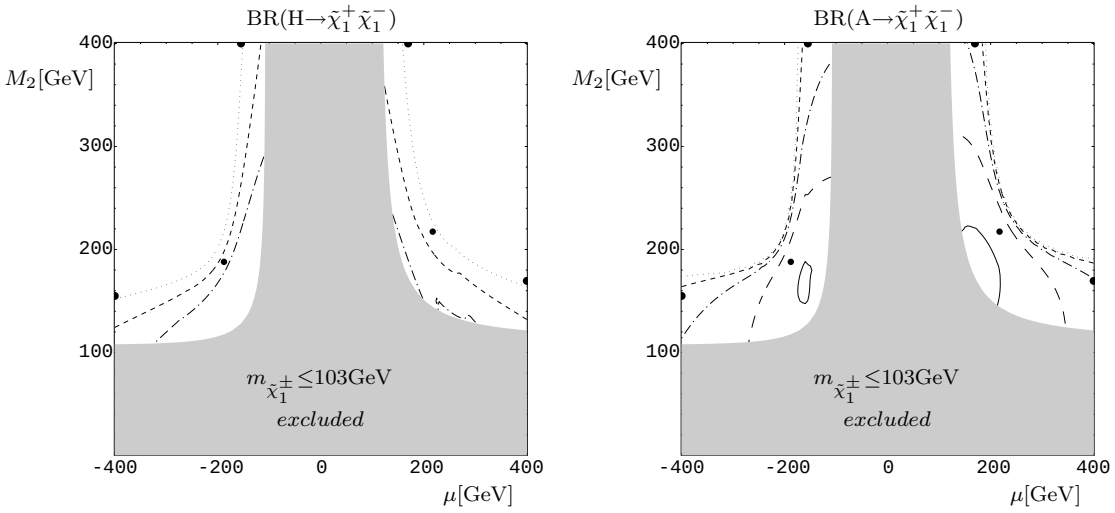

Figure 2.3: Branching ratios of the heavy Higgs bosons H and A into light chargino pairs for $m_A = 350$ GeV, $\tan\beta = 5$ and sfermions masses larger than $M_H/2$, computed with the program HDECAY [32]. The contour lines correspond to 0.1 (dashed), 0.3 (dash-dotted) and 0.5 (dotted). The gray area is the experimentally excluded region given here by $m_{\chi_1^\pm} < 103$ GeV, the thick dots are the scenarios **A** – **F** of table 2.1.

additional scenarios in Table 2.2 are derived from the mixed scenario **B** and the gaugino scenario **C** by varying $\tan\beta$ and the masses of the light chargino and the pseudoscalar Higgs boson.

In order to study the influence of the Higgs mass, m_A is increased from $m_A = 350$ GeV to $m_A = 400$ GeV in scenarios **B400** and **C400**. The influence of the chargino mass will be analyzed with the help of scenarios **B180** and **C180** where $m_{\tilde{\chi}_1^\pm} = 180$ GeV and $m_A = 400$ GeV in order to ensure $m_A > m_{\tilde{\chi}_1^\pm}/2$. However, the character of the light chargino is nearly identical in scenarios **B**, **B180** and **B400** (gaugino-higgsino mixing) and in scenarios **C**, **C180** and **C400** (gaugino like), respectively.

Finally we study the influence of higher values of $\tan\beta = 7$ and $\tan\beta = 8$ for $m_A = 350$ GeV and $m_{\tilde{\chi}_1^\pm} = 155$ GeV in scenarios **B7**, **B8** and **C7**, **C8**. To obtain a similar chargino mixing character the parameters M_2 and μ are slightly changed compared to scenarios **B** and **C** with $\tan\beta = 5$.

2.2.2.2 Branching ratios and cross sections

The branching ratios for the decays of the Higgs bosons H and A into a light chargino pair are crucial for obtaining sufficient cross sections. Therefore we show in Fig. 2.3 contour plots for the branching ratios in the $M_2 - \mu$ plane for $\tan\beta = 5$ and $m_A = 350$ GeV and indicate our scenarios **A** – **F**.

Since the Higgs bosons couple to both the gaugino and higgsino component

of the chargino, the couplings and branching ratios are large in the parameter region $|M_2| \approx |\mu|$ of the mixed scenarios **A** and **B**. In scenario **A** (**B**) with $\mu < 0$ ($\mu > 0$) one obtains branching ratios up to 45% (20%) for the A decay and up to 20% (15%) for the H decay. In scenarios **C** and **D** with a gaugino dominated light chargino as well as in scenarios **E** and **F** with a higgsino-like light chargino branching ratios between 20% and 30% for the A decay and between 10% and 20% for the H decay can be observed. The production cross sections σ^{11} (eq. (2.11)) for the scenarios **A** – **F** are shown in Figs. 2.4 a – f.

The heights of the Higgs resonances depend both on their total widths and on the Higgs-chargino couplings (cf. eqs. (2.12) and (2.13))

$$\sigma_\phi^{11} \propto |c_{11}^{(\phi)R}|^2/\Gamma_\phi^2, \quad \phi = H, A. \tag{2.25}$$

The interplay of these parameters (see table 2.1) can be observed in Fig. 2.4. In our scenarios the pattern of the A resonance is determined by the width, whereas for the H peaks the influence of the different H-chargino couplings generally predominates. So the A peaks are of equal height in the mixed and gaugino scenarios Fig. 2.4a and Fig. 2.4c and larger than in the higgsino scenario Fig. 2.4e, inversely proportional to the widths. The H resonance is largest in the scenario with the largest Higgs-chargino coupling Fig. 2.4a. Only comparing Fig. 2.4e and Fig. 2.4f the relative height of the H peak is determined by their width since the couplings are equal due to an approximate symmetry under $|\mu| \leftrightarrow M_2$.

Essential requirements for a precise determination of the Higgs-chargino couplings are distinct resonance peaks and a clear separation of the Higgs resonances. Near threshold the A resonance peak is suppressed by a factor β, compared to a suppression by β^3 of the H resonance. This effect explains the relative height of the resonances in Fig. 2.4.

Whether the resonances can be separated depends on both the Higgs line shape and the energy spread of the muon beams. In Figs. 2.4 a – f we compare the cross sections without and with a Gaussian energy spread of 150 MeV which corresponds to an energy resolution $R \approx 0.06\%$.

The energy spread clearly suppresses the resonance peaks especially in scenarios with gaugino-like and higgsino-like light charginos where the resonances are narrower than in the mixed scenarios. However, also with an energy spread of 150 MeV the H and A resonances are well separated in all scenarios (**A** – **F**).

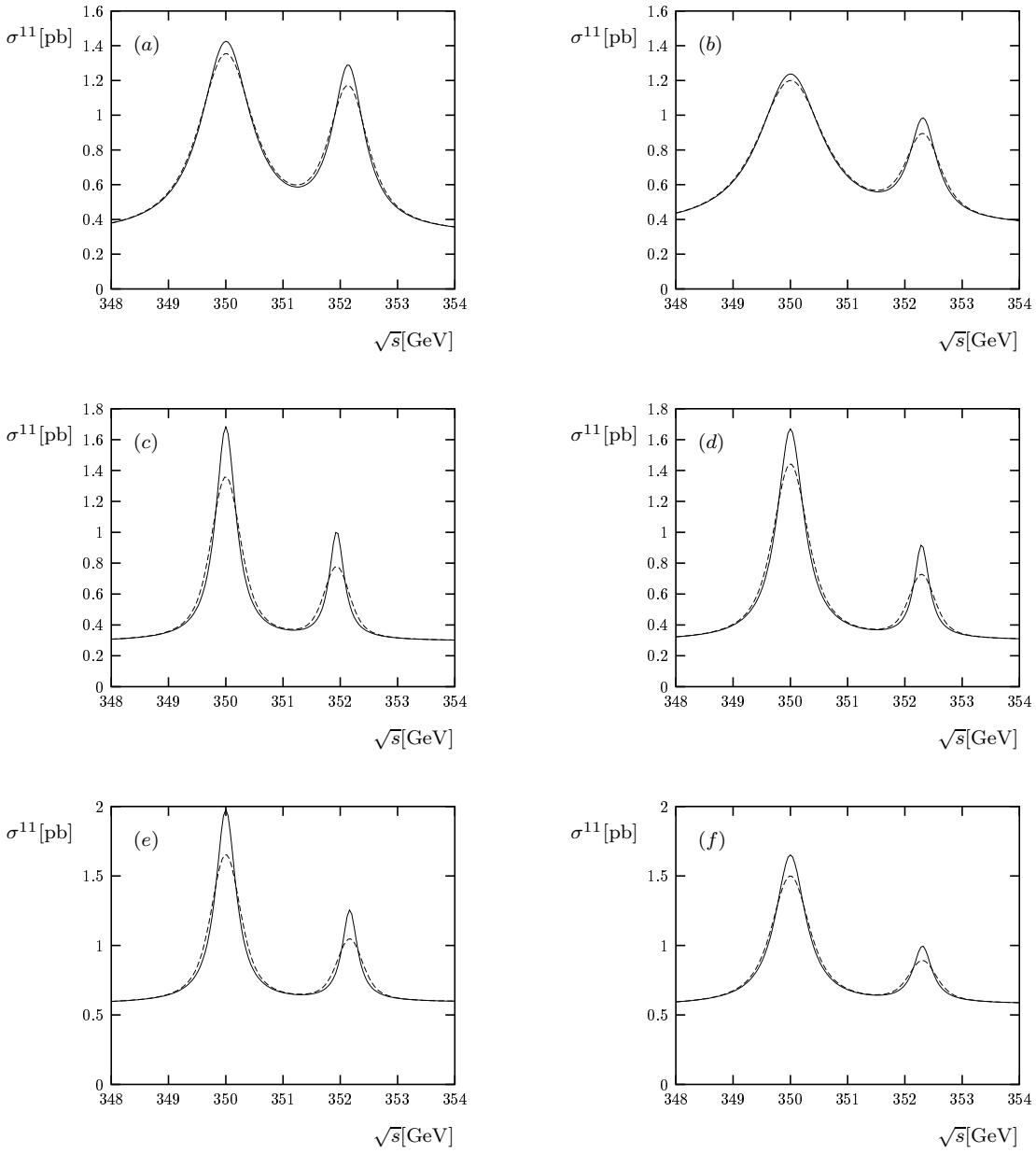

Figure 2.4: Total cross section σ^{11} for $\mu^+\mu^- \to \tilde{\chi}_1^+\tilde{\chi}_1^-$ in mixed, gaugino and higgsino scenarios with $\mu < 0$ ($\mu > 0$), a (b), c (d) and e (f) respectively, corresponding to the scenarios **A** (**B**), **C** (**D**) and **E** (**F**) of table 2.1. In all scenarios $\tan\beta = 5$, $m_A = 350$ GeV, $m_{\tilde{\chi}_1^+} = 155$ GeV and $m_{\tilde{\nu}_\mu} = 261$ GeV. The dashed line corresponds to an energy spread of 150 MeV, the solid line to no energy spread.

Scenarios	**B400**	**C400**	**B180**	**C180**	**B7**	**B8**	**C7**	**C8**
M_2[GeV]	217.3	154.9	242.8	180.7	214	212.8	156.9	157.5
μ[GeV]	217.3	-400	242.8	-420	214	212.8	-400	-400
$\tan\beta$	5	5	5	5	7	8	7	8
$m_{\chi_1^\pm}$	155	155	180	180	155	155	155	155
U_{11}	-0.632	0.958	-0.640	0.959	-0.625	-0.622	0.955	0.954
U_{12}	0.775	0.288	0.768	0.283	0.781	0.783	0.297	0.300
V_{11}	0.775	0.9984	0.768	0.9977	0.781	0.783	0.9972	0.9967
V_{12}	-0.632	-0.056	-0.640	-0.068	-0.625	-0.622	-0.075	-0.081
m_A[GeV]	400	400	400	400	350	350	350	350
m_H[GeV]	402.0	401.6	402.0	401.6	351.2	350.9	351.0	350.7
Γ_H[GeV]	1.17	0.61	0.82	0.52	0.71	0.80	0.44	0.53
Γ_A[GeV]	2.43	1.09	1.96	1.00	1.42	1.50	0.57	0.67

Table 2.2: Reference scenarios with different mass m_A (scenarios **B400** and **C400**), with different masses $m_{\tilde{\chi}_1^\pm}$ and m_A, (scenarios **B180** and **C180**) and different values of $\tan\beta$ (scenarios **B7**, **B8** and **C7**, **C8**) as in the reference scenarios (table 2.1). U_{11} and V_{11} (U_{12} and V_{12}) are the gaugino (higgsino) components of the charginos [33], see Appendix A.

The influence of the Higgs mass m_A and the chargino mass $m_{\tilde{\chi}_1^\pm}$ is illustrated in Fig. 2.5 for mixed scenarios with $\mu > 0$ and for scenarios with a gaugino-like light chargino and $\mu < 0$. In scenarios **B400** and **C400** with $m_A = 400$ GeV and $m_{\tilde{\chi}_1^\pm} = 155$ GeV the overlap of the Higgs resonances is larger than in the corresponding scenarios with $m_A = 350$ GeV and the same chargino mass, see Figs. 2.4 b and 2.4 c. The overlap diminishes when the chargino mass is increased to $m_{\tilde{\chi}_1^\pm} = 180$ GeV in scenarios **B180** and **C180** due to the smaller phase space of the Higgs decays.

For larger values of $\tan\beta$ the H and A resonances tend to overlap since the mass difference diminishes. As an example we compare in Fig. 2.6 for $m_A = 350$ GeV the total cross sections for the gaugino scenarios **C**, **C7** and **C8** with $\tan\beta = 5$, $\tan\beta = 7$ and $\tan\beta = 8$ respectively, without and with an energy spread of 150 MeV. Without energy spread both resonances are well separated up to $\tan\beta = 7$ whereas for $\tan\beta = 8$ the H resonance can barely be discerned. With energy spread, however, the overlap for $\tan\beta = 7$ is already so large that the resonances nearly merge. Here the separation of the resonance contributions may not be possible with a good precision. The same conclusion applies to other chargino scenarios, as can be seen for the mixed scenarios **B** ($\tan\beta = 5$), **B7** ($\tan\beta = 7$) and **B8** ($\tan\beta = 8$) in Figs. 2.6c and Fig. 2.6d without and with

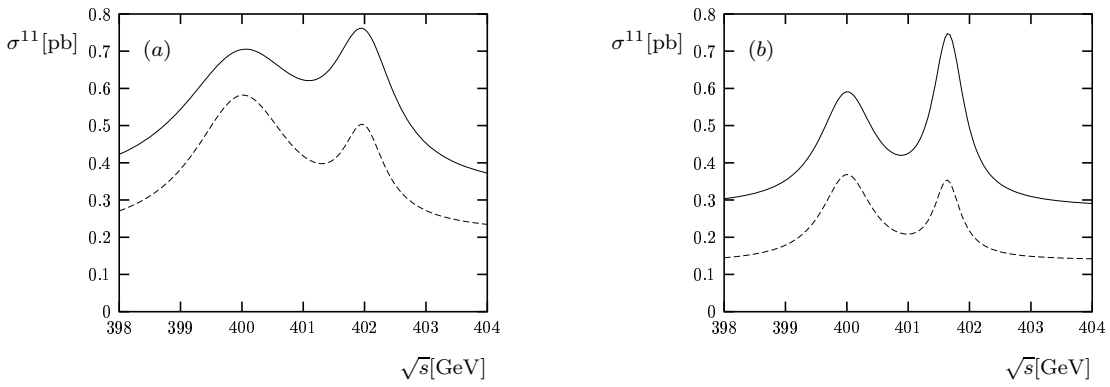

Figure 2.5: Total cross section σ^{11} for $\mu^+\mu^- \to \tilde{\chi}_1^+\tilde{\chi}_1^-$ with $\tan\beta = 5$, $m_A = 400$ GeV, $m_{\tilde{\nu}_\mu} = 261$ GeV and $m_{\tilde{\chi}_1^+} = 155$ GeV (solid) and $m_{\tilde{\chi}_1^+} = 180$ GeV (dashed). (a) shows the mixed scenarios of table 2.2 with $\mu > 0$, **B400** and **B180**, and (b) the gaugino scenarios with $\mu < 0$, **C400** and **C180**, given in table 2.2.

energy spread of 150 MeV, respectively.

2.2.3 Precision measurements of the Higgs-chargino couplings

In this section we study the errors of a measurement of the ratio of couplings x resulting from the uncertainties due to the energy spread of the beams and to the background.

The error in the determination of the ratio x of the squared Higgs-chargino couplings eq. (2.18) depends both on the energy resolution R of the muon beams and on the error $\Delta\sigma_B/\sigma_B$ in the measurement of the non-resonant channels (γ, Z, $\tilde{\nu}_\mu$ and h exchange as well as irreducible standard model background) at the H and A resonances. This background contribution can be estimated from cross section measurements sufficiently far off the Higgs resonances.

In Fig. 2.7 we plot contours of the relative error in the determination of x in the R and $\Delta\sigma_B/\sigma_B$ plane for the scenarios **A** – **F**. The contours are shown for the two cases that the irreducible standard model background is neglected or reduced to 25% of the non-resonant supersymmetric channels by appropriate cuts, respectively. For a detailed background analysis Monte Carlo simulations taking into account the detailed detector characteristics have to be performed and are expected to correspond to the considered range in Fig. 2.7 [29].

As a result of the error propagation one observes a stronger dependence on R than on $\Delta\sigma_B/\sigma_B$. Since the energy spread only changes the shape of the resonances the relative errors in the peak cross sections and in the widths are correlated. Generally, an irreducible standard model background up to 25% of

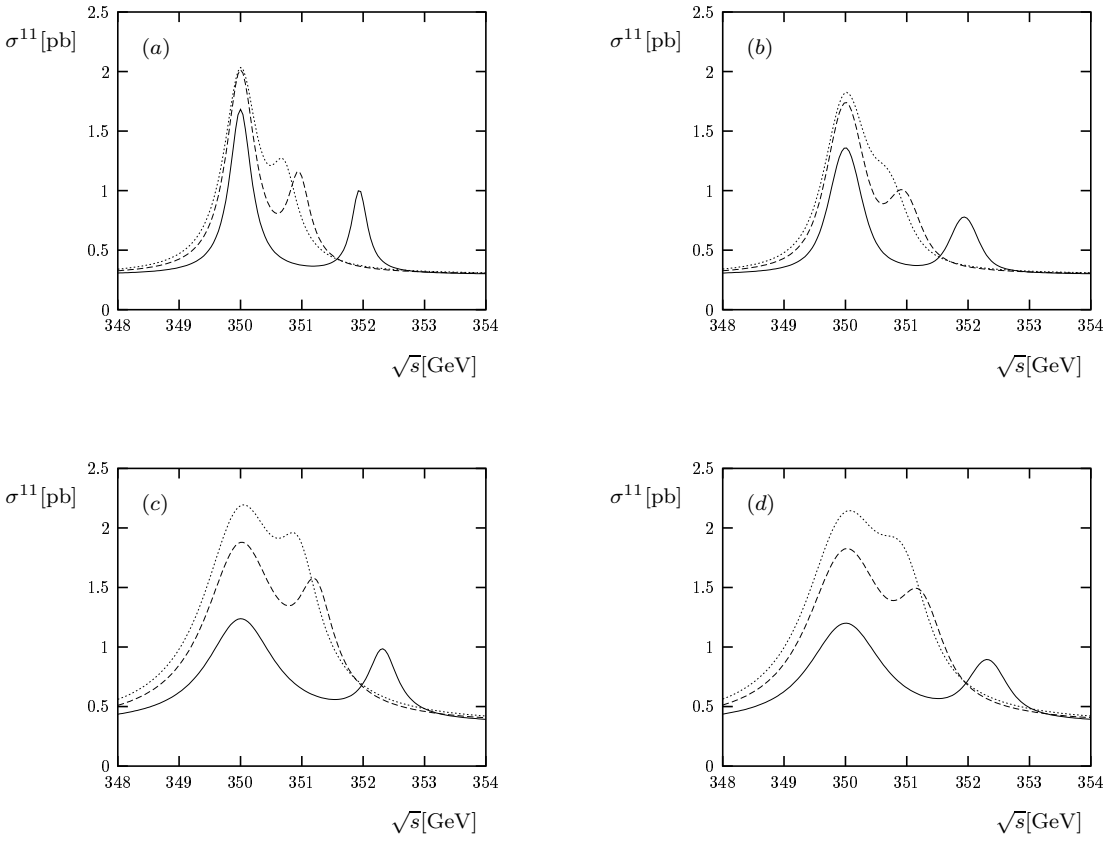

Figure 2.6: Dependence on $\tan\beta$ of the total cross section σ^{11} for $\mu^+\mu^- \to \tilde{\chi}_1^+\tilde{\chi}_1^-$ with $m_A = 350$ GeV and $m_{\tilde{\nu}_\mu} = 261$ GeV. The gaugino scenarios with $\mu < 0$, **C**, **C7** and **C8**, are plotted without energy spread (a) and with an energy spread of 150 MeV (b), for $\tan\beta = 5$ (solid), 7 (dashed) and 8 (dotted), and the mixed scenarios with $\mu > 0$, **B**, **B7** and **B8**, in (c) and (d), without and with energy spread respectively and $\tan\beta = 5$ (solid), 7 (dashed) and 8 (dotted).

the supersymmetric background leads to a slightly reduced precision for the determination of x.

Due to the narrower resonance widths the energy resolution R affects the relative error in x in scenarios **C**, **D** and **E**, **F** with gaugino-like or higgsino-like light charginos significantly more than in the mixed scenarios **A** and **B**. The influence of the error in the background measurement is largest in the scenarios with a higgsino-like light chargino and much smaller in the other chargino mixing scenarios. In all cases only minor differences appear between the scenarios with positive and negative μ.

In order to achieve a relative error $\Delta x/x < 10\%$ an energy resolution $R < 0.04\%$ is necessary in the mixed scenarios and better than 0.02% in the gaugino and higgsino scenarios. These values lie in the range between 0.01% and 0.06%

of the expected energy resolution at a muon collider [12, 16]. In addition, the background contributions have to be known with a relative error $\Delta\sigma_B/\sigma_B < 10\%$ in the mixed and gaugino scenarios whereas in the higgsino scenarios a much higher precision $\Delta\sigma_B/\sigma_B < 6\%$ is necessary.

For a energy resolution $R = 0.04\%$ the error in the measurement of x becomes $\Delta x/x \approx 40\%$ in the scenarios **C** and **D** with gaugino-like charginos and practically independent of the background error. A similar error is expected in scenario **E** with higgsino-like charginos, which decreases to 27% for $\Delta\sigma_B/\sigma_B < 10\%$.

If on the other hand an energy resolution $R = 0.01\%$ is achieved and the contributions of the background channels are well known ($\Delta\sigma_B/\sigma_B < 5\%$ in the mixed and gaugino scenarios and $\Delta\sigma_B/\sigma_B < 2.5\%$ in the higgsino scenarios) the error can be reduced to the order of a few percent.

2.2.4 Summary of Section 2.2

In this Section we have studied equal chargino pair production at a future muon collider via resonant heavy Higgs boson exchange in the MSSM. This process yields large cross sections of up to a few pb in relevant regions of the supersymmetric parameter space. Due to the sharp energy resolution that allows to separate the CP-even and CP-odd resonances a muon collider is an accurate tool to investigate the Higgs couplings to its decay products. Here we have focused on the determination of the Higgs-chargino couplings. We have shown that the ratio of H-chargino and A-chargino couplings can be precisely determined independently of the chargino decay mechanism. This method avoids reference to other experiments and makes only a few model dependent assumptions, namely the existence of a CP-even and a CP-odd resonance and the approximate decoupling limit for the Higgs-muon couplings.

In representative supersymmetric scenarios we have analyzed the effect of the energy spread and of the error from the non-resonant channels including an irreducible standard model background up to 25% of the supersymmetric background. With a good energy resolution a precision as good as a few percent can be obtained for $\tan\beta < 8$ and $m_A \leq 400$ GeV, where the Higgs resonances can be separated.

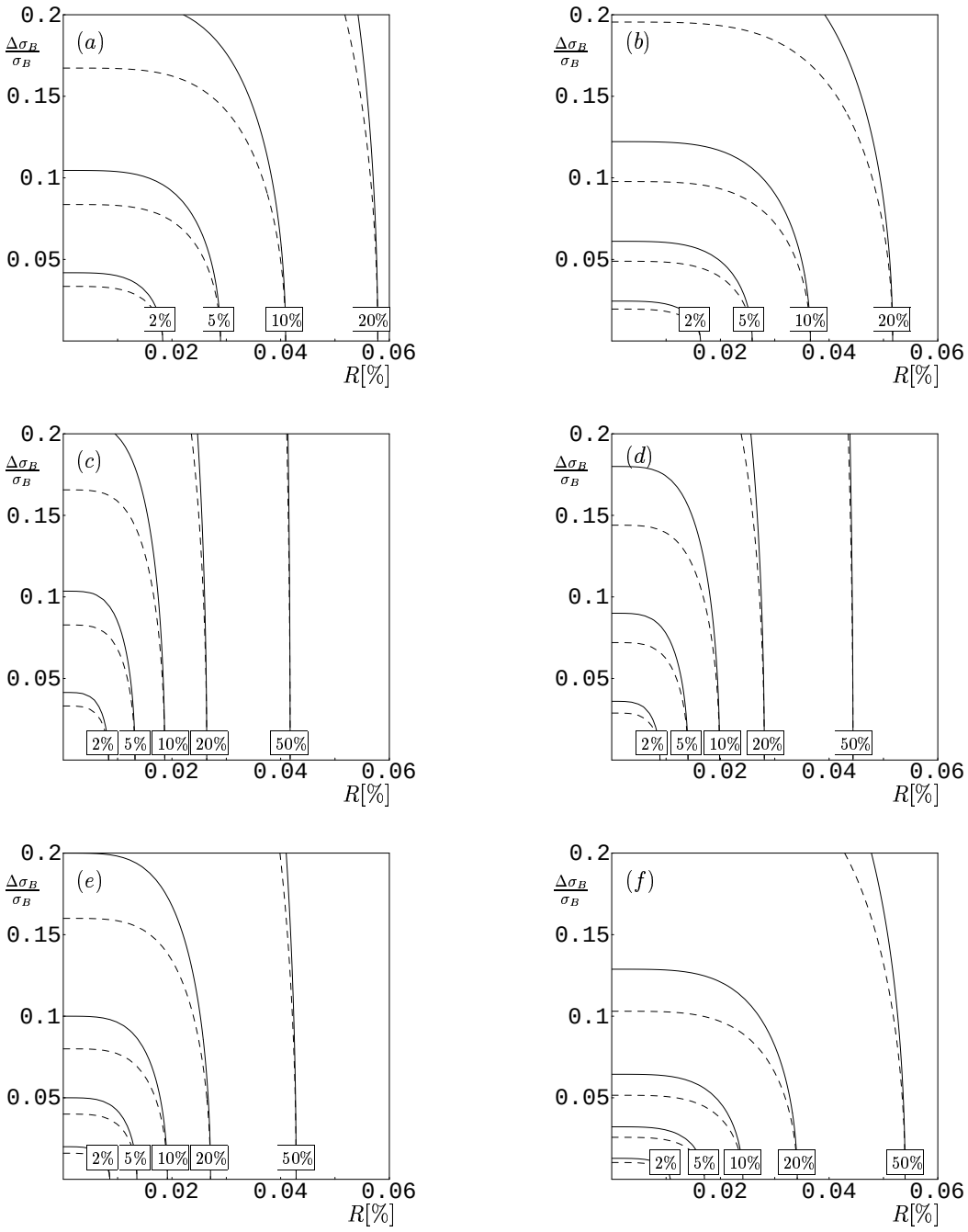

Figure 2.7: Relative error in the ratio of the Higgs-chargino couplings x as a function of the energy resolution and the relative error in the non-resonant contributions. The irreducible standard model background is neglected (solid) and 25% of the supersymmetric background (dashed). Plots (a) – (f) correspond to the scenarios **A** – **F** in Table 2.1.

2.3 Production of $\tilde{\chi}_1^\pm\tilde{\chi}_2^\mp$

In this section we study $\tilde{\chi}_1^\pm\tilde{\chi}_2^\mp$ production with longitudinally polarized beams. Unlike the couplings for equal charginos, the left and right-handed Higgs-chargino couplings are independent, and therefore a larger number of observables is necessary to probe the interaction structure. We show that the interference of scalar exchange channels with different CP quantum numbers does not in general vanish. Therefore the $\tilde{\chi}_1^+\tilde{\chi}_2^-$ and $\tilde{\chi}_1^-\tilde{\chi}_2^+$ production cross sections differ for longitudinally polarized beams. We show that, when H and A are nearly degenerate, the resulting asymmetries are large.

The production density matrix for chargino pair production via Higgs exchange, given in eqs. (C.39-C.42), are functions of the combinations of couplings $a_\pm^{\alpha\beta}$ and $b_\pm^{\alpha\beta}$, eqs. (C.50) and (C.51). Here α and β denote the Higgs boson exchange channel. The coefficient for production of unpolarized charginos P_r, depends on two terms proportional to the combinations $a_+^{\alpha\beta}$ and $b_+^{\alpha\beta}$. In principle, given the different center of mass energy dependence of the two terms both $a_+^{\alpha\beta}$ and $b_+^{\alpha\beta}$ could be obtained from the production process. In practice, however, since the resonance region is not large, a study of the chargino polarizations is necessary. Therefore, for the production process, the aim is not to determine but to test the Higgs-chargino interaction.

For pure Higgs exchange channels eq. (C.39) can be expressed as

$$P_r^{(\phi\phi)} = \frac{g^4}{4}(1+\mathcal{P}_+^L\mathcal{P}_-^L)\,|\Delta(\phi)|^2|c^{(\phi\mu)}|^2 s[(s-m_{\chi_i^\pm}^2-m_{\chi_j^\pm}^2)a_+^{\phi\phi}-2m_{\chi_i^\pm}m_{\chi_j^\pm}b_+^{\phi\phi}]. \quad (2.26)$$

Note that, while the first term inside the square brackets is positive, the second term may be positive or negative, depending on the sign of $b_+^{\phi\phi} = \mathrm{Re}(c_{L\,ij}^{(\phi)}c_{R\,ij}^{(\phi)*})$. The partial p-wave suppression of the Higgs exchange amplitudes for $\tilde{\chi}_i^+\tilde{\chi}_j^-$ production is given by the parameter $\delta_p^\phi = (a_+^{\phi\phi}+b_+^{\phi\phi})/2a_+^{\phi\phi}$, which vanishes for $c_{Lij}^{(\phi\phi)} = -c_{Rij}^{(\phi\phi)}$ and is maximal for $c_{Lij}^{(\phi\phi)} = c_{Rij}^{(\phi\phi)}$.

For the H-A interference eq. (C.39) simplifies to

$$\begin{aligned} P_r^{(HA)} &= -\frac{g^4}{2}(\mathcal{P}_+^L+\mathcal{P}_-^L)\,\mathrm{Re}\{\Delta(H)\Delta(A)^*\}\,\mathrm{Im}(c^{(H\mu)}c^{(A\mu)*}) \\ &\quad s[(s-m_{\chi_i^\pm}^2-m_{\chi_j^\pm}^2)\mathrm{Im}(a_+^{HA})-2m_{\chi_i^\pm}m_{\chi_j^\pm}\mathrm{Im}(b_+^{HA})]. \end{aligned} \quad (2.27)$$

Since the interference term is proportional to the sum of longitudinal beam polarizations, it changes sign under parity, contrary to the pure exchange contributions, eq. (2.26). Therefore, beam polarization can be used to separate the contributions. The interference term also changes sign under exchange of the chargino indices, $i \leftrightarrow j$ and thus cancels out for the sum of production cross sections $\sigma(\tilde{\chi}_1^+\tilde{\chi}_2^- + \tilde{\chi}_2^+\tilde{\chi}_1^-)$.

Table 2.3: Scenarios **P1** and **P2** for $\mu^+\mu^- \to \tilde{\chi}_1^\mp \tilde{\chi}_2^\pm$

	P1	**P2**		**P1**	**P2**
$\tan\beta$	10	10	$m_{\chi_1^\pm}$[GeV]	138	106
μ[GeV]	-250	-110	$m_{\chi_2^\pm}$[GeV]	281	322
M_2[GeV]	150	300	$m_{\tilde{\chi}_1^0}$[GeV]	74	89
m_0[GeV]	200	200	$m_{\tilde{\nu}_\mu}$[GeV]	232	327
m_A[GeV]	500	500	Γ_A[GeV]	3.7	3.4
m_H[GeV]	500.3	500.4	Γ_H[GeV]	3.6	3.3

To isolate the resonant contributions we define the charge asymmetry

$$\mathcal{A}^C_{prod} = \frac{\sigma(\tilde{\chi}_1^+\tilde{\chi}_2^-) - \sigma(\tilde{\chi}_2^+\tilde{\chi}_1^-)}{\sigma(\tilde{\chi}_1^+\tilde{\chi}_2^-) + \sigma(\tilde{\chi}_2^+\tilde{\chi}_1^-)} = \frac{P_r^{(HA)}}{\bar{P}_{cont} + P_r^{(HH)} + P_r^{(AA)}}, \tag{2.28}$$

as well as the polarization asymmetry

$$\mathcal{A}^{pol}_{prod} = \frac{\sigma(\tilde{\chi}_1^+\tilde{\chi}_2^-)(\mathcal{P}) - \sigma(\tilde{\chi}_1^+\tilde{\chi}_2^-)(-\mathcal{P})}{\sigma(\tilde{\chi}_1^+\tilde{\chi}_2^-)(\mathcal{P}) + \sigma(\tilde{\chi}_1^+\tilde{\chi}_2^-)(-\mathcal{P})} = \frac{P_r^{(HA)}(\mathcal{P})}{[\bar{P}_{cont} + P_r^{(HH)} + P_r^{(AA)}](\mathcal{P})}, \tag{2.29}$$

for $\mathcal{P}_+^L = \mathcal{P}_-^L \equiv \mathcal{P}$. To obtain eq. (2.29) we used, in addition to the dependence of the resonant channels on the beam polarization, as previously noted, also the dependence of the continuum contributions. The polarization dependence of the latter is relatively complicated, since it consists of several channels with different dependencies. However, choosing equal polarizations we obtain $P_{cont}(-\mathcal{P}) = P_{cont}(\mathcal{P})$ [20, 22].

2.3.1 Numerical analysis

In Fig. 2.8a we show the production cross sections of the charge conjugated processes $\mu^+\mu^- \to \tilde{\chi}_1^+\tilde{\chi}_2^-$ and $\mu^+\mu^- \to \tilde{\chi}_1^-\tilde{\chi}_2^+$ for scenario **P1** of Table 2.3. Both cross sections are equal for unpolarized beams and differ for polarized beams $\mathcal{P}_+^L = \mathcal{P}_-^L = -0.3$. In this case the H–A interference, eq. (2.7), enhances the $\tilde{\chi}_1^-\tilde{\chi}_2^+$ cross section and suppresses that for the conjugated process. The corresponding charge asymmetry, eq. (2.28), is $\mathcal{A}^C_{prod} = -48\%$ at $\sqrt{s} = 500$ GeV. The asymmetry almost reaches its maximum absolute value of $|\mathcal{P}_+^L + \mathcal{P}_-^L|/(1 + \mathcal{P}_+^L\mathcal{P}_-^L) \approx 55\%$, here for $\mathcal{P}_+^L = \mathcal{P}_-^L = -0.3$, which would be obtained in the ideal case of vanishing continuum contributions. For scenario **P2**, shown in Fig. 2.8b, the $\tilde{\chi}_1^-\tilde{\chi}_2^+$ production is instead suppressed by the H–A interference and the $\tilde{\chi}_1^+\tilde{\chi}_2^-$ production

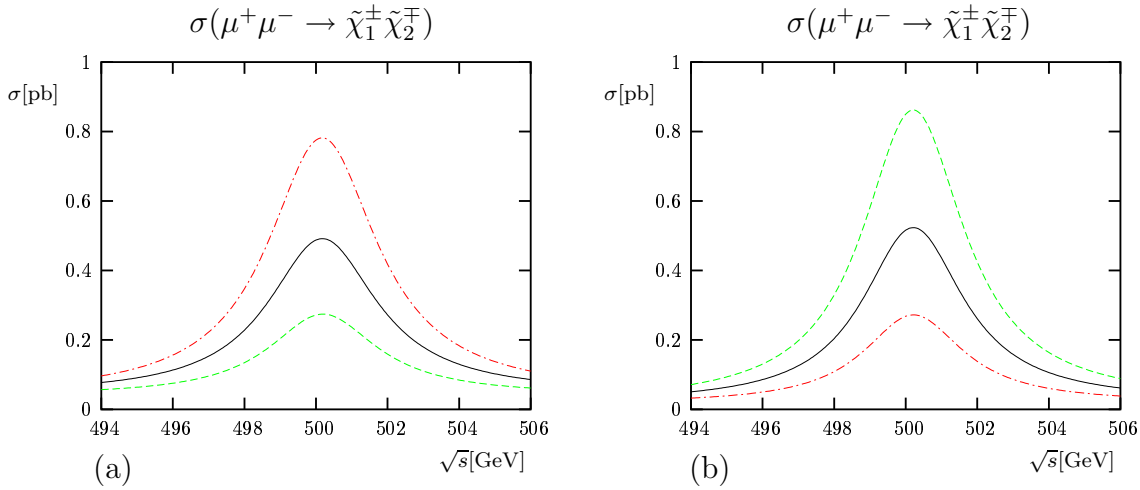

Figure 2.8: $\mu^+\mu^- \to \tilde{\chi}_1^\pm \tilde{\chi}_2^\mp$. Cross sections $\sigma(\mu^+\mu^- \to \tilde{\chi}_1^+ \tilde{\chi}_2^-)$ (dashed) and $\sigma(\mu^+\mu^- \to \tilde{\chi}_1^- \tilde{\chi}_2^+)$ (dash-dotted) for longitudinal beam polarizations $\mathcal{P}_+^L = \mathcal{P}_-^L = \mathcal{P} = -0.3$, and $\sigma(\mu^+\mu^- \to \tilde{\chi}_1^\pm \tilde{\chi}_2^\mp)$ (solid) for $\mathcal{P} = 0$, for scenario **P1 (a)** and scenario **P2 (b)**, given in Table 2.3.

is enhanced, such that $\mathcal{A}_{prod}^C = 45\%$ changes sign. In scenario **P1** (**P2**) the lightest chargino has mainly gaugino (higgsino) character, i.e., the gaugino (higgsino) components are larger. Since Higgs bosons couple to a gaugino-Higgsino pair, the corresponding couplings, eqs. (B.5-B.7), transform as

$$c_{L,Rij}^{(\phi)} \leftrightarrow c_{L,Rji}^{(\phi)} \tag{2.30}$$

under $M_2 \leftrightarrow |\mu|$. This symmetry relates the resonant amplitude for $\tilde{\chi}_1^+ \tilde{\chi}_2^-$ ($\tilde{\chi}_1^- \tilde{\chi}_2^+$) production for scenario **P1** with the amplitude for $\tilde{\chi}_1^- \tilde{\chi}_2^+$ ($\tilde{\chi}_1^+ \tilde{\chi}_2^-$) production for scenario **P2** and explains the different signs of $\mathcal{A}_{prod}^C$. Consequently, for $M_2 = |\mu|$ the asymmetries vanish.

In Fig. 2.9 we show the branching ratios of H and of A into $\tilde{\chi}_1^+ \tilde{\chi}_2^-$ and $\tilde{\chi}_2^+ \tilde{\chi}_1^-$ pairs. Branching ratios larger than 30% are found for H decays and 20% for A decays. This decay channel is therefore important for this set of parameters. Contrary to what we found for the decays into lighter charginos, the decays are slightly suppressed in the mixed regions, for $\mu \approx M_2$, mainly due to the competing channels from lighter charginos and neutralinos, see Sections 2.2 and 3.1.

Note that, if the mass difference between the charginos and the Higgs boson is small, the branching ratios for the CP-even Higgs H are larger than those for the CP-odd Higgs A. This behavior hints at a stronger p-wave suppression of the CP-odd amplitude, contrary to the case of equal charginos where the CP-even amplitude is suppressed.

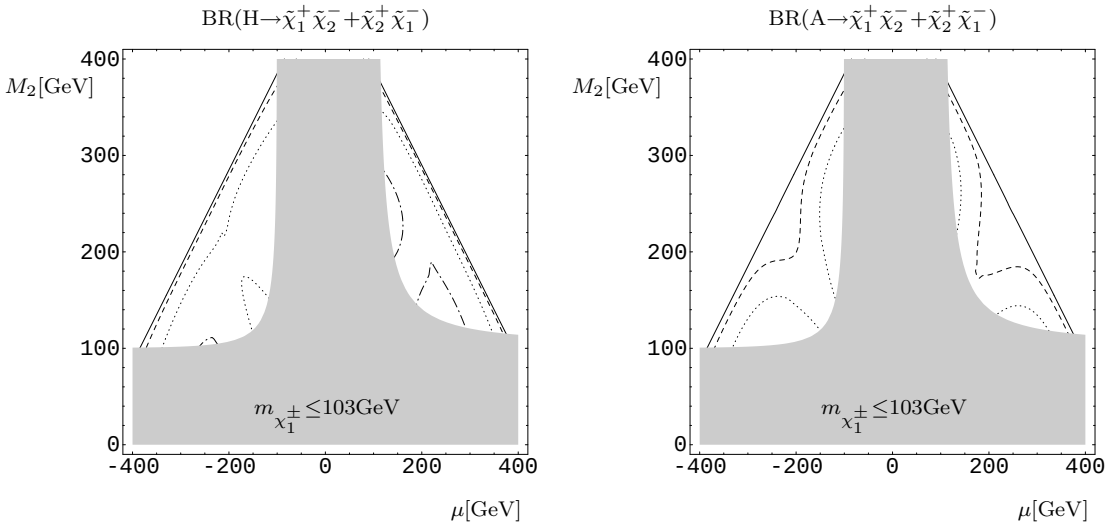

Figure 2.9: Branching ratios of the heavy Higgs bosons H and A into light chargino pairs for $m_A = 500$ GeV, $\tan\beta = 10$ and sfermions masses larger than $M_H/2$, computed with the program HDECAY [32]. The contour lines correspond to 0.1 (dashed), 0.2 (dotted) and 0.3 (dash-dotted). The solid line corresponds to the threshold for chargino pair production. The gray area is the experimentally excluded region given here by $m_{\chi_1^\pm} < 103$ GeV.

2.3.2 Summary of Section 2.3

Here we discussed $\tilde{\chi}_1^\pm\tilde{\chi}_2^\mp$ production in $\mu^+\mu^-$-annihilation with longitudinally polarized beams. We have shown that the interference of scalar exchange channels with different CP quantum numbers can be large, provided the resonances are nearly degenerate. For two example scenarios we have shown the dependence of the cross sections for $\tilde{\chi}_1^+\tilde{\chi}_2^-$ and $\tilde{\chi}_1^-\tilde{\chi}_2^+$ on the center of mass energy.

2.4 Chargino production with subsequent decay of one of the charginos

In the preceding two sections we have analyzed the chargino pair production process in $\mu^+\mu^-$-annihilation at the heavy Higgs resonances with longitudinally polarized beams. In this section we study the decay of one of the charginos in order to gain information from its polarization. Since we focus on the resonant exchange of neutral Higgs bosons, which do not contribute to the transverse polarizations of the charginos, eqs. (C.40) and (C.41), we only need to consider longitudinal chargino polarization. The chargino polarizations are determined through the energy distributions of the lepton or W boson from the two-body decays $\tilde{\chi}_j^\pm \to \ell^\mp\tilde{\nu}_\ell$ or $\tilde{\chi}_j^\pm \to W^\pm\tilde{\chi}_1^0$, respectively. We show that the interference of the CP-even and

CP-odd Higgs bosons can be analyzed using these energy distributions. Therefore we define asymmetries in these energy distributions which allow a determination of the H and A couplings to the charginos and in particular of their relative phase.

We analyze the asymmetries, cross sections and branching ratios in CP conserving MSSM scenarios. For nearly degenerate Higgs bosons we find large asymmetries which can be measured with high statistical significance.

2.4.1 Decay channels

Provided the following channels are kinematically allowed, charginos decay predominantly into a fermion-sfermion pair, into a neutralino and a W or a charged Higgs boson. The heavier chargino may also decay into the lighter one and a Z or Higgs boson, shown in Fig. 2.10. The corresponding interaction Lagrangians are given in Appendix B.4. We assume that squarks are heavier than charginos.

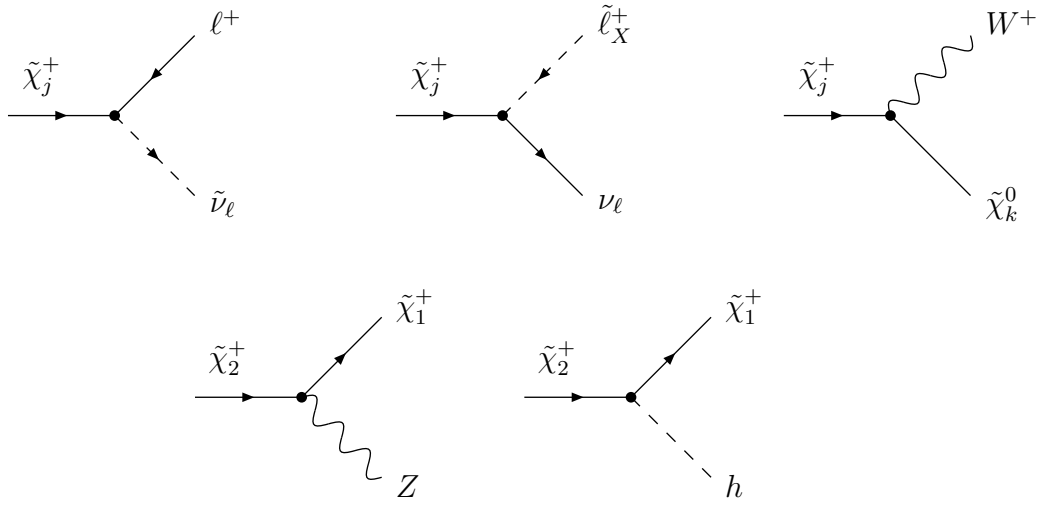

Figure 2.10: Two-body decays of charginos. Here $\tilde{\ell}_X^+ = \tilde{\ell}_{L,R}^+$ for $\ell = e, \mu$ and $\tilde{\ell}_X^+ = \tilde{\tau}_{1,2}^+$ for $\ell = \tau$. The charged conjugated processes are obtained inverting the arrows and the electric charges in the Feynman diagrams.

2.4.2 Chargino polarization

To study the polarization of the produced charginos we decompose the production spin density matrix and the decay matrix in terms of Pauli matrices and the Kronecker delta function, eqs. (C.25) and (C.26).

With our choice of the spin vectors, eqs. (C.18) and (C.21), $\Sigma^3_{P_j}/P$ is the longitudinal polarization of $\tilde{\chi}_j^\pm$, $\Sigma^1_{P_j}/P$ is its transverse polarization in the production plane and $\Sigma^2_{P_j}/P$ is its polarization perpendicular to the production plane.

As discussed in Section 2.1, the expansion coefficients of the chargino production matrix, eq. (C.25), subdivide into contributions from the Higgs resonances $\Sigma^a_{r_j}$ and the continuum $\Sigma^a_{cont_j}$, eq. (2.4). The spin correlation coefficients of the resonant contributions from s-channel exchange of the Higgs bosons H and A, are separated into pure exchange and interference terms

$$\Sigma^3_{rj} = \sum_{\phi=H,A} \Sigma^{3\,(\phi\phi)}_{rj} + \Sigma^{3\,(HA)}_{rj}, \tag{2.31}$$

while resonant contributions Σ^1_r and Σ^2_r to the transverse polarizations of the chargino vanish since the s-channel exchange is due to scalar Higgs bosons. Evaluating the production amplitudes with the interaction Lagrangians eqs. (B.1) and (B.2) in the CMS we obtain for $\mu^+\mu^- \to \tilde{\chi}^-_i \tilde{\chi}^+_j$

$$\Sigma^{3\,(\phi\phi)}_{rj} = \frac{g^4}{8}(1 + \mathcal{P}^L_+\mathcal{P}^L_-)|\Delta(\phi)|^2|c^{(\phi\mu)}|^2(|c^{(\phi)}_L|^2 - |c^{(\phi)}_R|^2)s\sqrt{\lambda_{ij}}, \tag{2.32}$$

$$\begin{aligned}\Sigma^{3\,(HA)}_{rj} = & -\frac{g^4}{4}(\mathcal{P}^L_+ + \mathcal{P}^L_-)\mathrm{Re}\{\Delta(H)\Delta(A)^*\} \\ & \mathrm{Im}\{c^{(H)}_L c^{(A)*}_L - c^{(H)}_R c^{(A)*}_R\}\mathrm{Im}\{c^{(H\mu)}c^{(A\mu)*}\}s\sqrt{\lambda_{ij}},\end{aligned} \tag{2.33}$$

where we used the short-hand notation $c^{(\phi)}_R \equiv c^{(\phi)}_{R\,ij}$ and $c^{(\phi)}_L \equiv c^{(\phi)}_{L\,ij}$ for the Higgs-chargino couplings, $\mathcal{P}^L_+$ and $\mathcal{P}^L_-$ denote the longitudinal beam polarizations, $\Delta(\phi)$ is the Breit-Wigner propagator, eq. (2.8) and and

$$\lambda_{ij} = \lambda(s, m^2_{\chi^\pm_i}, m^2_{\chi^\pm_j}), \tag{2.34}$$

with the triangle function λ defined in eq. (E.11).

Note that $\Sigma^{3\,(\phi\phi)}_{rj}$ vanishes for production of equal charginos $i = j$ since in this case the Higgs-chargino couplings are parity conserving, with $c^{(\phi)}_{L\,ii} = c^{(\phi)*}_{R\,ii}$. This term is thus only present for $\tilde{\chi}^\pm_1\tilde{\chi}^\mp_2$ production since, in general, $c^{(\phi)}_{L\,ij} \neq c^{(\phi)*}_{R\,ij}$ for $i \neq j$.

2.4.3 Kinematics of chargino two-body decay

The two-body decay $\tilde{\chi}^+_j \to \lambda^+ + \tilde{N}$ has $2 \times 3 - 4 = 2$ degrees of freedom, which can be parametrized by the polar and azimuth angles of the momentum of one of the decay particles. In the center of mass system of the decaying chargino the energies of the decay particles λ^+ and $\tilde{N}$ are fixed. If the chargino is not at rest the decay angle θ_j and the energy E_λ of the decay particle λ^+ are related due to four-momentum conservation, by

$$E_\lambda E_{\chi^+_j} - |\vec{p}_\lambda||\vec{p}_{\chi^+_j}|\cos\theta_j = \frac{1}{2}(m^2_{\chi^\pm_j} + m^2_\lambda - m^2_{\tilde{N}}). \tag{2.35}$$

If $m_\lambda > \bar{m}_\lambda$, with $\bar{m}_\lambda = (m^2_{\chi_j^\pm} - m^2_\lambda - m^2_{\tilde{N}})/2E_{\chi_j^+}$, eq. (2.35) admits two solutions of E_λ for every value of θ_j, with $0 \leq \theta_j \leq \theta_{max} < \pi/2$. The energy E_λ is thus a better parameter to parametrize the decay.

If $m_\lambda < \bar{m}_\lambda$, eq. (2.35) simplifies to

$$E_\lambda = \frac{m^2_{\chi_j^\pm} - m^2_{\tilde{N}}}{2(E_{\chi_j^+} - |\vec{p}_{\chi_j^+}| \cos\theta_j)} \tag{2.36}$$

with $0 \leq \theta_j \leq \pi$ and a one-to-one correspondence between θ_j and E_λ.

2.4.4 Energy distribution

The energy distribution of the charged lepton or W boson from the decay of $\tilde{\chi}_j^\pm$ is obtained integrating the differential cross section for production and decay, eqs. (C.23) and eq. (C.24), where the amplitude squared is given by (here we suppress the chargino index of the density matrix coefficients)

$$|T|^2 = |\Delta(\tilde{\chi}_j^\pm)|^2 \sum_{\lambda_i\lambda_j\lambda_i'\lambda_j'} \rho^P_{\lambda_i\lambda_i'\lambda_j\lambda_j'} \rho^D_{\lambda_j'\lambda_j} \delta_{\lambda_i\lambda_i'} = 4|\Delta(\tilde{\chi}_j^\pm)|^2 (P\cdot D + \Sigma_P^a \cdot \Sigma_D^a). \tag{2.37}$$

Here we summed over the helicity indices λ_i and λ_i' of $\tilde{\chi}_i^\mp$ whose decay is not observed. The resonant contributions to the production density matrix coefficients P and Σ_P^a are given in eqs. (2.6), (2.7), (2.32) and (2.33). The expansion coefficients of the chargino decay matrix (C.26) for the chargino decays $\tilde{\chi}_j^+ \to \ell^+ \, \tilde{\nu}_\ell$, with $\ell = e, \mu, \tau$ and $\tilde{\chi}_j^+ \to W^+ \tilde{\chi}_k^0$ are given in Appendix C.3.1.

In the CMS we can rewrite the factor Σ_D^3 that multiplies the longitudinal chargino polarization coefficient Σ_P^3 in eq. (C.30),

$$\Sigma_D^3 \;=\; \eta_{\lambda^\pm} \frac{D}{\Delta_\lambda} (E_\lambda - \bar{E}_\lambda), \quad \lambda = e, \mu, \tau, W, \tag{2.38}$$

where we have used the relation

$$m_{\chi_j^\pm}(s^3_{\chi_j^\pm} \cdot p_\lambda) = -\frac{m^2_{\chi_j^\pm}}{|\vec{p}_{\chi_j^\pm}|}(E_\lambda - \bar{E}_\lambda) \tag{2.39}$$

and the kinematical factors $\bar{E}_\lambda$ and Δ_λ have been defined in eqs. (D.12-D.15). The factor $\eta_{\lambda^\pm}$ in eq. (2.38) is a measure of parity violation in the decay process. It is thus maximal, $\eta_{\ell^\pm} = \pm 1$, for the decay $\tilde{\chi}_j^\pm \to \ell^\pm \, \tilde{\nu}_\ell^{(*)}$, for $\ell = e, \mu$, since the sneutrino couples purely left handed. For $\ell = \tau$ or for chargino decays into a W and a neutralino, the factors $\eta_{\tau^\pm}$, eq. (C.60), and $\eta_{W^\pm}$, eq. (C.61), respectively, are generally smaller, thus reducing Σ_D^3.

The energy distribution of the decay particle $\lambda^\pm$ is now given by

$$\frac{d\sigma_{\lambda^\pm}}{dE_\lambda} = \frac{\sigma_\lambda}{2\Delta_\lambda} \left[1 + \eta_{\lambda^\pm} \frac{\bar{\Sigma}_P^3}{\bar{P}} \frac{(E_\lambda - \bar{E}_\lambda)}{\Delta_\lambda} \right], \tag{2.40}$$

where we have defined averages of the production density matrix coefficients over the chargino production angles in the CMS

$$\bar{P} = \frac{1}{4\pi}\int P d\Omega_{\chi^\pm}, \qquad \bar{\Sigma}^3_P = \frac{1}{4\pi}\int \Sigma^3_P d\Omega_{\chi^\pm}. \tag{2.41}$$

Further, the cross section for production and subsequent decay σ_λ is obtained multiplying the cross section for production σ^{jj}, eq. (2.11), times the branching ratio $\mathrm{BR}(\tilde{\chi}^\pm_\mathrm{j} \to \lambda^\pm \tilde{\mathrm{N}})$.

Two examples of energy distributions of the decay particles ℓ^+ and ℓ^- are shown in Fig. 2.11. The linear dependence of the distributions on the lepton energy for ℓ^+ and ℓ^- is similar if the two end-points are exchanged. The slope of the curves is proportional to $\bar{\Sigma}^3_P/\bar{P}$, the average longitudinal polarization of the decaying chargino, as follows from eq. (2.41). Note that the energy distribution might be difficult to measure for a small chargino-sneutrino mass difference, since the energy range of the observed lepton is proportional to the difference of their squared masses, see (D.13).

The form of the energy distribution, eq. (2.40), can be interpreted with help of the decay $\tilde{\chi}^-_j \to e^- \tilde{\nu}^*_e$, in which the electron is left handed. Orbital angular momentum conservation along the direction of motion of the chargino, here $\hat{z}$, leads to conservation of the z spin component s_z. Since the sneutrino is a scalar, the electron and chargino have the same spin component in z direction. Therefore, a right-handed (left-handed) chargino decays then preferably into an electron in backward (forward) direction, which implies slower (faster) electrons. Averaging with the chargino polarization $\bar{\Sigma}^3_P/\bar{P}$ leads to eq. (2.40).

2.4.5 Asymmetries in the energy distribution

For the cross section $\sigma_{\lambda^\pm}$ of chargino production (2.1) with subsequent two-body decay of one of the charginos into a lepton and a sneutrino (2.2) or into a W boson and a neutralino (2.3), we define the asymmetries $\mathcal{A}_{\lambda^+}$ and $\mathcal{A}_{\lambda^-}$ for the charge conjugated processes $\mu^+\mu^- \to \tilde{\chi}^-_i\tilde{\chi}^+_j$, $\tilde{\chi}^+_j \to \lambda^+\tilde{N}$ and $\mu^+\mu^- \to \tilde{\chi}^+_i\tilde{\chi}^-_j$, $\tilde{\chi}^-_j \to \lambda^-\tilde{N}$, respectively,

$$\mathcal{A}_{\lambda^\pm} = \frac{\sigma^>_{\lambda^\pm} - \sigma^<_{\lambda^\pm}}{\sigma^>_{\lambda^\pm} + \sigma^<_{\lambda^\pm}} \qquad \lambda = e, \mu, \tau, W. \tag{2.42}$$

with the short hand notation

$$\sigma^<_{\lambda^\pm} = \int_{E^{min}_\lambda}^{\bar{E}_\lambda} \frac{d\sigma_{\lambda^\pm}}{dE_\lambda} dE_\lambda, \qquad \sigma^>_{\lambda^\pm} = \int_{\bar{E}_\lambda}^{E^{max}_\lambda} \frac{d\sigma_{\lambda^\pm}}{dE_\lambda} dE_\lambda. \tag{2.43}$$

Using the formula for the energy distribution of the decay particle $\lambda^\pm$, eq. (2.40), we find that the asymmetries are proportional to the averaged longitudinal polarization of the decaying chargino (here we suppress the chargino index)

$$\mathcal{A}_{\lambda^\pm} = \frac{1}{2}\eta_{\lambda^\pm}\frac{\bar{\Sigma}^3_P}{\bar{P}}. \tag{2.44}$$

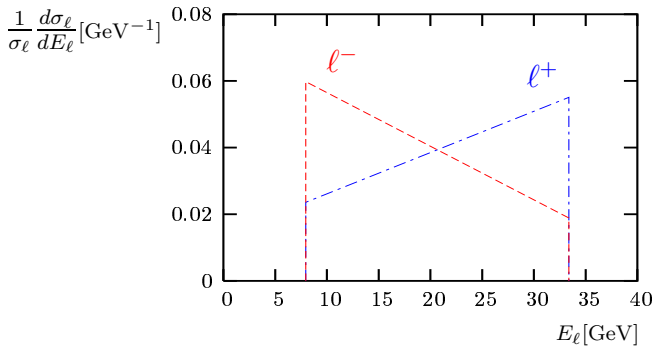

Figure 2.11: Normalized energy distributions of the lepton for the process $\mu^+\mu^- \to \tilde{\chi}_1^+\tilde{\chi}_1^-$ and decay $\tilde{\chi}_1^+ \to \ell^+\tilde{\nu}_\ell$ (dot-dashed) or $\tilde{\chi}_1^- \to \ell^-\tilde{\nu}_\ell^*$ (dashed) with $\sqrt{s} = 500$ GeV and longitudinal beam polarizations $\mathcal{P}_-^L = \mathcal{P}_+^L = -0.3$. The MSSM parameters are given in Table 2.4. The shown distributions have asymmetries $\mathcal{A}_{\ell^+} = 0.2$ and $\mathcal{A}_{\ell^-} = -0.26$, see eq. (2.42).

In order to separate the resonant contributions of the Higgs exchange channels to $\bar{\Sigma}_P^3$ from those of the continuum contributions, see eqs. (2.4) and (2.41), we study the transformation properties of the production density matrix expansion coefficients under charge conjugation and parity.

For the production of the charge conjugated pair of charginos $\mu^+\mu^- \to \tilde{\chi}_i^+\tilde{\chi}_j^-$, instead of $\mu^+\mu^- \to \tilde{\chi}_i^-\tilde{\chi}_j^+$, the coefficients transform into

$$\Sigma_{cont}^3 \to -\Sigma_{cont}^3, \tag{2.45}$$
$$P_r^{(HA)} \to -P_r^{(HA)}, \tag{2.46}$$
$$\Sigma_r^{3\,(\phi\phi)} \to -\Sigma_r^{3\,(\phi\phi)}, \tag{2.47}$$

while P_{cont}, $P_r^{(\phi\phi)}$ and $\Sigma_r^{3\,(HA)}$ do not change. The coefficients for the continuum contributions from γ, Z and sneutrino exchange can be found in [20, 22].

For equal beam polarizations $\mathcal{P}_+^L = \mathcal{P}_-^L \equiv \mathcal{P}$ the resonant contributions transform under $\mathcal{P} \to -\mathcal{P}$ into

$$P_r^{(HA)} \to -P_r^{(HA)}, \tag{2.48}$$
$$\Sigma_r^{3\,(HA)} \to -\Sigma_r^{3\,(HA)}, \tag{2.49}$$

while the terms $P_r^{(\phi\phi)}$, $\Sigma_r^{3\,(\phi\phi)}$ and the continuum contributions P_{cont} and Σ_{cont}^3, given in [20, 22], are invariant.

It is useful to discuss the production of equal and unequal charginos separately.

2.4.5.1 Production of equal charginos

If equal charginos are produced, $\mu^+\mu^- \to \tilde{\chi}_j^+\tilde{\chi}_j^-$, the resonant contributions $\Sigma_{rj}^{3\,(HA)}$ for the longitudinal polarization of $\tilde{\chi}_j^+$ and those for the longitudinal

polarization of $\tilde{\chi}_j^-$ are equal. The corresponding continuum contributions, however, differ by a sign, see eq. (2.45), and are thus eliminated in the numerator of the charge asymmetries

$$\mathcal{A}_\lambda^C = \frac{1}{2}[\mathcal{A}_{\lambda^+} - \mathcal{A}_{\lambda^-}] \tag{2.50}$$

$$= \frac{1}{2}\eta_{\lambda^+}\frac{\Sigma_{rj}^{3\,(HA)}}{\bar{P}}, \tag{2.51}$$

with $\bar{\Sigma}_{rj}^{3\,(HA)} = \Sigma_{rj}^{3\,(HA)}$, see eq. (2.41). The resonant contributions can also be isolated from the continuum contributions by taking into account their different dependence on the beam polarizations for $\mathcal{P} \equiv \mathcal{P}_+^L = \mathcal{P}_-^L$, given in eqs. (2.48) and (2.49). Then the invariant continuum contributions are eliminated in the polarization asymmetries

$$\mathcal{A}_{\lambda^\pm}^{pol} = \frac{1}{2}[\mathcal{A}_{\lambda^\pm}(\mathcal{P}) - \mathcal{A}_{\lambda^\pm}(-\mathcal{P})] \tag{2.52}$$

$$= \frac{1}{2}\eta_{\lambda^\pm}\frac{\Sigma_{rj}^{3\,(HA)}(\mathcal{P})}{\bar{P}}. \tag{2.53}$$

Since $\Sigma_{rj}^{3\,(HA)}$, eq. (2.33), describes the interference of the H and A exchange amplitudes, non-vanishing asymmetries $\mathcal{A}_\lambda^C$ and $\mathcal{A}_{\lambda^\pm}^{pol}$ are a clear indication of nearly degenerate scalar resonances with opposite CP quantum numbers in the production of equal charginos.

2.4.5.2 Production of $\tilde{\chi}_1^\mp\tilde{\chi}_2^\pm$

The asymmetries $\mathcal{A}_\lambda^C$, eq. (2.51), and $\mathcal{A}_{\lambda^\pm}^{pol}$, eq. (2.53), have to be generalized for the production of unequal charginos, $\mu^+\mu^- \to \tilde{\chi}_1^+\tilde{\chi}_2^-$, since the coefficient $P_r^{(HA)}$, eq. (2.7), does not vanish. We define the generalized charge asymmetry

$$\tilde{\mathcal{A}}_\lambda^C = \frac{\sigma_{\lambda^+}^> - \sigma_{\lambda^+}^< - \sigma_{\lambda^-}^> + \sigma_{\lambda^-}^<}{\sigma_{\lambda^+}^> + \sigma_{\lambda^+}^< + \sigma_{\lambda^-}^> + \sigma_{\lambda^-}^<}, \qquad \lambda = e, \mu, \tau, W, \tag{2.54}$$

with the short hand notation of eq. (2.43).

Using the definition of $\sigma_{\lambda^\pm}$, eq. (2.40) and the chargino charge transformation properties of the coefficients P and Σ_{Pj}^3, eqs. (2.45)-(2.47), the resonant contributions can be separated, in analogy to eq. (2.51),

$$\tilde{\mathcal{A}}_\lambda^C = \frac{1}{2}\eta_{\lambda^+}\frac{\Sigma_{rj}^{3\,(HA)}}{\bar{P}_{cont} + P_r^{(HH)} + P_r^{(AA)}}, \tag{2.55}$$

with $\bar{P}_r^{(\phi\phi)} = P_r^{(\phi\phi)}$.

Analogously we define the generalized polarization asymmetry obtained from the energy distribution of $\lambda^\pm = e^\pm, \mu^\pm, \tau^\pm, W^\pm$ from the two-body decay of one of the charginos

$$\tilde{\mathcal{A}}^{pol}_{\lambda^\pm} = \frac{\sigma^{>}_{\lambda^\pm}(\mathcal{P}) - \sigma^{<}_{\lambda^\pm}(\mathcal{P}) - \sigma^{>}_{\lambda^\pm}(-\mathcal{P}) + \sigma^{<}_{\lambda^\pm}(-\mathcal{P})}{\sigma^{>}_{\lambda^\pm}(\mathcal{P}) + \sigma^{<}_{\lambda^\pm}(\mathcal{P}) + \sigma^{>}_{\lambda^\pm}(-\mathcal{P}) + \sigma^{<}_{\lambda^\pm}(-\mathcal{P})}, \tag{2.56}$$

$$= \frac{1}{2}\eta_{\lambda^\pm}\frac{\Sigma^{3\,(HA)}_{rj}(\mathcal{P})}{\bar{P}_{cont} + P^{(HH)}_r + P^{(AA)}_r}, \tag{2.57}$$

for equal beam polarizations $\mathcal{P}^L_+ = \mathcal{P}^L_- \equiv \mathcal{P}$. For the production of equal charginos these asymmetries reduce to their equivalents $\mathcal{A}^C_\lambda$ and $\mathcal{A}^{pol}_{\lambda^\pm}$, defined in eqs. (2.51) and (2.53), respectively.

2.4.6 Determination of the Higgs-chargino couplings in production and decay

In the previous sections we have shown that the coefficient Σ^3_{rj} (2.33) of the longitudinal chargino polarization is sensitive to the interference of the H and A Higgs bosons. Their interference determines the sign γ of the product of couplings

$$\kappa = \mathrm{Im}\{c^{(H\mu)}c^{(A\mu)*}\}\mathrm{Im}\{c^{(H)}_R c^{(A)*}_R\} = \gamma\,|c^{(H\mu)}c^{(A\mu)}c^{(H)}_R c^{(A)}_R|, \tag{2.58}$$

which appears in

$$\Sigma^{3(HA)}_{rj} = g^4\mathcal{P}\mathrm{Re}\{\Delta(H)\Delta(A)^*\}\mathrm{Im}\{c^{(H\mu)}c^{(A\mu)*}\}\mathrm{Im}\{c^{(H)}_R c^{(A)*}_R\}s\sqrt{\lambda_{jj}}, \tag{2.59}$$

where we focus on the pair production of charginos $\mu^+\mu^- \to \tilde{\chi}^+_j\tilde{\chi}^-_j$ with equal muon beam polarizations $\mathcal{P}^L_+ = \mathcal{P}^L_- \equiv \mathcal{P}$. Since we assume CP conservation, γ can take the value ± 1 for interfering amplitudes of opposite CP eigenvalues, and vanishes for interfering amplitudes with same CP eigenvalues. A measurement of γ would thus be a unique test of the CP properties of the Higgs sector in the underlying supersymmetric model.

The coefficient $\Sigma^{3(HA)}_{rj}$ can be obtained from the chargino production cross section

$$\sigma(\mu^+\mu^- \to \tilde{\chi}^+_j\tilde{\chi}^-_j) = \frac{\sqrt{\lambda_{jj}}}{4\pi s^2}\bar{P}, \tag{2.60}$$

and the charge asymmetry $\mathcal{A}^C_\lambda$, eq. (2.51)

$$\Sigma^{3(HA)}_{rj} = \frac{8\pi s^2}{\eta_{\lambda^+}\sqrt{\lambda_{jj}}}\,\sigma(\mu^+\mu^- \to \tilde{\chi}^+_j\tilde{\chi}^-_j)\,\mathcal{A}^C_\lambda. \tag{2.61}$$

Now the product of couplings κ can be determined by a comparison of eq. (2.61) with eq. (2.59). Alternatively, using the polarization asymmetry $\mathcal{A}^{pol}_{\lambda^\pm}$ (2.53), we find

$$\Sigma^{3(HA)}_{rj} = \frac{8\pi s^2}{\eta_{\lambda^\pm}\sqrt{\lambda_{jj}}}\,\sigma(\mu^+\mu^- \to \tilde{\chi}^+_j\tilde{\chi}^-_j)\,\mathcal{A}^{pol}_{\lambda^\pm}. \tag{2.62}$$

In addition, a measurement of the asymmetries $\mathcal{A}^C_\lambda$, eq. (2.51), or $\mathcal{A}^{pol}_{\lambda^\pm}$ eq. (2.53), allows the determination of the ratio

$$\frac{\Sigma^3_{rj}}{P_r} = \frac{\sigma(\mu^+\mu^- \to \tilde{\chi}^+_j\chi^-_j)}{\sigma_r(\mu^+\mu^- \to \tilde{\chi}^+_j\chi^-_j)}\frac{2}{\eta_{\lambda^+}}\mathcal{A}^C_\lambda \tag{2.63}$$

$$= \frac{\sigma(\mu^+\mu^- \to \tilde{\chi}^+_j\chi^-_j)}{\sigma_r(\mu^+\mu^- \to \tilde{\chi}^+_j\chi^-_j)}\frac{2}{\eta_{\lambda^\pm}}\mathcal{A}^{pol}_{\lambda^\pm}, \tag{2.64}$$

using the charge or polarization asymmetry, respectively. The resonant contributions

$$\sigma_{rj}(\mu^+\mu^- \to \tilde{\chi}^+_j\tilde{\chi}^-_j) = \frac{\sqrt{\lambda_{jj}}}{4\pi s^2}P_r, \quad \text{with} \quad P_r = \bar{P}_r, \tag{2.65}$$

to the cross section can be obtained by subtracting the continuum contributions. The latter can be estimated by extrapolating the production line shape below and above the resonance region [25]. Uncertainties due to detection efficiencies of the chargino decay products cancel out in the ratio

$$\frac{\sigma_{rj}(\mu^+\mu^- \to \tilde{\chi}^+_j\chi^-_j)}{\sigma(\mu^+\mu^- \to \tilde{\chi}^+_j\chi^-_j)} = \frac{P_r}{\bar{P}}. \tag{2.66}$$

After inserting the expressions of $\Sigma^{3(HA)}_r$ (2.59) and P_r (2.6) we obtain

$$\frac{\Sigma^3_{rj}}{P_r} = \frac{2\mathcal{P}}{1+\mathcal{P}^2}\,\frac{2\gamma\,\mathrm{Re}\{\Delta(H)\Delta^*(A)\}\sqrt{s^+ s}}{q\,|\Delta(H)|^2\,s^+ + q^{-1}\,|\Delta(A)|^2\,s}, \tag{2.67}$$

with

$$s^+ = s - 4m^2_{\chi^\pm_j} = \frac{\lambda_{jj}}{s}, \tag{2.68}$$

$$q = \frac{|c^{(H\mu)}c^{(H)}_R|}{|c^{(A\mu)}c^{(A)}_R|}. \tag{2.69}$$

It is now possible to solve (2.67) for q as well as for γ.

For our analysis we have assumed that the masses and widths of the Higgs resonances H and A can be measured. The resonance parameters of nearly degenerate Higgs bosons with different CP quantum numbers may e.g. be determined by using transverse beam polarizations, which enhances or suppresses the Higgs exchange channels depending on their CP quantum numbers [34]. Alternatively,

the if both chargino decays are observed, their transverse polarizations can be used to separate the CP-even and CP-odd Higgs exchange contributions, see Section 2.5.2.

Note that γ (2.58) can only be determined by measuring the charge or polarization asymmetries $\mathcal{A}_\lambda^C$ and $\mathcal{A}_{\lambda^\pm}^{pol}$, which are sensitive to the H–A interference channels. A determination of γ from a measurement of the cross section $\sigma(\mu^+\mu^- \to \tilde{\chi}_j^+\tilde{\chi}_j^-)$ is not possible, since it contains contributions from pure H or A exchange only.

2.4.7 Numerical results

We analyze numerically the charge asymmetry $\mathcal{A}_\ell^C$ (2.50) of the lepton energy distribution for the production of equal charginos $\mu^+\mu^- \to \tilde{\chi}_1^+\tilde{\chi}_1^-$ in Section 2.4.8, The feasibility of measuring the asymmetries depends also on the corresponding production cross sections which we discuss in our scenarios. For the calculation of the Higgs masses and widths we use the program HDECAY [32]. For the calculation of the branching ratios and widths of the decaying charginos we include the two-body decays

$$\tilde{\chi}_1^\pm \;\to\; e^\pm\tilde{\nu}_e,\ \mu^\pm\tilde{\nu}_\mu,\ \tau^\pm\tilde{\nu}_\tau,\ \tilde{e}_L^\pm\nu_e,\ \tilde{\mu}_L^\pm\nu_\mu,\ \tilde{\tau}_{1,2}^\pm\nu_\tau,\ W^\pm\tilde{\chi}_n^0, \tag{2.70}$$

and neglect three-body decays. In order to reduce the number of parameters, we assume GUT relations for the gaugino mass parameters, related by $M_1 = 5/3\, M_2 \tan^2\theta_W$, and for the slepton masses, related to the scalar mass parameter m_0 at the GUT scale by the approximate renormalization group equations [35] given in Appendix A.4.1 In the stau sector we fix the trilinear scalar coupling parameter $A_\tau = 250$ GeV.

2.4.8 Production of $\tilde{\chi}_1^+\tilde{\chi}_1^-$

In the following subsections we study the dependence of the asymmetries and cross sections on the MSSM parameters μ, M_2, $\tan\beta$ and m_A, as well as on the center of mass energy $\sqrt{s}$.

2.4.8.1 μ and M_2 dependence

In Fig. 2.12a we show the contour lines of the chargino production cross section $\sigma(\mu^+\mu^- \to \tilde{\chi}_1^+\tilde{\chi}_1^-)$ in the μ–M_2 plane for $\sqrt{s} = m_A$ and beam polarizations $\mathcal{P}_-^L = \mathcal{P}_+^L = -0.3$, with $m_A = 500$ GeV, $\tan\beta = 10$ and $m_0 = 70$ GeV.

At $\sqrt{s} = m_A \approx m_H$ the production cross section is close to its peak value, since the two Higgs resonances are nearly degenerate. The main contributions to the cross section, which reaches up to 2 pb, are from the resonant ones. For increasing values of $|\mu|$ the couplings of both H and A to the charginos decrease,

leading to smaller resonant contributions. The continuum contributions from h, γ, Z and $\tilde{\nu}_\mu$ exchange reach 0.5 pb at most.

We show contour lines of the chargino branching ratio $\mathrm{BR}(\tilde{\chi}_1^+ \to \mathrm{e}^+\tilde{\nu}_\mathrm{e})$ in the μ–M_2 plane in Fig. 2.12b, where also the allowed region for the chargino two-body decay $\tilde{\chi}_1^+ \to e^+\tilde{\nu}_e$ is indicated. The sneutrinos are rather light for $m_0 = 70$ GeV, such that this chargino decay mode is open for $|\mu| \gtrsim 200$ GeV and reaches values of up to 20%.

For the chargino decay into an electron $\tilde{\chi}_1^\pm \to e^\pm\tilde{\nu}_e^{(*)}$, we show in Fig. 2.12c contour lines of the charge asymmetry $\mathcal{A}_e^C$ (2.50) which reaches values of up to 24%. The asymmetry depends only weakly on the character of chargino mixing, since $\mathcal{A}_e^C$ is proportional to a ratio of the couplings, see (2.63) and (2.67). In the ideal case of maximal H-A interference and vanishing continuum contributions, the asymmetry could reach its maximum absolute value of $|\mathcal{P}_+^L + \mathcal{P}_-^L|/(1 + \mathcal{P}_+^L\mathcal{P}_-^L)/2 \approx 28\%$, as follows from (2.51) for $\mathcal{P}_+^L = \mathcal{P}_-^L = -0.3$.

Thus the shown values of $\mathcal{A}_e^C$ in Fig. 2.12c are large, since the amplitudes of the interfering H and A Higgs bosons are roughly of the same magnitude in the resonance region $\sqrt{s} = m_A$. Near the production threshold $\sqrt{s} = 2m_{\chi_1^\pm}$ the asymmetry decreases due to the p-wave suppression of the CP-even scalar exchange amplitude.

In Fig. 2.12d we show the contour lines of the significance $\mathcal{S}_e^C$, eq. (D.31), for an integrated effective luminosity $\mathcal{L}_{eff} = 1\ \mathrm{fb}^{-1}$. Due to the large asymmetry $\mathcal{A}_e^C$ and cross section $\sigma(\mu^+\mu^- \to \tilde{\chi}_1^+\tilde{\chi}_1^-) \times \mathrm{BR}(\tilde{\chi}_1^+ \to e^+\tilde{\nu}_e)$ for chargino production and subsequent decay, $\mathcal{A}_e^C$ can be measured with a significance $\mathcal{S}_e^C > 1$ for a luminosity $\mathcal{L}_{eff} = \mathcal{O}(\mathrm{fb}^{-1})$. The same values of the significance are obtained for the muonic chargino decay mode $\tilde{\chi}_1^+ \to \mu^+\tilde{\nu}_\mu$.

In Fig. 2.13 we show similar contours as in Fig. 2.12 for $\mu > 0$. For $\tan\beta \gg 1$ the chargino sector is not very sensitive to the sign of μ. Here, for $\tan\beta = 10$, we observe that the chargino production cross section $\sigma(\mu^+\mu^- \to \tilde{\chi}_1^+\tilde{\chi}_1^-)$, shown in Fig. 2.13a, is indeed almost the same for both values of μ. However, for $\mu > 0$ charginos are slightly lighter. This implies that the kinematical limit for the two-body decay $\tilde{\chi}_1^+ \to e^+\tilde{\nu}_e$ is found at larger values of $|\mu|$, as can be observed in Fig. 2.13b for the branching ratios for this process, which are slightly smaller. The asymmetry $\mathcal{A}_e^C$ (2.50) and the statistical significance $\mathcal{S}_e^C$ for an integrated effective luminosity $\mathcal{L}_{eff} = 1\ \mathrm{fb}^{-1}$ are shown in Figs. 2.13c and 2.13d, respectively.

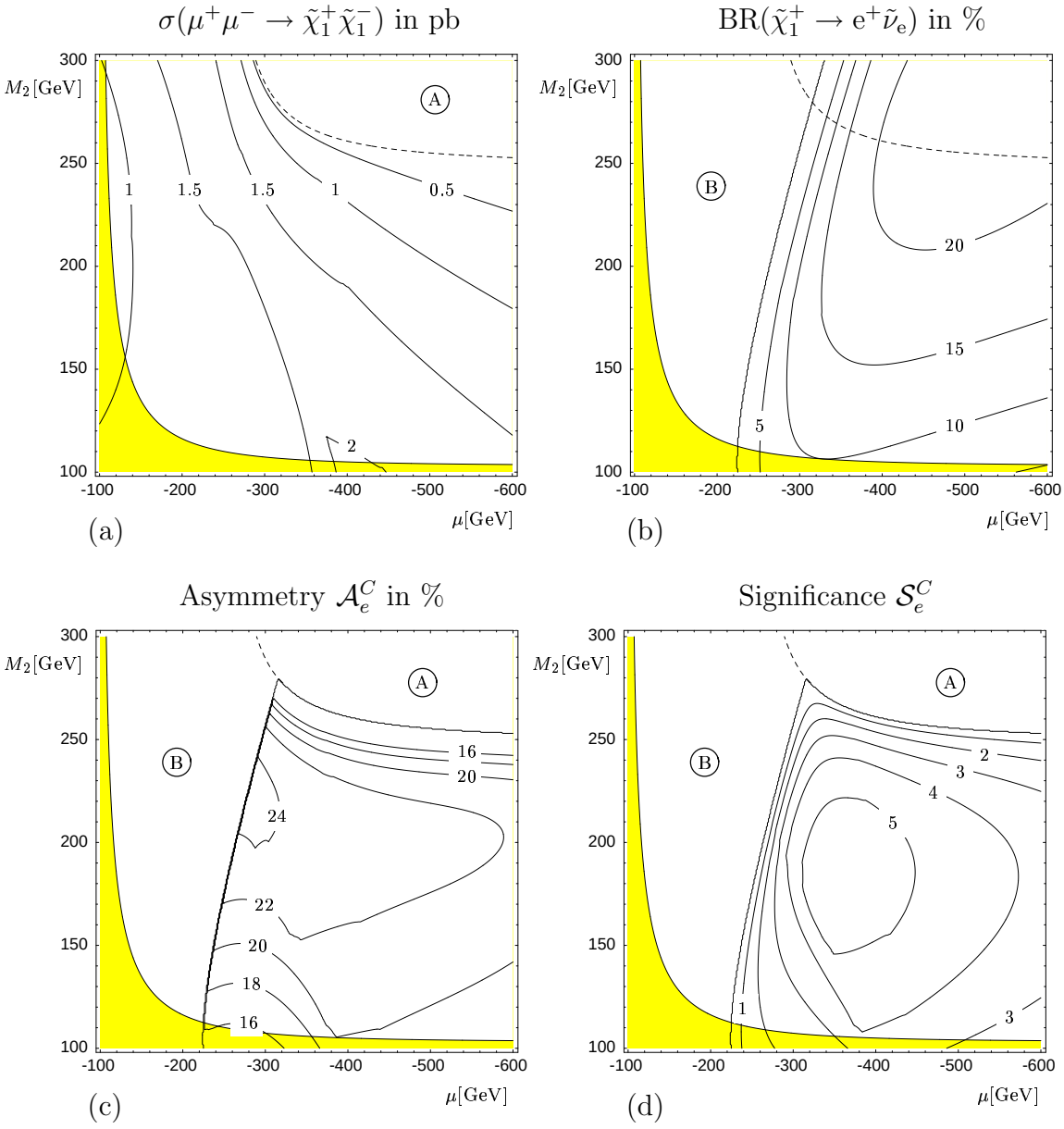

Figure 2.12: $\mu^+\mu^- \to \tilde{\chi}_1^+\tilde{\chi}_1^-$, $\tilde{\chi}_1^+ \to \tilde{\nu}_e e^+$. Contour lines of the cross section $\sigma(\mu^+\mu^- \to \tilde{\chi}_1^+\tilde{\chi}_1^-)$ **(a)**, the branching ratio BR($\tilde{\chi}_1^+ \to e^+\tilde{\nu}_e$) **(b)**, the charge asymmetry $\mathcal{A}_e^C$ **(c)** and the significance $\mathcal{S}_e^C$ for an integrated effective luminosity $\mathcal{L}_{eff} = 1$ fb^{-1} **(d)** in the μ–M_2 plane for $\mu < 0$, $m_A = 500$ GeV, $\tan\beta = 10$, $m_0 = 70$ GeV, $\sqrt{s} = 500$ GeV and longitudinal beam polarizations $\mathcal{P}_+^L = \mathcal{P}_-^L = -0.3$. The dashed line indicates the kinematical limit $2m_{\chi_1^\pm} = \sqrt{s}$. The area A (B) is kinematically forbidden by $2m_{\chi_1^\pm} > \sqrt{s}$ ($m_{\tilde{\nu}_e} > m_{\chi_1^\pm}$). The shaded area is excluded by $m_{\chi_1^\pm} < 103$ GeV.

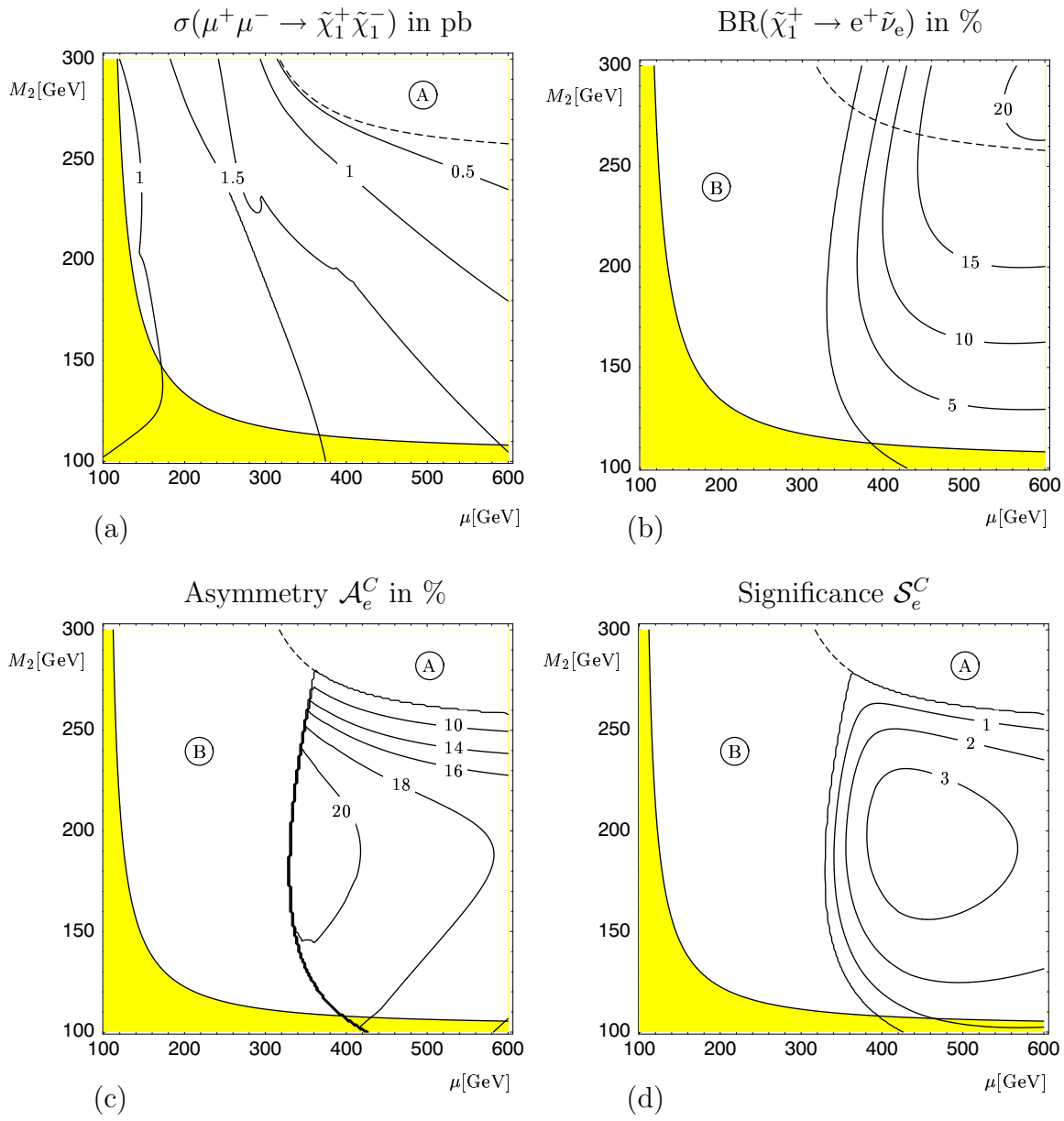

Figure 2.13: $\mu^+\mu^- \to \tilde{\chi}_1^+\tilde{\chi}_1^-$, $\tilde{\chi}_1^+ \to \tilde{\nu}_e e^+$. Contour lines of the cross section $\sigma(\mu^+\mu^- \to \tilde{\chi}_1^+\tilde{\chi}_1^-)$ **(a)**, the branching ratio BR($\tilde{\chi}_1^+ \to e^+\tilde{\nu}_e$) **(b)**, the charge asymmetry $\mathcal{A}_e^C$ **(c)** and the significance $\mathcal{S}_e^C$ for an integrated effective luminosity $\mathcal{L}_{eff} = 1$ fb^{-1} **(d)** in the μ–M_2 plane for $\mu > 0$, $m_A = 500$ GeV, $\tan\beta = 10$, $m_0 = 70$ GeV, $\sqrt{s} = 500$ GeV and longitudinal beam polarizations $\mathcal{P}_+^L = \mathcal{P}_-^L = -0.3$. The dashed line indicates the kinematical limit $2m_{\chi_1^\pm} = \sqrt{s}$. The area A (B) is kinematically forbidden by $2m_{\chi_1^\pm} > \sqrt{s}$ ($m_{\tilde{\nu}_e} > m_{\chi_1^\pm}$). The shaded area is excluded by $m_{\chi_1^\pm} < 103$ GeV.

Table 2.4: Scenario **A** for $\mu^+\mu^- \to \tilde{\chi}_1^+\tilde{\chi}_1^-$.

$\tan\beta = 10$	$m_A = 500$ GeV	$m_{\chi_1^\pm} = 197$ GeV	$\mathrm{BR}(\tilde{\chi}_1^+ \to e^+\tilde{\nu}_e) = 19\%$
$\mu = -500$ GeV	$\Gamma_A = 1.41$ GeV	$m_{\chi_2^\pm} = 514$ GeV	$\mathrm{BR}(\tilde{\chi}_1^+ \to \mu^+\tilde{\nu}_\mu) = 19\%$
$M_2 = 200$ GeV	$m_H = 500.07$ GeV	$m_{\chi_1^0} = 100$ GeV	$\mathrm{BR}(\tilde{\chi}_1^+ \to \tau^+\tilde{\nu}_\tau) = 19\%$
$m_0 = 70$ GeV	$\Gamma_H = 1.20$ GeV	$m_{\tilde{\nu}_e} = 180$ GeV	$\mathrm{BR}(\tilde{\chi}_1^+ \to \tilde{\tau}_1^+\nu_\tau) = 43\%$

Table 2.5: Scenario **B7** for $\mu^+\mu^- \to \tilde{\chi}_1^+\tilde{\chi}_1^-$, chargino and slepton parameters.

$\tan\beta = 7$	$m_{\chi_1^\pm} = 158$ GeV	$\mathrm{BR}(\tilde{\chi}_1^+ \to e^+\tilde{\nu}_e) = 22\%$
$\mu = -400$ GeV	$m_{\chi_2^\pm} = 417$ GeV	$\mathrm{BR}(\tilde{\chi}_1^+ \to \mu^+\tilde{\nu}_\mu) = 22\%$
$M_2 = 160$ GeV	$m_{\chi_1^0} = 81$ GeV	$\mathrm{BR}(\tilde{\chi}_1^+ \to \tau^+\tilde{\nu}_\tau) = 22\%$
$m_0 = 70$ GeV	$m_{\tilde{\nu}_e} = 145$ GeV	$\mathrm{BR}(\tilde{\chi}_1^+ \to \tilde{\tau}_1^+\nu_\tau) = 33\%$

2.4.8.2 $\sqrt{s}$ dependence

In order to study the dependence of the asymmetries and the chargino production cross sections on the center of mass energy, we choose a representative point in the μ–M_2 plane with $\mu = -500$ GeV and $M_2 = 200$ GeV. The parameters and resulting Higgs masses and widths for this point, called scenario **A**, are given in Table 2.4. The branching ratios for $\tilde{\chi}_1^+ \to W^+\tilde{\chi}_1^0$ and $\tilde{\chi}_1^+ \to \tilde{e}_L^+\nu_e$ are smaller than 0.3%.

In Fig. 2.14a we show the energy distribution asymmetry $\mathcal{A}_{e^+}$, eq. (2.42), for the decay $\tilde{\chi}_1^+ \to e^+\tilde{\nu}_e$, and the asymmetry $\mathcal{A}_{e^-}$ for the charge conjugated process, with longitudinal beam polarizations $\mathcal{P}_+^L = \mathcal{P}_-^L = -0.3$. In addition we show the charge asymmetry $\mathcal{A}_e^C = (\mathcal{A}_{e^+} - \mathcal{A}_{e^-})/2$, see eq. (2.50), which reaches its maximal value of 23% at $\sqrt{s} \approx m_A = 500$ GeV. Since the continuum contributions from γ, Z and $\tilde{\nu}_\mu$ exchange cancel out in $\mathcal{A}_e^C$, it asymptotically vanishes far from the resonance region. The $\sqrt{s}$ dependence of the chargino production cross section is shown in Fig. 2.14b. We show the corresponding statistical significance $\mathcal{S}_e^C$, defined in eq. (D.31), for an effective integrated luminosity $\mathcal{L}_{eff} = 1\mathrm{fb}^{-1}$ in Fig. 2.14c.

2.4.8.3 m_A and $\tan\beta$ dependence

In Fig. 2.15a we compare the charge asymmetries $\mathcal{A}_e^C$ (2.50) for scenarios **B7**, **B7'** and **B7"** of Tables 2.5 and 2.6, that differ only in $m_A = \{350, 400, 500\}$ GeV, as a

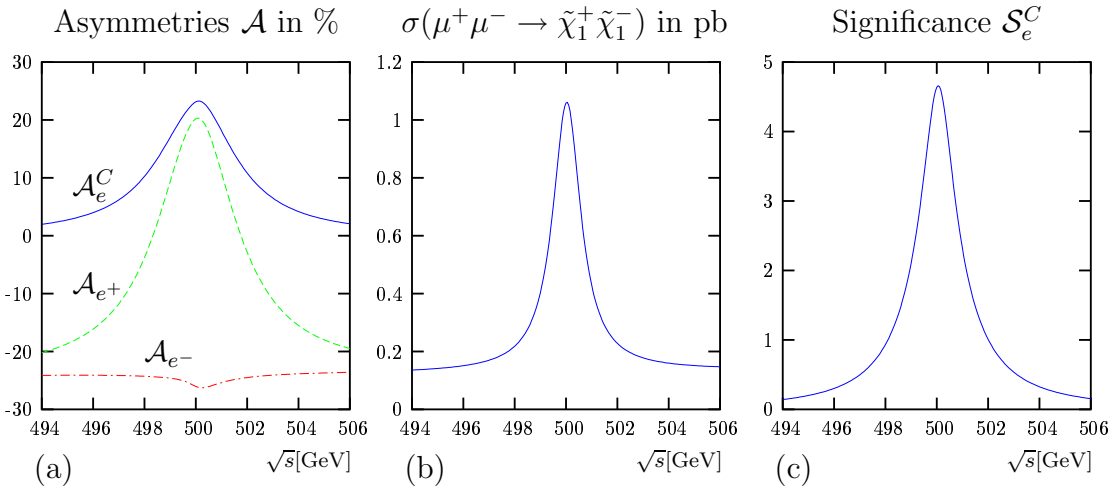

Figure 2.14: $\mu^+\mu^- \to \tilde{\chi}_1^+\tilde{\chi}_1^-$, $\tilde{\chi}_1^\pm \to e^\pm\tilde{\nu}^{(*)}$. Asymmetries **(a)**, chargino production cross section **(b)** and significance for $\mathcal{L}_{eff} = 1\text{fb}^{-1}$ **(c)**, with longitudinal beam polarizations $\mathcal{P}_+^L = \mathcal{P}_-^L = -0.3$ for Scenario **A**, given in Table 2.4.

Table 2.6: Scenarios **B7**, **B7'** and **B7"**, Higgs sector parameters.

	B7	**B7'**	**B7"**
m_A[GeV]	350	400	500
m_H[GeV]	350.7	400.6	500.4
Γ_A[GeV]	0.56	1.00	1.4
Γ_H[GeV]	0.43	0.65	1.1

function of $\sqrt{s}-m_A$. We show the corresponding cross sections for $\mu^+\mu^- \to \tilde{\chi}_1^+\tilde{\chi}_1^-$ in Fig. 2.15b. For increasing Higgs masses their widths increase, and thus the interference of the H and A exchange amplitudes. However, the maxima of the asymmetries are reduced by larger continuum contributions to the cross section. For smaller Higgs masses, here $m_A = 350$ GeV, the threshold effects are stronger. Since a Dirac fermion-antifermion pair has negative intrinsic parity, and thus the CP-even H resonance is p-wave suppressed, the peak cross section is found at $\sqrt{s} \approx m_A$, where the asymmetry nearly vanishes. The asymmetry changes sign between the two resonances, whose mass difference is larger than their widths, due to the complex phases of the propagators. Its maximum is found at center of mass energies slightly above m_H where the phases of the propagators are roughly equal and the amplitudes of similar magnitude. In Fig. 2.15c we show the statistical significance $\mathcal{S}_e^C$ for an integrated effective luminosity $\mathcal{L}_{eff} = 1$ fb^{-1}. We find statistical significances of $\mathcal{S}_e^C > 3$, albeit not in the entire resonance region for

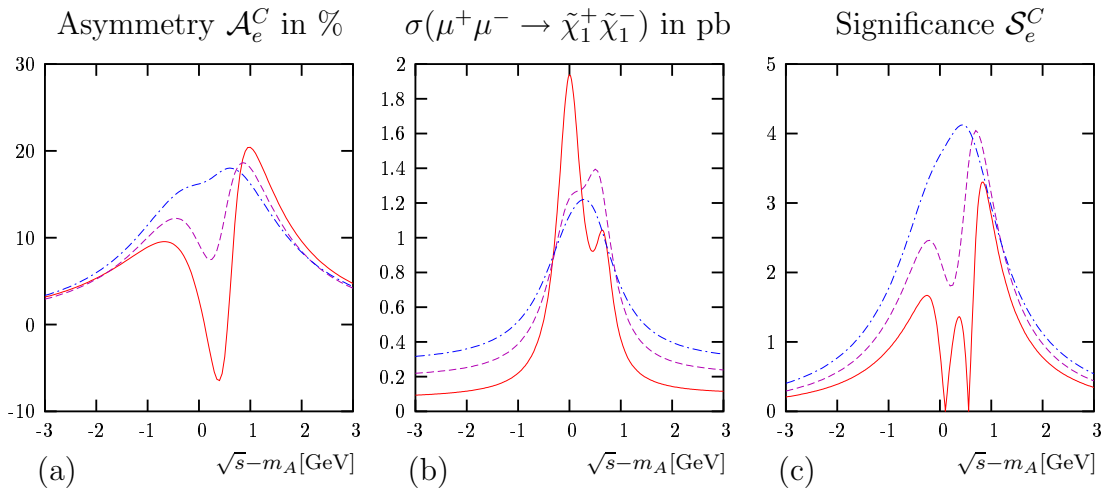

Figure 2.15: $\mu^+\mu^- \to \tilde{\chi}_1^+\tilde{\chi}_1^-$, $\tilde{\chi}_1^\pm \to e^\pm\tilde{\nu}_e^{(*)}$. Asymmetry $\mathcal{A}_e^C$ **(a)**, cross section $\sigma(\mu^+\mu^- \to \tilde{\chi}_1^+\tilde{\chi}_1^-)$ **(b)** and significance $\mathcal{S}_e^C$ for $\mathcal{L}_{eff} = 1$ fb^{-1} **(c)** for scenarios **B7** (solid), **B7'** (dashed) and **B7"** (dot-dashed) of Table 2.5 and 2.6 with $m_A = 350$ GeV, 400 GeV and 500 GeV, respectively, and longitudinal beam polarizations $\mathcal{P}_+^L = \mathcal{P}_-^L = -0.3$.

scenarios **B7** and **B7'** with smaller m_A.

Increasing $\tan\beta$ the mass difference $m_H - m_A$ decreases and the widths Γ_H and Γ_A increase. This results in a larger overlap of the resonances, leading to large asymmetries $\mathcal{A}_e^C$ in the resonance region. In addition, since the couplings of the muons to the Higgs bosons (B.3) and (B.4) are proportional to $\tan\beta$, larger values imply smaller relative continuum contributions that enhance the asymmetries. The influence of these effects can be observed comparing the plot of $\mathcal{A}_e^C$ in Fig. 2.15a for scenario **B7"**, where $\tan\beta = 7$, with the plot of $\mathcal{A}_e^C$ in Fig. 2.14a for scenario **A**, where $\tan\beta = 10$.

2.4.8.4 Chargino decay into W bosons

If the sleptons are heavier than the charginos, the chargino decay into a W boson, $\tilde{\chi}_1^\pm \to W^\pm\tilde{\chi}_1^0$, might be the only allowed two-body decay channel. In this case only the asymmetries of the energy distribution of the W boson, $\mathcal{A}_W^C$ and $\mathcal{A}_{W^\pm}^{pol}$, eqs. (2.50) and (2.52), respectively, are accessible. These asymmetries are reduced by a factor $\eta_{W^\pm}$, eq. (C.61), with respect to the asymmetries for leptonic chargino decay modes. In Fig. 2.12c we have shown the contour lines of the leptonic charge asymmetry $\mathcal{A}_e^C$ (2.50) in the μ–M_2 plane for $\tan\beta = 10$. The values of $\mathcal{A}_e^C$ have to be multiplied by $\eta_{W^+} = -\eta_{W^-}$, which we show in Fig. 2.16, to obtain the asymmetry $\mathcal{A}_W^C = \eta_{W^+} \times \mathcal{A}_e^C$. Although the asymmetries are suppressed by $|\eta_{W^\pm}| \approx 0.2 - 0.4$, and uncertainties in the energy measurement of the W boson lead to lower effective integrated luminosities, statistics will be gained from large

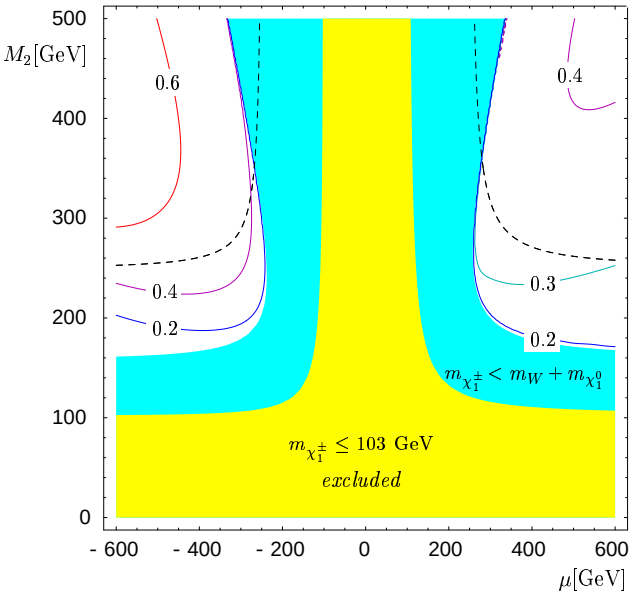

Figure 2.16: Contour lines of η_{W^-} (C.61) for the decay $\tilde{\chi}_1^- \to W^-\tilde{\chi}_1^0$ in the μ–M_2 plane for $\tan\beta = 10$. The dashed line indicates the kinematical limit for $2m_{\chi_1^\pm} = \sqrt{s} = 500$ GeV. The dark shaded area is kinematically forbidden by $m_{\chi^\pm} < m_W + m_{\chi_1^0}$. The light shaded area is experimentally excluded by $m_{\chi_1^\pm} < 103$ GeV.

branching ratios, $\mathrm{BR}(\tilde{\chi}_1^\pm \to W^\pm\tilde{\chi}_1^0) = 1$.

2.4.9 Summary of Section 2.4

We studied the energy distributions of the lepton or W-boson from the decay $\tilde{\chi}_j^\pm \to \ell^\pm\tilde{\nu}_\ell$, $\ell = e, \mu, \tau$, or $\tilde{\chi}_j^\pm \to W^\pm\tilde{\chi}_1^0$, respectively, from a chargino produced in $\mu^+\mu^-$-annihilation with longitudinally polarized beams. These energy distributions are correlated to the chargino longitudinal polarization. We have shown that the interference of H and A can be analyzed using asymmetries in these energy distributions. The asymmetries allow a determination of chargino couplings to the H and A bosons and in particular a determination of their relative phase. In a numerical study we have analyzed the production of $\tilde{\chi}_1^+\tilde{\chi}_1^-$ for different MSSM scenarios and found asymmetries which are maximal for nearly degenerate H and A bosons. In the numerical analysis of the chargino cross sections and branching ratios, we have shown that the asymmetries are accessible at a future muon collider with polarized beams.

2.5 Production of chargino pairs with subsequent decay of both charginos

We can further probe the Higgs-chargino interaction with the correlation of the polarizations of both charginos in the process $\mu^+\mu^- \to \tilde{\chi}_i^\mp \tilde{\chi}_j^\pm$. Therefore we study the subsequent two-body decay of both charginos. We build asymmetries of the energy and angular distributions of the final particles and discuss their dependence on the Higgs-chargino couplings.

In the preceding section we have discussed the spin correlation between production and decay of one of the charginos in the production process (2.1). We found that two-body decays in which parity is not conserved are very useful probes of the chargino polarizations. The parity violation in the decay is given by the coefficient $\eta_{\lambda^\pm}$, where λ denotes the observed final particle.

Now we analyze the spin-spin correlation terms of the charginos, described by the last term of the spin density matrix, eq. (C.25). We analyze the polarizations of the charginos using their two-body decays. Therefore, the spin-spin correlations are related to correlations of the momenta of the final particles.

As discussed in Section 2.1, we subdivide the expansion coefficients of the chargino production density matrix into contributions from the Higgs resonances $\Sigma_{r_j}^{ab}$ and the continuum $\Sigma_{cont_j}^{ab}$, eq. (2.4). The resonant contributions are further separated into pure Higgs exchange and interference terms

$$\Sigma_r^{ab} = \sum_{\phi=H,A} \Sigma_r^{ab\,(\phi\phi)} + \Sigma_r^{ab\,(HA)}, \qquad a,b = 1,\ldots,3. \tag{2.71}$$

Evaluating the spin density matrix in the CMS and using the notation of Section 2.4.2, these coefficients are given by

$$\begin{aligned}
\Sigma_r^{ab\,(\phi\phi)} &= \delta_{ab}\,\frac{g^4}{8}(1+\mathcal{P}_+^L\mathcal{P}_-^L)|\Delta(\phi)|^2|c^{(\phi\mu)}|^2 \\
&\quad \left[(|c_L^{(\phi)}|^2+|c_R^{(\phi)}|^2)A^{(a)} + 2\mathrm{Re}\{c_L^{(\phi)}c_R^{(\phi)\,*}\}B^{(a)}\right] s, \qquad (2.72)\\
\Sigma_r^{ab\,(HA)} &= \Sigma_{r,0}^{ab\,(HA)} + \Sigma_{r,abs}^{ab\,(HA)}, \qquad (2.73)\\
\Sigma_{r,0}^{ab\,(HA)} &= \delta_{ab}\,\frac{g^4}{4}(\mathcal{P}_+^L+\mathcal{P}_-^L)\mathrm{Re}\{\Delta(H)\Delta(A)^*\}\mathrm{Im}\{c^{(H\mu)}c^{(A\mu)^*}\} \qquad (2.74)\\
&\quad \left[\mathrm{Im}\{c_L^{(H)}c_L^{(A)\,*}+c_R^{(H)}c_R^{(A)\,*}\}A^{(a)} + \mathrm{Im}\{c_L^{(H)}c_R^{(A)\,*}+c_R^{(H)}c_L^{(A)\,*}\}B^{(a)}\right] s,\\
\Sigma_{r,abs}^{ab\,(HA)} &= \frac{g^4}{4}(\mathcal{P}_+^L+\mathcal{P}_-^L)\mathrm{Im}\{\Delta(H)\Delta(A)^*\}\mathrm{Im}\{c^{(H\mu)}c^{(A\mu)^*}\}\\
&\quad \mathrm{Im}\{c_L^{(H)}c_R^{(A)\,*}-c_R^{(H)}c_L^{(A)\,*}\}C^{(ab)}\,s, \qquad (2.75)
\end{aligned}$$

with

$$A^{(1)} = -A^{(2)} = -B^{(3)} = 2m_{\chi_i^\pm}m_{\chi_j^\pm}, \tag{2.76}$$

$$B^{(1)} = -B^{(2)} = -A^{(3)} = -(s - m^2_{\chi_i^\pm} - m^2_{\chi_j^\pm}), \tag{2.77}$$

$$C^{(12)} = C^{(21)} = -\sqrt{\lambda_{ij}}, \quad C^{(ab)} = 0 \quad \text{otherwise}, \tag{2.78}$$

and λ_{ij} defined in eq. (2.34).

It is instructive to compare the spin-spin correlation coefficient Σ_r^{ab} with the spin density matrix coefficient P_r, eqs. (2.6) and (2.7).

The non-absorptive parts of the spin-spin correlation coefficients, eqs. (2.72) and (2.74), depend on the same combinations of couplings as the spin independent coefficients P_r. Setting $a = b = 3$ in eqs. (2.72) and (2.73) for the longitudinal chargino polarization leads to

$$P_r^{(\alpha\beta)} = \Sigma_r^{33(\alpha\beta)}, \tag{2.79}$$

with $\alpha, \beta = H, A$. This relation implies that the longitudinal polarizations of the charginos produced via scalar exchange are equal, as follows from angular momentum conservation and from the requirement that the orbital angular momentum in the direction of motion of the charginos is zero.

More interesting are the transverse polarizations of the charginos. There is no preferred direction in a process that proceeds via s-channel scalar exchange, as in the case of the resonant contributions to chargino pair production. Therefore, for the transverse polarizations of the charginos, there is a symmetry under rotations around the direction of motion of the charginos. In Section 2.4 we found that, summing over the transverse polarization of one of the chargino, the transverse polarization of the other chargino had thus to vanish. For the spin-spin correlation terms, this symmetry implies that observables will depend only the relative direction of the polarizations and not on the production plane. Therefore we expect to find two observables, one which relates parallel transverse polarizations and one which relates polarizations orthogonal to each other.

The non-absorptive parts of Σ_r^{ab}, eqs. (2.72) and (2.74), relate only equal polarizations, i.e. $\Sigma_r^{ab} \propto \delta_{ab}$. The transverse polarization spin-spin correlation coefficients Σ_r^{11} and Σ_r^{22} depend on the same combinations of couplings as P_r, as found for Σ_r^{33}. However, these combinations of couplings appear with different coefficients $A^{(a)}$ and $B^{(a)}$. Therefore, the transverse polarization coefficients contain complementary information on the Higgs-chargino interaction.

For unequal charginos, the spin-spin polarizations provide unique information which allows to separate the first and second term in the right hand side of eqs. (2.72) and (2.74).

For equal charginos the relations between $\Sigma_r^{aa(\phi\phi)}$, $a = 1, 2$, and $P_r^{(\phi\phi)}$ simplify to

$$\Sigma_r^{11\,(\phi\phi)} = -\Sigma_r^{22\,(\phi\phi)} = -\eta^\phi P_r^{(\phi\phi)}, \tag{2.80}$$

where $\eta^\phi = \pm 1$ is the CP quantum number of the exchanged Higgs boson ϕ.

Therefore, for a single resonance, this relation allows to measure η^ϕ. For two overlapping resonances with different CP quantum numbers, we may use eq. (2.80) to separate the production cross sections. For H and A we obtain

$$P_r = P_r^{(AA)} + P_r^{(HH)}, \tag{2.81}$$
$$\Sigma_r^{11} = P_r^{(AA)} - P_r^{(HH)}, \tag{2.82}$$

from which follows

$$P_r^{(HH)} = \frac{1}{2}(P_r - \Sigma_r^{11}), \tag{2.83}$$
$$P_r^{(AA)} = \frac{1}{2}(P_r + \Sigma_r^{11}). \tag{2.84}$$

Note that, since for equal charginos the interference coefficients $P_r^{(HA)}$ and $\Sigma_r^{aa(HA)}$, $a = 1, 2$, vanish, eqs. (2.83) and (2.84) just separate the CP-even and CP-odd contributions to the coefficient P_r and may be generalized to

$$P_r^{(CP+)} = \frac{1}{2}(P_r - \Sigma_r^{11}), \tag{2.85}$$
$$P_r^{(CP-)} = \frac{1}{2}(P_r + \Sigma_r^{11}). \tag{2.86}$$

However, these relations do not allow to distinguish between two overlapping resonances with different CP quantum numbers and a single resonance with CP violating couplings. To prove the existence of interfering resonances we need to study the spin-correlations between production and decay as in Section 2.4.

The absorptive part of the spin-spin coefficient, eq. (2.75), which correlates orthogonal transverse polarizations, has no analogous term in the spin independent coefficients. Both for equal as for different charginos pairs, eq. (2.75) depends on a new combination of couplings. It is significant if the resonances overlap but are not exactly degenerate, so that

$$\frac{|\mathrm{Im}\{\Delta(H)\Delta(A)^*\}|}{|\Delta(H)||\Delta(A)|} \sim \mathcal{O}(1). \tag{2.87}$$

2.5.1 Energy distribution

The amplitude squared for chargino pair production with subsequent decay of both charginos, shown in eq. (C.32), is used to evaluate the double energy distribution in E_λ and $E_{\lambda'}$ for the decays $\tilde{\chi}_i^\mp \to \lambda^\mp \tilde{N}$ and $\tilde{\chi}_j^\pm \to \lambda'^\pm \tilde{N}'$, respectively, as in Section 2.4.4, eqs. (2.38) and (2.40). Denoting with $\sigma_{\lambda,\lambda'}$ the cross section for our process of chargino production and decay and using the notation of Section 2.4.4 for the kinematical limits, the double energy distribution can be expressed in the form

$$\frac{d^2\sigma_{\lambda,\lambda'}}{dE_\lambda dE_\lambda} = \frac{\sigma_{\lambda,\lambda'}}{4\Delta_\lambda\Delta_{\lambda'}}[1 + B_\lambda(E_\lambda - \bar{E}_\lambda) + B_{\lambda'}(E_{\lambda'} - \bar{E}_{\lambda'}) + C_{\lambda\lambda'}(E_\lambda - \bar{E}_\lambda)(E_{\lambda'} - \bar{E}_{\lambda'})], \tag{2.88}$$

with

$$B_\lambda = \eta_{\lambda^\mp}\frac{1}{\Delta_\lambda}\frac{\bar{\Sigma}^3_P}{\bar{P}}, \tag{2.89}$$

$$B_{\lambda'} = \eta_{\lambda'^\pm}\frac{1}{\Delta_{\lambda'}}\frac{\bar{\Sigma}^3_P}{\bar{P}}, \tag{2.90}$$

$$C_{\lambda\lambda'} = \eta_{\lambda^\mp}\eta_{\lambda'^\pm}\frac{1}{\Delta_\lambda\Delta_{\lambda'}}\frac{\bar{\Sigma}^{33}_P}{\bar{P}}. \tag{2.91}$$

Here we have defined averages over the chargino production angles in the CMS

$$\bar{P} = \frac{1}{(4\pi)^2}\int P d\Omega_{\chi^+}d\Omega_{\chi^-}, \tag{2.92}$$

$$\bar{\Sigma}^a_P = \frac{1}{(4\pi)^2}\int \Sigma^a_P d\Omega_{\chi^+}d\Omega_{\chi^-}, \tag{2.93}$$

$$\bar{\Sigma}^{ab}_P = \frac{1}{(4\pi)^2}\int \Sigma^{ab}_P d\Omega_{\chi^+}d\Omega_{\chi^-}. \tag{2.94}$$

In order to isolate the spin-spin correlation contribution in the energy distribution, eq. (2.88), we define the asymmetry

$$\mathcal{A}_{\lambda\lambda'} = \frac{\sigma^{<<}_{\lambda\lambda'}+\sigma^{>>}_{\lambda\lambda'}-\sigma^{<>}_{\lambda\lambda'}-\sigma^{><}_{\lambda\lambda'}}{\sigma^{<<}_{\lambda\lambda'}+\sigma^{>>}_{\lambda\lambda'}+\sigma^{<>}_{\lambda\lambda'}+\sigma^{><}_{\lambda\lambda'}} \tag{2.95}$$

$$= \frac{1}{4}\eta_{\lambda^\mp}\eta_{\lambda'^\pm}\frac{\bar{\Sigma}^{33}_P}{\bar{P}}, \tag{2.96}$$

with the short hand notation

$$\sigma^{<<}_{\lambda\lambda'} = \int_{E^{min}_\lambda}^{\bar{E}_\lambda}\int_{E^{min}_{\lambda'}}^{\bar{E}_{\lambda'}}\frac{d\sigma_{\lambda\lambda'}}{dE_\lambda dE'_\lambda}dE_\lambda dE_{\lambda'}, \tag{2.97}$$

$$\sigma^{<<}_{\lambda\lambda'} = \int_{\bar{E}_\lambda}^{E^{max}_\lambda}\int_{\bar{E}_{\lambda'}}^{E^{max}_{\lambda'}}\frac{d\sigma_{\lambda\lambda'}}{dE_\lambda dE'_\lambda}dE_\lambda dE_{\lambda'}, \tag{2.98}$$

$$\sigma^{<>}_{\lambda\lambda'} = \int_{\bar{E}_\lambda}^{E^{max}_\lambda}\int_{E^{min}_{\lambda'}}^{\bar{E}_{\lambda'}}\frac{d\sigma_{\lambda\lambda'}}{dE_\lambda dE'_\lambda}dE_\lambda dE_{\lambda'}, \tag{2.99}$$

$$\sigma^{><}_{\lambda\lambda'} = \int_{\bar{E}_\lambda}^{E^{max}_\lambda}\int_{E^{min}_{\lambda'}}^{\bar{E}_{\lambda'}}\frac{d\sigma_{\lambda\lambda'}}{dE_\lambda dE'_\lambda}dE_\lambda dE_{\lambda'}. \tag{2.100}$$

As discussed in the preceding section, if only scalar s-channel exchange contributes to the spin-spin correlation terms inserting (2.79) into (2.96) we obtain

$$\mathcal{A}_{\lambda\lambda'} = \frac{1}{4}\eta_{\lambda^\mp}\eta_{\lambda'^\pm}. \tag{2.101}$$

We conclude that, assuming that the resonant contributions can be well separated, the asymmetry of the energy distributions is only sensitive to the scalar character of the exchange channel and to the product of decay factors $\eta_{\lambda^\mp}\eta_{\lambda'^\pm}$.

2.5.2 Angular distributions

In this section we analyze the dependence of the differential cross section on the azimuth angles of the decay particles $\lambda^\mp$ and $\lambda'^\pm$. The non-absorptive and absorptive parts of the production spin density matrix depending on the transverse polarizations can be thus extracted with two asymmetries.

To obtain the dependence of the amplitude squared of production with subsequent decays, eq. (C.32), on the azimuth angles of the decay particles we express the decay matrix coefficients $\Sigma_D^a,\ a = 1, 2$ given explicitly in Section C.3.1, in the CMS. For the decay $\tilde{\chi}_j^\pm \to \lambda'^\pm \tilde{N}'$, $\lambda' = e, \mu, \tau, W$, we obtain

$$\Sigma_D^1 = \eta_{\lambda'^\pm} D \sin\theta_j \cos\varphi_j, \tag{2.102}$$

$$\Sigma_D^2 = \eta_{\lambda'^\pm} D \sin\theta_j \sin\varphi_j. \tag{2.103}$$

Here θ_j and φ_j are the polar and azimuth angles of $\lambda'^\pm$ with respect to the momentum of $\tilde{\chi}_j^\pm$, see Section D.2.

For the decay $\tilde{\chi}_i^\mp \to \lambda^\mp \tilde{N}$ the decay matrix coefficients are

$$\Sigma_D^1 = -\eta_{\lambda^\mp} D \sin\theta_i \cos\varphi_i \tag{2.104}$$

$$\Sigma_D^2 = \eta_{\lambda^\mp} D \sin\theta_i \sin\varphi_i, \tag{2.105}$$

with θ_i and φ_i the polar and azimuth angles of $\lambda^\mp$ in the reference frame R_{χ_j} given in Section C.1.4, where the momentum of $\tilde{\chi}_j^\pm$, $\vec{p}_{\chi_j^\pm}$ defines the z-axis.

The differential cross section can then be expressed in the form

$$\begin{aligned}\frac{d^2\sigma_{\lambda,\lambda'}}{d\varphi_i d\varphi_j} &= \frac{\sigma_{\lambda,\lambda'}}{4\pi^2}[1 + K^{11}\cos\varphi_i\cos\varphi_j + K^{22}\sin\varphi_i\sin\varphi_j \\ &\qquad + \mathrm{K}^{12}\cos\varphi_\mathrm{i}\sin\varphi_\mathrm{j} + \mathrm{K}^{21}\sin\varphi_\mathrm{i}\cos\varphi_\mathrm{j}],\end{aligned} \tag{2.106}$$

where the coefficients K^{ab} depend on the spin-spin correlation coefficients Σ_P^{ab}.

For the resonant contributions of H and A exchange, eq. (2.106) further simplifies due to the relations $\Sigma_r^{11} = -\Sigma_r^{22}$ and $\Sigma_r^{12} = \Sigma_r^{21}$, see eqs. (2.76) and (2.77),

$$\frac{d^2\sigma_{\lambda,\lambda'}}{d\varphi_i d\varphi_j} = \frac{\sigma_{\lambda,\lambda'}}{4\pi^2}[1 + K^{11}\cos(\varphi_i - \varphi_j) + K^{12}\sin(\varphi_i - \varphi_j)], \tag{2.107}$$

with

$$K^{11} = -\eta_{\lambda^\mp}\eta_{\lambda'^\pm} K_\lambda K_{\lambda'} \frac{\bar{\Sigma}_r^{11}}{\bar{P}}, \tag{2.108}$$

$$K^{12} = -\eta_{\lambda^\mp}\eta_{\lambda'^\pm} K_\lambda K_{\lambda'} \frac{\bar{\Sigma}_r^{12}}{\bar{P}}, \tag{2.109}$$

where the average over the chargino production angles $\bar{\Sigma}_P^{ab}$ is defined in eq. (2.94). Further, the coefficients K_λ and $K_{\lambda'}$ result from the integration over the polar

angles of the decay particles λ and λ', respectively. Since the kinematics of the decay depends on the mass difference between the chargino and its decay particles, we need to distinguish the two cases, see Section 2.4.3. For $m_\lambda < \bar{m}_\lambda$, with $\bar{m}_\lambda = (m^2_{\chi_j^\pm} - m^2_\lambda - m^2_{\tilde{N}})/2E_{\chi_j^\pm}$, the polar angle θ is not bounded and we have

$$K_\lambda = \frac{1}{2}\int_0^\pi d\theta \, \sin^2\theta = \frac{\pi}{4}, \tag{2.110}$$

while for $m_\lambda > \bar{m}_\lambda$

$$K_\lambda = \int_0^{\theta_{max}} d\theta \, \sin^2\theta = \frac{1}{2}\theta_{max}. \tag{2.111}$$

Analogous expressions follow for $K_{\lambda'}$.

Note that the differential cross section, eq. (2.107), only depends on the difference of the azimuth angles $\varphi_i - \varphi_j$. The absolute value $|\varphi_i - \varphi_j|$ is independent of the production plane since it is obtained from the relation

$$\cos\theta_{\lambda\lambda'} \;=\; \cos\theta_i\cos\theta_j + \sin\theta_i\sin\theta_j\cos(\varphi_i - \varphi_j), \tag{2.112}$$

where $\theta_{\lambda\lambda'}$ denotes the angle between λ and λ' and θ_j and θ_i are functions of the energies E_λ and $E_{\lambda'}$, see eq. (2.35). The sign of $\varphi_i - \varphi_j$ depends on the orientation of the momenta of the decay particles with respect to one of the charginos, with the formalism chosen here $\tilde{\chi}_j^\pm$. Therefore, the momentum of the charginos, and thus the production plane, needs to be determined. This is possible if the subsequent decay of either $\tilde{N}$ or $\tilde{N}'$ can be reconstructed.

If the continuum contributions need to be taken into account we must substitute in eqs. (2.108) and (2.109)

$$\bar{\Sigma}^{11}_r \to \bar{\Sigma}^{11}_r + \frac{1}{2}(\bar{\Sigma}^{11}_{cont} - \bar{\Sigma}^{22}_{cont}) \equiv \bar{\Sigma}^{\parallel}, \tag{2.113}$$

$$\bar{\Sigma}^{12}_r \to \bar{\Sigma}^{12}_r + \frac{1}{2}(\bar{\Sigma}^{12}_{cont} + \bar{\Sigma}^{21}_{cont}) \equiv \bar{\Sigma}^{\perp}. \tag{2.114}$$

To isolate the two coefficients, $\bar{\Sigma}^{\parallel}$ and $\bar{\Sigma}^{\perp}$ we define the angular distribution asymmetries

$$\mathcal{A}^{T\parallel} = \frac{\sigma(\cos(\varphi_i - \varphi_j) > 0) - \sigma(\cos(\varphi_i - \varphi_j) < 0)}{\sigma(\cos(\varphi_i - \varphi_j) > 0) + \sigma(\cos(\varphi_i - \varphi_j) < 0)} = -\frac{2}{\pi}\eta_{\lambda^\mp}\eta_{\lambda'^\pm}K_\lambda K_{\lambda'}\frac{\bar{\Sigma}^{\parallel}}{\bar{P}} \tag{2.115}$$

and

$$\mathcal{A}^{T\perp} = \frac{\sigma(\sin(\varphi_i - \varphi_j) > 0) - \sigma(\sin(\varphi_i - \varphi_j) < 0)}{\sigma(\sin(\varphi_i - \varphi_j) > 0) + \sigma(\sin(\varphi_i - \varphi_j) < 0)} = -\frac{2}{\pi}\eta_{\lambda^\mp}\eta_{\lambda'^\pm}K_\lambda K_{\lambda'}\frac{\bar{\Sigma}^{\perp}}{\bar{P}}. \tag{2.116}$$

2.5.3 Summary of Section 2.5

In order to analyze the spin-spin correlation terms in chargino pair production in $\mu^+\mu^-$-annihilation with longitudinally polarized beams we have studied the two-body decays of both charginos. We have defined three independent asymmetries in the momenta of the decay particles: an asymmetry in the energy distributions of the decay particles, and two asymmetries in their transverse momentum distributions.

For Higgs exchange channels the energy distribution asymmetry does not provide additional information on the production process. It is thus ideal to determine the decay factor $\eta_{\lambda^\mp}\eta_{\lambda'^\pm}$, which are needed to extract information from the angular asymmetries $\mathcal{A}^{T\parallel}$ and $\mathcal{A}^{T\perp}$. While the decay factors $\eta_{\lambda^\mp}$ and $\eta_{\lambda'^\pm}$ will be determined at an e^+e^- collider, a measurement in the same process may allow to cancel systematic uncertainties.

The azimuth angular distribution asymmetry $\mathcal{A}^{T\parallel}$, which is sensitive to parallel transverse chargino polarizations, is of greatest interest for unequal chargino production, since in this process it is not possible to determine the couplings in a model independent way with the production process alone. For equal charginos $\mathcal{A}^{T\parallel}$ may be used to determine the CP quantum number of a single resonance, or, for overlapping resonances, to separate the CP-even and CP-odd contributions.

The asymmetry $\mathcal{A}^{T\perp}$ is sensitive to the absorptive parts of the production spin density matrix, which is possible for partially interfering scalar and pseudoscalar resonances.

2.6 Production and decay with transverse beam polarization

Here we briefly discuss the effect of transverse polarization on pair production and decay of charginos in $\mu^+\mu^-$ annihilation at the neutral Higgs resonances H and A.

The dependence of the chargino production process on transverse polarization introduces new possibilities to probe the Higgs-neutralino interactions. Specifically, for completely polarized beams, transverse polarization would allow to create states with any CP phase. The CP-even (CP-odd) state would then be obtained for parallel (anti-parallel) μ^+ and μ^- polarizations.

A general expression for the resonant contributions to the spin-density matrix coefficients is given in Appendix C.2.1. For polarization independent coefficient P_r for the pure Higgs exchange channels we can refer to Section 3.4, where the effects of the transverse polarization on neutralino production is analyzed. The analysis for charginos is analogous, in what regards the beam polarization additional effects. Transverse polarizations allow to enhance or suppress states the

CP components of the $\mu^+\mu^-$ pair.

For the interference of H and A, however, there is no analog in neutralino production. In addition to the term which depends on the longitudinal beam polarizations there is an absorptive term given by, in the formalism of Appendix C.2.1.

The chargino polarization independent coefficient P_r of the production spin density matrix, for longitudinally *and* transversely polarized beams, is obtained from eqs. (2.6) and (2.7). with the new dependence on the beam polarization for

$$\begin{aligned} P_r(HA) &= -2g^4\,\mathrm{Im}\{\Delta(H)\Delta(A)^*\},\mathrm{Re}[\ell^{(HA)}(\vec{\mathcal{P}}_,\vec{\mathcal{P}}_-)] \\ &\quad \mathrm{Im}[a_+^{HA}\,(p_{\chi_i^\pm}p_{\chi_j^\pm}) - b_+^{HA}m_{\chi_i^\pm}m_{\chi_j^\pm}]\}(p_{\mu^+}p_{\mu^-}), \end{aligned} \tag{2.117}$$

where the couplings a_+^{HA} and b_+^{HA} can be found in Appendix C.2.1.

The additional most interesting term arises in the spin-spin correlation terms, where a non-absorptive term is obtained, which contributes to the asymmetry $\mathcal{A}^{T\perp}$, eq. 2.116.

$$\begin{aligned} \Sigma_{r,T}^{ab\,(HA)} &= \frac{g^4}{4}[(\vec{\mathcal{P}}_+ \times \vec{\mathcal{P}}_-)\cdot\hat{n}_{\mu^+}]\,\mathrm{Re}\{\Delta(H)\Delta(A)^*\}\mathrm{Im}\{c^{(H\mu)}c^{(A\mu)}\} \\ &\quad \mathrm{Im}\{c_L^{(H)}c_R^{(A)\,*} - c_R^{(H)}c_L^{(A)\,*}\}C^{(ab)}\,s, \end{aligned} \tag{2.118}$$

where the coefficient $C^{(ab)}$ is defined in eq. (2.78), for the notation for the couplings see e.g. Section 2.5.

For detailed conclusions on the effect of transverse beam polarization of the pure Higgs exchange contributions to the production process see Section 3.4.

Chapter 3

Neutralino production and decay in $\mu^+\mu^-$-annihilation

In this chapter we study the pair production of neutralinos in $\mu^+\mu^-$-annihilation for center of mass energies $\sqrt{s}$ around the masses of the heavy neutral Higgs bosons H and A in the MSSM,

$$\mu^+ \ \mu^- \to \tilde{\chi}_i^0 \ \tilde{\chi}_j^0, \tag{3.1}$$

with $i, j = 1, \ldots, 4$.

In order to probe the Higgs-neutralino interaction we study cross sections, energy and angular distributions, in analogy to the chargino production process in Chapter 2, using beam and neutralino polarizations.

The analysis of neutralino production and decay is strongly correlated to that of charginos since both are mixing states of the supersymmetric partners of the Higgs and electroweak gauge bosons. Therefore the structures of the Higgs-neutralino and of the Higgs-chargino interaction are very similar. An important difference, however, lies in the fact that neutralinos are Majorana fermions. The couplings of the Higgs bosons to their left-handed and right-handed components must then be related, as follows from the interaction Lagrangian, eq. (B.10). An analogous relation is fulfilled for the Higgs-chargino couplings for equal chargino pairs, see eq. (B.7). We thus expect the analysis of neutralino production via Higgs boson exchange to have a strong similarity to the analysis of pair production of equal charginos.

A phenomenological analysis of neutralino pair production is complicated by the fact that in the MSSM there are four neutralinos and the lighter one is the lightest supersymmetric particle (LSP) and thus escapes undetected from the detector. We focus on the production of the lighter neutralino pairs $\tilde{\chi}_i^0\tilde{\chi}_j^0$ with $i = 1, j = 2, 3$ and $i = 2, j = 2$. These neutralinos are expected to be among the lightest observed supersymmetric particles.

We first study in Section 3.1 the dependence of the neutralino pair production cross sections on $\sqrt{s}$ for longitudinally polarized beams. In order to study

the Higgs-neutralino interactions we need to separate the contributions from the Higgs resonances from each other and from the non-resonant Z boson in s-channel and $\tilde{\mu}_{L,R}$ in t- and u-channel exchange. If the resonances do not overlap this is straightforward and we can build ratios of cross sections which allow to determine the Higgs-neutralino couplings, in analogy to Section 2.1 for chargino production. An additional complication appears in neutralino production, however, since for some neutralino pairs their couplings to one of the Higgs bosons may be small, strongly suppressing one of the resonances.

In Section 3.2 we study neutralino pair production with the subsequent two-body decay of one of the neutralinos

$$\tilde{\chi}_j^0 \to \ell^\pm \tilde{\ell}^\mp, \quad \ell = e, \mu, \tau, \tag{3.2}$$

for $j = 2, \ldots, 4$ [27]. We can thus analyze the longitudinal polarizations of the neutralinos through the energy distributions of their decays, eq. (3.2). The neutralino polarizations allow to measure the interference of the overlapping Higgs boson resonances with different CP quantum numbers. For the remaining contributions to neutralino pair production from pure Higgs exchange as well as from the continuum, the neutralino polarizations, averaged over their production angles, must vanish due to their Majorana character. Here we build asymmetries in the energy distribution of the decay leptons and numerically investigate the cross sections, asymmetries and statistical significances for a set of sample scenarios.

In Section 3.3, we analyze the two-body decays of both neutralinos, which are sensitive to the neutralino spin-spin correlations. and build asymmetries in the energy and angular distributions of their final particles. Finally, in Section 3.4, we analyze the effect of transverse beam polarization in neutralino pair production. Both the transverse polarizations of the beams and those of the neutralinos are sensitive to the CP quantum number of the resonant contributions and are thus ideal to separate their CP-even and odd contributions.

3.1 Neutralino production

Here we show that, for scenarios where the two resonances can be separated, we can probe the Higgs-neutralino interactions studying the line-shape of neutralino pair production in $\mu^+\mu^-$-annihilation with longitudinally polarized beams.

At center of mass energies around the heavy Higgs bosons H and A neutralinos are produced via the resonant s-channel exchange of H and A bosons, shown in Fig. 3.1, as well as via the non-resonant exchange of the Z boson and of the light Higgs boson h in the s-channel and of the t- and u-channel exchange of $\tilde{\mu}_{L,R}$, shown in Fig. 3.2. The interaction Lagrangians of the Higgs exchange channels are given in Appendix B, eqs. (B.1) and (B.10). The Lagrangians for the non-Higgs exchange channels can be found in [22]. Assuming that the masses

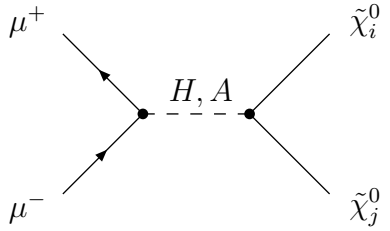

Figure 3.1: Resonant neutralino pair production

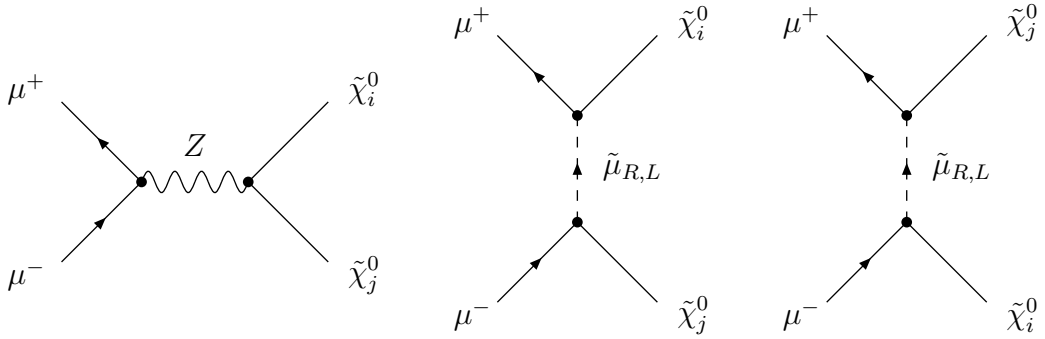

Figure 3.2: Continuum contribution to neutralino pair production

and couplings of the smuons and selectrons are equal, the contributions from the non-Higgs channels to the production process are equivalent to those in e^+e^- collisions.

For the calculation of the cross section for the combined process of neutralino production eq. (3.1) and decay, eq. (3.2), which depends on the neutralino $\tilde{\chi}_j^0$ polarization, we use the spin density matrix formalism of [28], see Appendix C. The unnormalized spin density matrix for neutralino pair production in $\mu^+\mu^-$-annihilation ρ^P, eq. (C.23), is a function of the polarization degrees of the μ^+ and μ^- beams, denoted with $\mathcal{P}_+^m$ and $\mathcal{P}_-^m$, respectively, for $m = 1, 2, 3$. With our choice of reference system, see Section D.1.3, $\mathcal{P}_\pm^3 \equiv \mathcal{P}_\pm^L$ denote the longitudinal beam polarizations, i.e. the average helicities of the incoming muons and antimuons, and $\mathcal{P}_\pm^1$ and $\mathcal{P}_\pm^2$ their transverse polarizations. In the following we consider only longitudinally polarized beams.

The expansion coefficients of the neutralino production matrix, see eqs. (C.25) and (C.39-C.42), subdivide into contributions from the Higgs resonances and the continuum, respectively,

$$P = P_r + P_{cont}, \qquad \Sigma^a_{P_j} = \Sigma^a_{rj} + \Sigma^a_{cont\,j}, \qquad \Sigma^{ab}_P = \Sigma^{ab}_r + \Sigma^{ab}_{cont}\ , \tag{3.3}$$

analogous to eq. (2.4) for chargino production. Here the continuum contributions P_{cont}, Σ^a_{cont} and Σ^{ab}_{cont} are those from the non-resonant Z and h in s-channel and $\tilde{\mu}_L$ and $\tilde{\mu}_R$ in t- and u-channel exchange. These coefficients can be found in [22].

The coefficients $\Sigma^a_{P_j}$ and Σ^{ab}_P describe the polarization of the charginos and are discussed in Sections 3.2 and 3.3.

The resonant contributions, from s-channel exchange of the Higgs bosons H and A, are separated into pure exchange and interference terms,

$$P_r = \sum_{\phi=H,A} P_r^{(\phi\phi)} + P_r^{(HA)}. \tag{3.4}$$

The H-A interference term $P_r^{(HA)}$ vanishes due to the Majorana nature of the neutralinos.

In the center of mass system (CMS) we obtain for $\mu^+\mu^- \to \tilde{\chi}^0_i\tilde{\chi}^0_j$

$$P_r^{(\phi\phi)} = \frac{g^4}{4}(1+\mathcal{P}^L_+\mathcal{P}^L_-)|\Delta(\phi)|^2|c^{(\phi\mu)}|^2|d_{ij}^{(\phi)}|^2 s[s-(m_{\chi^0_i}+\eta^\phi_{ij}m_{\chi^0_j})^2], \tag{3.5}$$

$$\eta^\phi_{ij} = \eta_\phi\eta_i\eta_j, \qquad \phi = H, A, \tag{3.6}$$

where η_ϕ is the CP quantum number of the Higgs boson ϕ, with $\eta_H = -\eta_A = 1$, and η_i and η_j are the signs of the neutralino mass matrix eigenvalues, see Section A.3.1.

The phase factor η^ϕ_{ij} can be plus or minus one for both H and A, depending on the signs η_i and η_j. Therefore, for unequal neutralinos, either the CP-even or the CP-odd exchange channel is p-wave suppressed, for $\eta_i = \eta_j$ or $\eta_i = -\eta_j$, respectively.

Since the interference of H and A vanishes due to CP conservation, the production cross section of $\tilde{\chi}^0_i\tilde{\chi}^0_j$ can be separated into the dominating contributions σ^{ij}_H and σ^{ij}_A from H and A exchange, respectively, and the background of non-resonant channels σ^{ij}_{cont} from Z boson, the light Higgs boson h, and t- and u-channel exchange of $\tilde{\mu}_{L,R}$

$$\sigma^{ij} = \sigma^{ij}_H + \sigma^{ij}_A + \sigma^{ij}_{cont}. \tag{3.7}$$

Neutralino production via the Z and $\tilde{\mu}_{L,R}$ exchange channels will have been thoroughly studied at linear colliders [9]. Here we neglect the contributions from h exchange at the H and A resonances.

At CMS energy $\sqrt{s}$ the cross sections σ^{ij}_H and σ^{ij}_A can be expressed in the form (see Appendix C.1.7)

$$\sigma^{ij}_\phi = (2-\delta_{ij})\frac{g^4}{8\pi}(1+\mathcal{P}^L_+\mathcal{P}^L_-)|c^{(\phi\mu)}|^2\cdot|d_{ij}^{(\phi)}|^2\cdot\sqrt{\lambda_{ij}(s)}\,B^{ij}_\phi(s)K_\phi(s), \quad \phi = H, A \tag{3.8}$$

with

$$B^{ij}_\phi(s) = 1 - \frac{(m_{\chi^0_i}+\eta^\phi_{ij}m_{\chi^0_j})^2}{s}, \tag{3.9}$$

$$K_\phi(s) = \left[(s-m^2_\phi)^2+\Gamma^2_\phi m^2_\phi\right]^{-1}, \tag{3.10}$$

and

$$\lambda_{ij}(s) \;=\; \lambda(s, m^2_{\tilde{\chi}^0_i}, m^2_{\tilde{\chi}^0_j}) \tag{3.11}$$

is the triangle function defined in (E.11).

Experimentally, cross sections of neutralino production and decay are observed. Therefore, for precision studies, their decays need to be taken into account. We neglect widths effects in the decays of neutralinos. Then, the total cross section $\sigma^{f_i f_j}$ for the pair production $\mu^+\mu^- \to \tilde{\chi}^0_i \tilde{\chi}^0_j$ with subsequent decays $\tilde{\chi}^0_k \to f_k$, $k = i, j$, factorizes into the production cross section σ^{ij} and the branching ratios for the respective decay channels:

$$\sigma^{f_i f_j}(\sqrt{s}) = \sigma^{ij}(\sqrt{s}) \times \mathrm{BR}(\tilde{\chi}^0_i \to f_i) \times \mathrm{BR}(\tilde{\chi}^0_j \to f_j). \tag{3.12}$$

Since this results holds independently of the production channel, the decay factors out in ratios of the cross sections.

3.1.1 Determination of the Higgs-neutralino couplings in production

Here we relate ratios of neutralino cross sections to the ratio of H-neutralino and A-neutralino couplings. In the preceding section we have seen that, for longitudinally polarized beams, the contributions from the scalar and pseudoscalar Higgs exchange, as well as those from the continuum, can be separated since their interference is negligible. To isolate the resonant contributions $\sigma_H^{f_+f_-} + \sigma_A^{f_+f_-}$ we subtract from the measured cross section $\sigma_{meas}^{f_+f_-}$ at $\sqrt{s} = m_H$ and $\sqrt{s} = m_A$ the continuum contributions $\sigma_{cont}^{f_+f_-}$. However, the measured cross section σ_{meas}^{ij} contains, in addition to the resonant and continuum contributions, the background from standard model sources. Here Z pair production constitutes the main source of standard model background, which can be significantly reduced with appropriate cuts. Therefore the resonances can be observed above the smooth standard model background σ_{SM}^{ij}.

We determine the total background contribution $\sigma_B^{f_+f_-} = \sigma_{cont}^{f_+f_-} + \sigma_{SM}^{f_+f_-}$ by linear interpolation of $\sigma_{meas}^{f_+f_-}$ far below and above the resonance energies. The precision of this estimate obviously depends on the variation of the background contributions around the heavy Higgs resonances. By this procedure we avoid, however, reference to other experiments at different energy scales as e. g. chargino production at e^+e^- colliders combined with specific model calculations.

We define the ratio

$$r = \frac{\sigma_{meas}^{f_i f_j}(m_H) - \sigma_B^{f_i f_j}(m_H)}{\sigma_{meas}^{f_i f_j}(m_A) - \sigma_B^{f_i f_j}(m_A)} = \frac{\sigma_H^{ij}(m_H) + \sigma_A^{ij}(m_H)}{\sigma_H^{ij}(m_A) + \sigma_A^{ij}(m_A)}, \tag{3.13}$$

where in the last equality the branching ratios for the decays of the neutralinos factor out. Therefore r is independent of the specific neutralino decay channel and probes only the production process. We can then express the ratio of couplings

$$x_{ij} = \left| \frac{d_{ij}^{(H)}}{d_{ij}^{(A)}} \right|^2 . \tag{3.14}$$

as a function of the ratio r, the masses and widths of H and A and the masses of the neutralinos.

From eqs. (3.8) and (3.13) results

$$x_{ij} = \frac{r}{C_{ij}} \cdot \frac{1 - C'_{ij}/r}{1 - C''_{ij} r} \cdot \frac{1}{x_\mu}, \tag{3.15}$$

with

$$C_{ij} = \frac{\beta_{ij}(m_H)}{\beta_{ij}(m_H)} \frac{B_H^{ij}(m_A^2)}{B_A^{ij}(m_A^2)} \frac{\Gamma_A^2}{\Gamma_H^2}, \tag{3.16}$$

$$C'_{ij} = \frac{\beta_{ij}(m_H)}{\beta_{ij}(m_A)} \frac{B_A^{ij}(m_A^2)}{B_A^{ij}(m_A^2)} K_A(m_H^2) \Gamma_A^2, \tag{3.17}$$

$$C''_{ij} = \frac{\beta_{ij}(m_A)}{\beta_{ij}(m_H)} \frac{B_H^{ij}(m_A^2)}{B_H^{ij}(m_H^2)} K_H(m_A^2) \Gamma_H^2, \tag{3.18}$$

$$\beta_{ij}(\sqrt{s}) = \frac{\sqrt{\lambda_{ij}(s)}}{s}, \tag{3.19}$$

$$x_\mu = \left| \frac{c^{(H\mu)}}{c^{(A\mu)}} \right|^2 , \tag{3.20}$$

where C_{ij}, C'_{ij} and C''_{ij} can be determined without model dependent assumptions, and $x_\mu = 1$ in the Higgs decoupling limit [30].

Assuming that the masses of the heavy Higgs bosons and the neutralino are precisely known [9, 31] the precision for the determination of x depends on the energy spread of the muon beams, the width of the H and A resonances and on the error in the determination of the background.

3.1.2 Numerical analysis

In the numerical analysis we study the dependence on the MSSM parameters μ, M_2, $\tan\beta$ and m_A of $\tilde{\chi}_i^0 \tilde{\chi}_j^0$ production in $\mu^+\mu^-$ annihilation for $i = 1, j = 2, 3$ and $i = j = 2$ near the H and A resonances. We show neutralino production cross sections for unpolarized beams for a set of representative scenarios.

The Higgs sector parameters and the branching ratios for the decays of H and A into neutralinos are computed with the program HDECAY [32].

Scenarios	**M1**	**M2**	**M2′**	**G1**	**H1**	**H2**
M_2[GeV]	200	200	240	150	350	350
μ[GeV]	-200	200	240	-300	-150	150
m_H[GeV]	352.1	352.3	352.3	352.0	352.1	352.3
Γ_H[GeV]	0.49	0.79	0.34	0.43	0.40	0.54
Γ_A[GeV]	0.82	1.65	0.53	0.64	0.53	0.85
$\eta_1 m_{\chi_1^0}$	95	84	110	76	131	113
$\eta_2 m_{\chi_2^0}$	164	146	185	147	-162	-156
$\eta_3 m_{\chi_3^0}$	-215	-207	- 246	-313	189	195

Table 3.1: Reference scenarios with fixed $m_A = 350$ GeV, $\tan\beta = 5$ and $m_0 = 200$ GeV.

3.1.2.1 Scenarios

We choose six representative scenarios with $m_A = 350$ GeV, and $\tan\beta = 5$ which differ by the mixing character of the neutralino and by the sign of the higgsino mass parameter μ.

3.1.2.2 Branching ratios

The branching ratios for the decays of the Higgs bosons H and A into neutralino pairs are crucial for obtaining sufficient cross sections.

In Figs. 3.3a and 3.3b we show contours in the $\mu - M_2$ plane of the branching ratios of H and A into $\tilde{\chi}_1^0\tilde{\chi}_2^0$ for $\tan\beta = 5$ and $M_A = 350$ GeV. For the decay of the pseudoscalar the largest branching ratios are obtained in the mixed region, with $|\mu| \approx M_2$. The enhancement of the mixed region is due to the larger Higgs-neutralino couplings. Higgs bosons couple to a gaugino-higgsino pair and are therefore larger in regions of parameter space where one of the neutralinos is gaugino-like while the other is higgsino-like. For the lighter neutralinos $\tilde{\chi}_1^0$ and $\tilde{\chi}_2^0$ this corresponds to the mixed region.

The couplings, however, are not necessarily the most important parameter which determines the branching ratios. The relative CP phase-factor of the neutralinos η_{ij} determines the threshold behavior. For instance, for $\tilde{\chi}_1^0\tilde{\chi}_2^0$ in the mixed region with $\mu > 0$, we find $\eta_{12} = 1$ which leads to a p-wave suppression of the CP-even amplitudes and results in small relative small branching ratios BR(H $\to \tilde{\chi}_1^0\tilde{\chi}_2^0$), compared with BR(A $\to \tilde{\chi}_1^0\tilde{\chi}_2^0$), see Figs. 3.3a and 3.3c. In the higgsino region $M_2 > 2\mu$ the opposite is true, with $\eta_{12} = -1$, CP-odd amplitudes suppressed and larger branching ratios of H into $\tilde{\chi}_1^0\tilde{\chi}_2^0$.

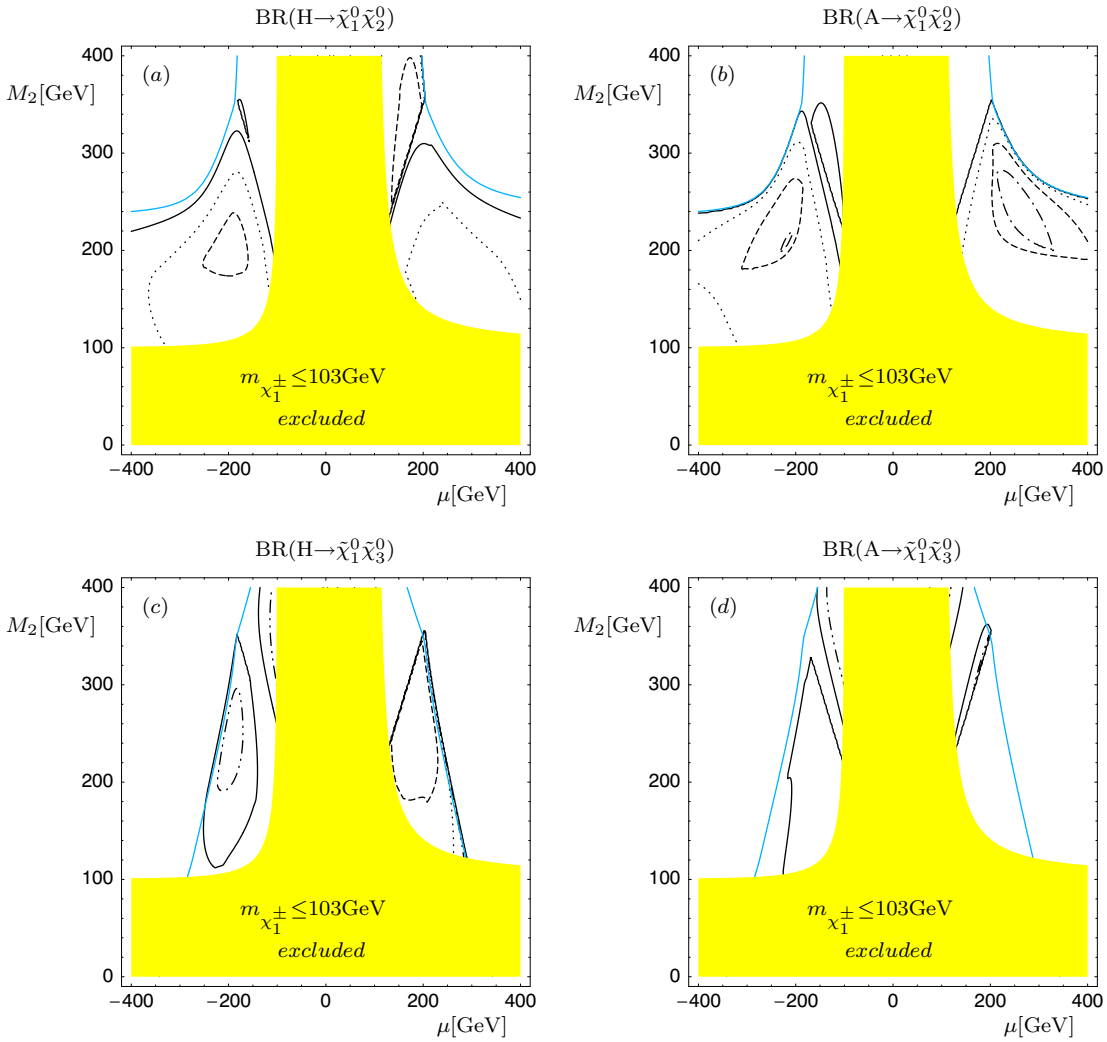

Figure 3.3: Branching ratios of the heavy Higgs bosons H and A into neutralino pairs into $\tilde{\chi}_1^0\tilde{\chi}_2^0$ and $\tilde{\chi}_1^0\tilde{\chi}_3^0$ for $m_A = 350$ GeV, $\tan\beta = 5$ and sfermions masses larger than $M_H/2$, computed with the program HDECAY [32]. The contour lines correspond to 2 % (solid), 10 % (dotted), 20 % (dashed) and 30 % (dash-dotted). For the decays into $\tilde{\chi}_1^0\tilde{\chi}_3^0$ the contour line for 5 % (dash-double-dotted) is also shown. The shaded area is the experimentally excluded region given here by $m_{\chi_1^\pm} < 103$ GeV. Also shown is the kinematical limit for the neutralino pair production processes.

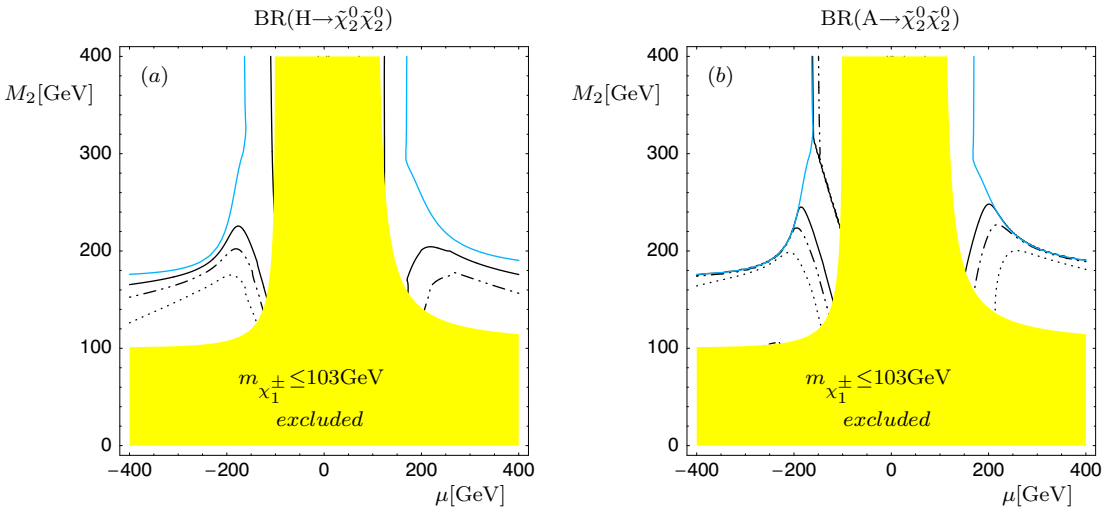

Figure 3.4: Branching ratios of the heavy Higgs bosons H and A into $\tilde{\chi}_2^0\tilde{\chi}_2^0$ for $m_A = 350$ GeV, $\tan\beta = 5$ and sfermions masses larger than $M_H/2$, computed with the program HDECAY [32]. The contour lines correspond to 2 % (solid), 5 % (dash-double-dotted) and 10 % (dotted). The shaded area is the experimentally excluded region given here by $m_{\chi_1^\pm} < 103$ GeV. Also shown is the kinematical limit for the neutralino pair production processes.

The two different values of η_{12} are due to the level crossing at $M_2 \approx 2\mu$, where the second and third lightest neutralinos are degenerate. The resulting exchange of parameters between $\tilde{\chi}_1^0$ and $\tilde{\chi}_2^0$ is clear comparing Figs 3.3a and Figs 3.3c, as well as Figs 3.3b and Figs 3.3d.

For mixed scenarios with $\mu > 0$ the scalar Higgs decays then predominantly into $\tilde{\chi}_1^0\tilde{\chi}_3^0$, with $\eta_{13} = -1$. The level crossing discussed here is a consequence of the convention used to label the neutralinos, namely through their masses, and introduces an additional complication to the dependence of the neutralino sector on the supersymmetric parameters. Therefore some care is needed in regions of parameter space where two neutralinos are nearly degenerate.

Note that the largest branching ratios for $A \to \tilde{\chi}_1^0\tilde{\chi}_2^0$, with BR(A $\to \tilde{\chi}_1^0\tilde{\chi}_2^0$) > 30 %, are found for relative large values of $|\mu| \approx M_2$, since in this parameter space region charginos are too heavy to be produced and the only competing supersymmetric process is pair production of LSPs.

3.1.2.3 Cross sections

In Figs. 3.5a-3.5f we show the production cross sections for $\tilde{\chi}_1^0\tilde{\chi}_2^0$, $\tilde{\chi}_1^0\tilde{\chi}_3^0$ and $\tilde{\chi}_2^0\tilde{\chi}_2^0$ in $\mu^+\mu^-$ annihilation as a function of the CMS energy around the H and A resonances for the scenarios of Table 3.1. In all scenarios we have chosen the same parameters as for the branching ratios, namely $\tan\beta = 5$, $m_A = 350$ GeV and $m_0 = 200$ GeV, as well as unpolarized beams.

In Fig. 3.5a, for the mixed scenario **M1** with $\mu < 0$, the production of $\tilde{\chi}_1^0\tilde{\chi}_2^0$ has peak sections of order $\mathcal{O}$(pb). As in chargino production, the contributions to $\tilde{\chi}_1^0\tilde{\chi}_2^0$ production can be well separated. The resonant production cross section for $\tilde{\chi}_1^0\tilde{\chi}_3^0$, on the contrary, is small for the A resonance and can be better observed via H exchange production, while for $\tilde{\chi}_2^0\tilde{\chi}_2^0$ the opposite is true.

In Fig. 3.5b, for the mixed scenario **M2** with $\mu > 0$, $\tilde{\chi}_1^0\tilde{\chi}_3^0$ becomes the main decay channel of the scalar Higgs boson. However, its resonant cross section at $\sqrt{s} = m_A$ cannot be clearly distinguished from the continuum and $\tilde{\chi}_1^0\tilde{\chi}_2^0$ production is necessary to test the Higgs-neutralino interactions.

In Fig. 3.5c we show the cross sections for scenario **M2′**, similar to scenario **M2** except for larger μ and M_2 values, so that only $\tilde{\chi}_1^0\tilde{\chi}_2^0$ is kinematically accessible. For this scenario, no other visible supersymmetric particles are produced. Therefore, the peak cross section at the A resonance is enhanced by the resulting narrower widths, despite the smaller available phase space, while at the H resonance the p-wave suppression can be clearly observed.

In Fig. 3.5d we show production cross sections for the gaugino scenario **G1**, for which the LSP is roughly bino-like while the second lightest neutralino is wino-like, with a larger higgsino component than the LSP. The only observable channels are $\tilde{\chi}_1^0\tilde{\chi}_2^0$ and $\tilde{\chi}_2^0\tilde{\chi}_2^0$ pair production. In this scenario the p-wave suppression of the scalar resonance is compensated by the narrower width. In scenarios in which $|\mu| \gg M_2$, as **G1**, the masses of the heavier two neutralinos are large and are in general not accessible. The threshold for $\tilde{\chi}_1^0\tilde{\chi}_3^0$ production is shown in Figs 3.3c and 3.3d.

In Figs. 3.5e and 3.5f we show cross sections for the higgsino scenarios **H1** and **H2**, with $\mu < 0$ and $\mu > 0$, respectively, in which the lightest two neutralinos have larger higgsino components. Since the Z boson couples to higgsino pairs, its couplings to the lighter neutralinos are large in these scenarios, resulting in large continuum contributions. For $\mu < 0$ the resonant cross sections are relatively small, compared to the remaining scenarios and the most promising channel is $\tilde{\chi}_2^0\tilde{\chi}_2^0$ production. For $\mu > 0$, however, large cross sections are expected for $\tilde{\chi}_1^0\tilde{\chi}_2^0$ at the scalar resonance. Note that this cross section is similar to $\tilde{\chi}_1^0\tilde{\chi}_3^0$ production the mixed scenario **M2**, as expected since at the level crossing the second and third lightest neutralinos are exchanged.

For larger values of $\tan\beta$ the resonances tend to overlap, see f.i. Section 2.1, and a separation of the resonances in total production is more difficult.

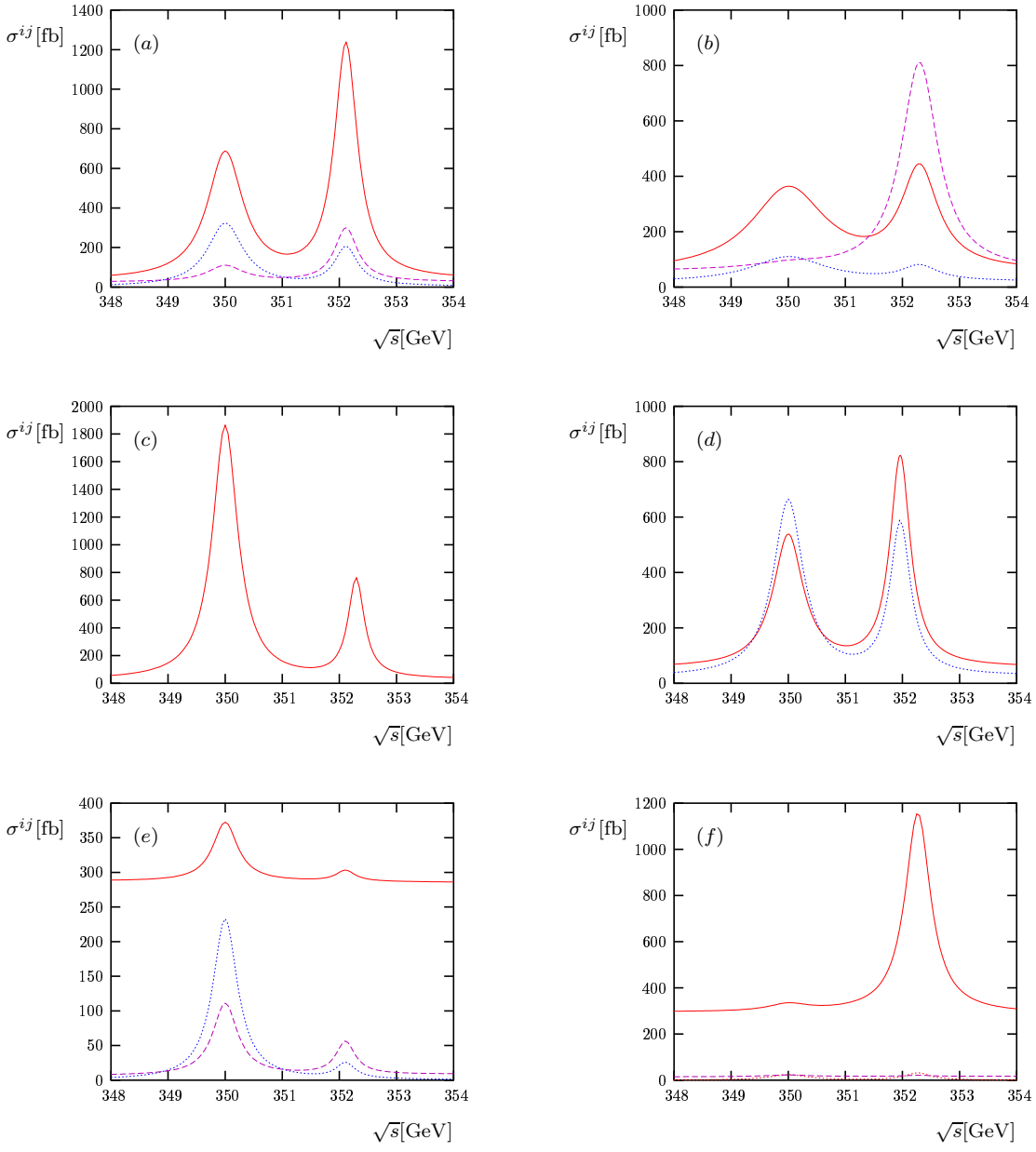

Figure 3.5: Total cross section σ^{ij} for $\mu^+\mu^- \to \tilde{\chi}_i^0\tilde{\chi}_j^0$, with $i = 1, j = 2$ (solid), $i = 1, j = 3$ (dashed) and $i = 2, j = 2$ (dotted), for scenarios **M1**, **M2**, **M2′**, **G1**, **H1** and **H2** of Table 3.1. In all scenarios $\tan\beta = 5$, $m_A = 350$ GeV and $m_0 = 200$ GeV.

3.1.3 Summary of Section 3.1

In this Section we have studied neutralino production at a muon collider via resonant heavy Higgs boson exchange in the MSSM. In analogy to chargino production, we have proposed to determine the ratio of couplings of H and A to neutralino pairs in a model independent way from the production cross section dependence on the center of mass energy. For a set of scenarios with $\tan\beta = 5$ and $m_A = 350$ GeV we have shown branching ratios of the neutral Higgs bosons into neutralinos, as well as production cross sections around the neutral Higgs boson resonances. The most important result is that, even though neutralino production cross sections are large, which neutralino pairs can be studied depends strongly on the μ and M_2 parameters. The dependence on $\tan\beta$ and m_A of the neutralino production process can be inferred from our analysis of chargino production since, in the regions of interest of parameter space, they affect mainly the Higgs sector.

3.2 Neutralino production with subsequent decay of one of the neutralinos

In this section we study the interference of resonant Higgs boson exchange in neutralino pair production in $\mu^+\mu^-$-annihilation with longitudinally polarized beams. We analyze the energy distribution of the decay lepton in the process $\tilde{\chi}_j^0 \to \ell^\pm\tilde{\ell}^\mp$, for $\ell = e, \mu, \tau$. In the CP conserving MSSM a non-vanishing asymmetry in the lepton energy spectrum is caused by the interference of Higgs boson exchange channels with different CP eigenvalues. The contribution of this interference is large if the heavy neutral bosons H and A are nearly degenerate. We show that the asymmetry can be used to determine the product of couplings of the neutral Higgs bosons to the neutralinos and their couplings to the muons. In particular, the asymmetry allows to determine the relative phase of the couplings. We find large asymmetries and cross sections for a set of reference scenarios with nearly degenerate neutral Higgs bosons.

3.2.1 Decay channels

Provided these decays are allowed, neutralinos decay dominantly into a fermion-sfermion pair or into a lighter neutralino and a Z or light Higgs boson, heavier neutralinos may also decay into a chargino and a W boson, shown in Fig. 3.6. The corresponding interaction Lagrangians are given in Appendix B.5.

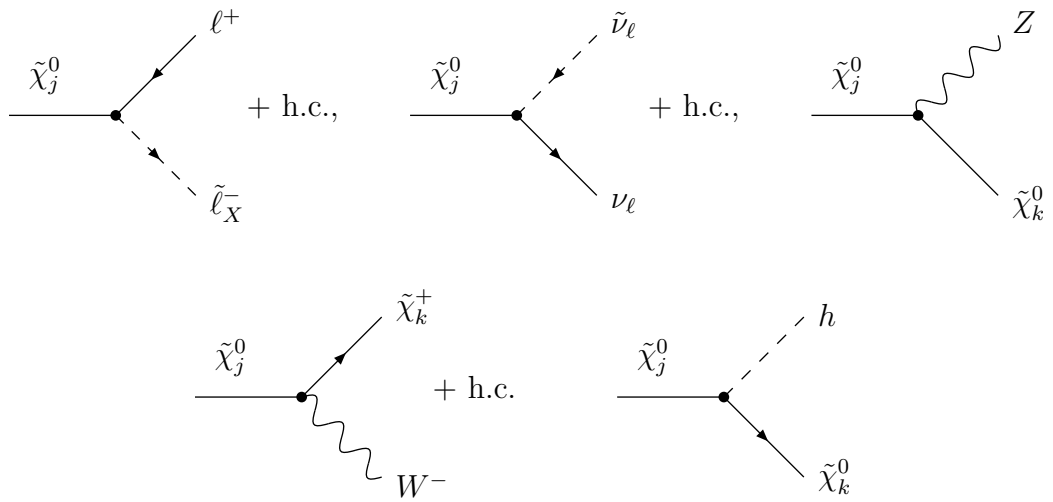

Figure 3.6: Two-body decays of the neutralinos. Here $\tilde{\ell}_X^- = \tilde{\ell}_{L,R}^-$ for $\ell = e, \mu$ and $\tilde{\ell}_X^- = \tilde{\tau}_{1,2}^-$ for $\ell = \tau$.

3.2.2 Neutralino polarization

With our choice of spin vectors, eqs. (C.18) and (C.21), $\Sigma^3_{P_j}/P$ is the longitudinal polarization of the decaying neutralino $\tilde{\chi}_j^0$, $\Sigma^1_{P_j}/P$ is its transverse polarization in the production plane and $\Sigma^2_{P_j}/P$ is its polarization perpendicular to the production plane.

As discussed in Section 3.1, the expansion coefficients of the neutralino production matrix subdivide into contributions from the Higgs resonances and the continuum, respectively, eq. (3.3). The spin correlation coefficients of the resonant contributions from s-channel exchange of the Higgs bosons H and A, are further separated into pure exchange and interference terms

$$\Sigma^3_{rj} = \sum_{\phi=H,A} \Sigma^{3\,(\phi\phi)}_{rj} + \Sigma^{3\,(HA)}_{rj}, \tag{3.21}$$

while resonant contributions Σ^1_{rj} and Σ^2_{rj} to the transverse polarizations of the neutralino vanish since the s-channel exchange is due to scalar Higgs bosons. The contributions from pure Higgs exchange $\Sigma^{3\,(\phi\phi)}_{rj}$ vanish due to the Majorana character of the neutralinos [36]. In the CMS we obtain for $\mu^+\mu^- \to \tilde{\chi}_i^0\tilde{\chi}_j^0$

$$\begin{aligned}\Sigma^{3\,(HA)}_{rj} = {} & \frac{g^4}{2}(\mathcal{P}_+^L + \mathcal{P}_-^L)\mathrm{Re}\{\Delta(H)\Delta(A)^*\} \\ & \mathrm{Im}\{d_{ij}^{(H)} d_{ij}^{(A)*}\}\mathrm{Im}\{c^{(H\mu)} c^{(A\mu)*}\} s\sqrt{\lambda_{ij}}\eta_j,\end{aligned} \tag{3.22}$$

where $\mathcal{P}_+^L$ and $\mathcal{P}_-^L$ denote the longitudinal beam polarizations of μ^+ and μ^-, respectively, $\Delta(\phi)$, is the Breit-Wigner propagator of the Higgs boson ϕ, eq. (2.8),

and

$$\lambda_{ij} \;=\; \lambda(s, m^2_{\chi^0_i}, m^2_{\chi^0_j}), \tag{3.23}$$

is the triangle function defined in eq. (E.11).

3.2.3 Energy distribution

The energy distribution of the lepton from the decay of $\tilde{\chi}^0_j$ is obtained integrating the differential cross section for production and decay, eqs. (C.23) and eq. (C.24), where the amplitude squared is given by (here we suppress the chargino index of the density matrix coefficients)

$$|T|^2 = |\Delta(\tilde{\chi}^0_j)|^2 \sum_{\lambda_i\lambda_j\lambda'_i\lambda'_j} \rho^P_{\lambda_i\lambda'_i\lambda_j\lambda'_j}\rho^D_{\lambda'_j\lambda_j}\delta_{\lambda_i\lambda'_i} = 4|\Delta(\tilde{\chi}^0_j)|^2(P\cdot D + \Sigma^a_P\cdot\Sigma^a_D). \tag{3.24}$$

Here we summed over the helicity λ_i of $\tilde{\chi}^0_i$ whose decay is not observed. The resonant contributions to the production density matrix coefficients P and Σ^a_P are given in eqs. (3.5) and (3.22). The expansion coefficients of the chargino decay matrix (C.26) for the neutralino decays $\tilde{\chi}^0_j \to \ell^\pm\,\tilde{\ell}^\mp_n$, with $n = R, L$ for $\ell = e, \mu$ (n=1,2 for $\ell = \tau$), are given in Appendix C.5.1.

In the CMS we can rewrite the factor Σ^3_D that multiplies the longitudinal chargino polarization coefficient Σ^3_P in eq. (C.30),

$$\Sigma^3_D \;=\; \eta^n_{\ell^\pm}\frac{D}{\Delta_\ell}(E_\ell - \bar{E}_\ell), \quad \ell = e, \mu, \tau, \tag{3.25}$$

where we have used the relation

$$m_{\chi^0_j}(s^3_{\chi^0_j}\cdot p_\ell) = -\frac{m^2_{\chi^0_j}}{|\vec{p}_{\chi^0_j}|}(E_\ell - \bar{E}_\ell) \tag{3.26}$$

and the kinematical factors $\bar{E}_\ell$ and Δ_ℓ have been defined in eq. (D.16-D.17).

The factor $\eta^n_{\ell^\pm}$ gives a measure of parity violation in decay. For the decays into leptons of the first two generations parity violation is maximal, with

$$\eta^R_{e^+} = \eta^R_{\mu^+} = -1, \quad \eta^L_{e^+} = \eta^L_{\mu^+} = 1, \tag{3.27}$$

and $\eta^n_{\ell^-} = -\eta^n_{\ell^+}$. For the decay $\tilde{\chi}^0_j \to \tau^\pm\tilde{\tau}^\mp_{1,2}$ the lepton energy dependent term in (3.25) is suppressed, due to stau mixing, by the factor $\eta^n_{\tau^\pm}$ given in eq. (C.84). The decays $\tilde{\chi}^0_j \to h\tilde{\chi}^0_k$ and $\tilde{\chi}^0_j \to Z\tilde{\chi}^0_k$ are thus uninteresting here, since, due to the Majorana character of the neutralinos, $\eta_h = \eta_Z = 0$.

The energy distribution of the lepton is

$$\frac{d\sigma^n_{\ell^\pm}}{dE_\ell} = \frac{\sigma^n_\ell}{2\Delta_\ell}\left[1 + \eta^n_{\ell^\pm}\frac{\bar{\Sigma}^3_P}{\bar{P}}\frac{(E_\ell - \bar{E}_\ell)}{\Delta_\ell}\right], \tag{3.28}$$

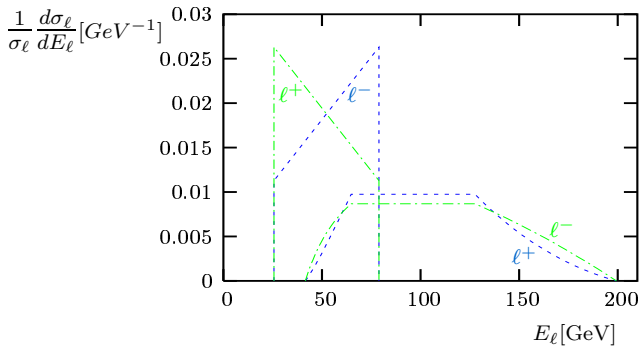

Figure 3.7: Normalized primary and secondary lepton energy distribution, with $\mathcal{A}_\ell^R = 0.2$, $m_{\chi_2^0} = 250$ GeV, $m_{\tilde{\ell}_R} = 200$ GeV, $m_{\chi_1^0} = 60$ GeV and $\sqrt{s} = 450$ GeV. The dashed curves correspond to the decay chain $\tilde{\chi}_2^0 \to \ell^-\tilde{\ell}_R^+$, $\tilde{\ell}_R^+ \to \tilde{\chi}_1^0\ell^+$ and the dash-dotted curves to $\tilde{\chi}_2^0 \to \ell^+\tilde{\ell}_R^-$, $\tilde{\ell}_R^- \to \tilde{\chi}_1^0\ell^-$.

where we have defined the averages over the neutralino production angles in the CMS by

$$\bar{P} = \frac{1}{4\pi}\int P d\Omega_{\tilde{\chi}^0}. \qquad \bar{\Sigma}_P^3 = \frac{1}{4\pi}\int \Sigma_P^3 d\Omega_{\tilde{\chi}^0}. \tag{3.29}$$

Further,

$$\sigma_\ell^n \;=\; \frac{2-\delta_{ij}}{128\pi^2}\frac{\sqrt{\lambda_{ij}}}{s^2}\frac{(m_{\chi_j^0}^2 - m_{\tilde{\ell}}^2)}{m_{\chi_j^0}^3\Gamma_{\chi_j^0}}\bar{P}D. \tag{3.30}$$

is the integrated cross section for neutralino production, eq. (3.1), and subsequent leptonic decay $\tilde{\chi}_j^0 \to \ell^\pm\tilde{\ell}_n^\mp$, with $n = R, L$ for $\ell = e, \mu$ ($n = 1, 2$ for $\ell = \tau$).

Explicit expressions for D are given in eqs. (C.76) and (C.80) for $\ell = e, \mu$ and $\ell = \tau$, respectively, and λ_{ij} is the triangle function, defined in eq. (E.11).

The lepton energy dependent part of the energy distribution eq. (3.28) is thus proportional to the average longitudinal polarization of the neutralinos $\bar{\Sigma}_P^3/\bar{P}$ times the factor $\eta_{\ell\pm}^n$ from the decay.

Due to the Majorana character of the neutralinos, the contribution to Σ_P^3 from the non-Higgs channels is forward-backward antisymmetric [36], whereas that from Higgs exchange is isotropic. Then, the non-resonant contribution in eq. (3.29) vanishes and, neglecting the interference of the resonant amplitudes with the Z and slepton exchange amplitudes,

$$\bar{\Sigma}_P^3 \;=\; \Sigma_r^3. \tag{3.31}$$

From eq. (C.71) follows that Σ_r^3, and thus the energy dependent term in eq. (3.28), are proportional to the interference of the H and A exchange amplitudes.

3.2.3.1 Lepton energy distribution asymmetry

For the processes $\mu^+\mu^- \to \tilde{\chi}^0_i\tilde{\chi}^0_j$ with subsequent decay $\tilde{\chi}^0_j \to \ell^+\tilde{\ell}^-_{R,L}$, with $\ell = e, \mu$, and $\tilde{\chi}^0_j \to \tau^+\tilde{\tau}^-_{1,2}$, as well as the charge conjugated decays, we define the asymmetries $\mathcal{A}^n_{\ell^+}$ and $\mathcal{A}^n_{\ell^-}$, with $n = R, L$ for $\ell = e$ and $\ell = \mu$, and $n = 1, 2$ for $\ell = \tau$,

$$\mathcal{A}^n_{\ell\pm} = \frac{\sigma^n_{\ell\pm}(E_\ell > \bar{E}_\ell) - \sigma^n_{\ell\pm}(E_\ell < \bar{E}_\ell)}{\sigma^n_{\ell\pm}(E_\ell > \bar{E}_\ell) + \sigma^n_{\ell\pm}(E_\ell < \bar{E}_\ell)} \tag{3.32}$$

$$= \frac{1}{2}\eta^n_{\ell\pm}\frac{\Sigma^3_r}{\bar{P}} \tag{3.33}$$

in order to isolate the H-A interference term in eq. (3.28).

We assume that the slepton decays subsequently into a neutralino and a secondary lepton. The latter needs to be distinguished from the primary lepton. Therefore, it is useful to define the charge asymmetry

$$\mathcal{A}^n_\ell = \frac{1}{2}(\mathcal{A}^n_{\ell^-} - \mathcal{A}^n_{\ell^+}). \tag{3.34}$$

From the relation $\mathcal{A}^n_{\ell^-} = -\mathcal{A}^n_{\ell^+}$, which is fulfilled for the primary lepton from neutralino decay, follows for the charge asymmetry $\mathcal{A}^n_\ell = \mathcal{A}^n_{\ell^-}$. The advantage of the new asymmetry, eq. (3.34), is that the largest part of the non-irreducible background from the secondary lepton drops out because its energy distribution is only weakly dependent on the sign of the lepton charge, as can be observed in Fig. 3.7, where we show the normalized energy distributions of the primary and secondary leptons for both charge cases, for a sample scenario with $\mathcal{A}^R_\ell = 0.2$.

Denoting by $\sigma_r(\mu^+\mu^- \to \tilde{\chi}^0_i\tilde{\chi}^0_j)$ the resonant contribution to the production cross section $\sigma(\mu^+\mu^- \to \tilde{\chi}^0_i\tilde{\chi}^0_j)$ we relate $\bar{P}$, eq. (3.29), to the resonant contribution P_r by:

$$\bar{P} = \frac{\sigma(\mu^+\mu^- \to \tilde{\chi}^0_i\tilde{\chi}^0_j)}{\sigma_r(\mu^+\mu^- \to \tilde{\chi}^0_i\tilde{\chi}^0_j)}P_r, \tag{3.35}$$

and express $\mathcal{A}^n_\ell$ in the form:

$$\mathcal{A}^n_\ell = \frac{1}{2}\,\eta^n_{\ell^-}\frac{\sigma_r(\mu^+\mu^- \to \tilde{\chi}^0_i\tilde{\chi}^0_j)}{\sigma(\mu^+\mu^- \to \tilde{\chi}^0_i\tilde{\chi}^0_j)}\,\mathcal{P}^r_j, \tag{3.36}$$

$$\mathcal{P}^r_j = \frac{\Sigma^3_r}{P_r}. \tag{3.37}$$

The contribution of the H-A interference to the asymmetry, eq. (3.36), is contained in the coefficient $\mathcal{P}^r_j$, which has the following dependence on the longitudinal beam polarizations $\mathcal{P}^L_+$ of μ^+ and $\mathcal{P}^L_-$ of μ^-:

$$\mathcal{P}^r_j = \frac{\mathcal{P}^L_+ + \mathcal{P}^L_-}{1 + \mathcal{P}^L_+\mathcal{P}^L_-}\mathcal{P}^r_{j,R_+R_-}, \tag{3.38}$$

where $\mathcal{P}^r_{j,R_+R_-} = \mathcal{P}^r_j$ for $\mathcal{P}^L_+ = \mathcal{P}^L_- = 1$, i.e. for right handed μ^+ and μ^- beams.

Since $\mathcal{P}^r_j$ is proportional to the interference of the H and A exchange amplitudes a non-vanishing asymmetry of the lepton energy distribution is a clear indication of nearly degenerate scalar resonances with opposite CP quantum numbers. The statistical significance of the asymmetry $\mathcal{A}^n_\ell$ is defined in Appendix D.4, eq. (D.33).

3.2.4 Determination of the Higgs-neutralino couplings in production and decay

In the previous sections we have shown that the production spin density matrix coefficient Σ^3_{rj} (3.22) of the longitudinal neutralino polarization is sensitive to the interference of the H and A Higgs bosons. Their interference in $\tilde{\chi}^0_i\tilde{\chi}^0_j$ production determines the sign γ_{ij} of the product of couplings

$$\kappa_{ij} = \mathrm{Im}(d^{(H)}_{ij} d^{(A)*}_{ij})\mathrm{Im}(c^{(H\mu)} c^{(A\mu)*}) \tag{3.39}$$

which appears in

$$\Sigma^{3\,(HA)}_{rj} = \frac{g^4}{2}(\mathcal{P}^L_+ + \mathcal{P}^L_-)\mathrm{Re}\{\Delta(H)\Delta(A)^*\}\kappa_{ij} s\sqrt{\lambda_{ij}}\eta_j. \tag{3.40}$$

The coefficient $\Sigma^{3\,(HA)}_{rj}$ can be obtained from the neutralino production cross section

$$\sigma_r(\mu^+\mu^- \to \tilde{\chi}^0_i\tilde{\chi}^0_j) \;=\; \frac{(2-\delta_{ij})\sqrt{\lambda_{ij}}}{2\pi s^2} P_r. \tag{3.41}$$

and the charge asymmetry $\mathcal{A}^n_\ell$, eq. (3.36),

$$\Sigma^{3(HA)}_{rj} = \frac{16\pi s^2}{(2-\delta_{ij})\sqrt{\lambda_{ij}}\,\eta_{\ell^-}}\,\sigma(\mu^+\mu^- \to \tilde{\chi}^0_i\tilde{\chi}^0_j)\,\mathcal{A}^n_\ell. \tag{3.42}$$

Now the product of couplings κ_{ij} can be obtained by comparison of eq. (3.40) and (3.42).

In general the factor γ_{ij} is defined by

$$\gamma_{ij} \;=\; \frac{\mathrm{Im}(d^{(H)}_{ij} d^{(A)*}_{ij})}{|d^{(H)}_{ij} d^{(A)}_{ij}|}\frac{\mathrm{Im}(c^{(H\mu)} c^{(A\mu)*})}{|c^{(H\mu)} c^{(A\mu)}|}. \tag{3.43}$$

Since we assume CP conservation γ_{ij} takes the values ± 1 for interfering amplitudes with opposing CP eigenvalues, as is here the case, and vanishes for interfering amplitudes of same CP.

It is also possible to determine the ratio of H and A couplings to the neutralinos with from the charge asymmetry $\mathcal{A}_\ell^n$, which allows to determine the ratio

$$\frac{\Sigma^3_{rj}}{P_r} = \frac{\sigma(\mu^+\mu^- \to \tilde{\chi}^0_j\chi^0_j)}{\sigma_r(\mu^+\mu^- \to \tilde{\chi}^0_j\chi^-_j)}\frac{2}{\eta_{\ell^-}}\mathcal{A}^n_\ell. \tag{3.44}$$

Inserting in eq. (3.44) the expressions of P_r and Σ^3_{rj}, eqs. (3.5) and (3.22), we obtain,

$$\frac{\Sigma^3_{rj}}{P_r} = \frac{\mathcal{P}^L_+ + \mathcal{P}^L_-}{1 + \mathcal{P}^L_+\mathcal{P}^L_-} \cdot \frac{2\gamma_{ij}\mathrm{Re}(\Delta(H)\Delta^*(A))\sqrt{s^+_{ij}s^-_{ij}}}{q_{ij}\,|\Delta(H)|^2\,s^+_{ij} + q^{-1}_{ij}\,|\Delta(A)|^2\,s^-_{ij}}, \tag{3.45}$$

where

$$s^\pm_{ij} = s - (\eta_i m_{\chi^0_i} \pm \eta_j m_{\chi^0_j})^2, \tag{3.46}$$

$$q_{ij} = \frac{|d^{(H)}_{ij}c^{(H\mu)}|}{|d^{(A)}_{ij}c^{(A\mu)}|}, \tag{3.47}$$

and $\Delta(H)$ and $\Delta(A)$ are the Breit-Wigner propagators. Note that the functions $s^\pm_{ij}$ depend on the relative CP phase factor of the neutralinos $\eta_{ij} = \eta_i\eta_j$, with η_i, η_j defined in Section B.5.

It is possible to solve eq. (3.45) for $\gamma_{ij}q_{ij}$. By comparison of eqs. (3.45) and (3.46) we then obtain the ratio q_{ij} and the sign of the product of couplings γ_{ij}.

For our analysis we have assumed that the masses and widths of the Higgs resonances H and A can be measured. The resonance parameters of nearly degenerate Higgs bosons with different CP quantum numbers may e.g. be determined by using transverse beam polarizations, which enhances or suppresses the Higgs exchange channels depending on their CP quantum numbers [34]. Alternatively, the if both neutralino decays are observed, their transverse polarizations can be used to separate the CP-even and CP-odd Higgs exchange contributions, see Section 3.3.

The neutralino-slepton couplings needed to evaluate η^n_ℓ will have been precisely studied at a linear collider, see, e.g., [9, 37], and the resonant cross section of neutralino production $\sigma_r(\mu^+\mu^- \to \tilde{\chi}^0_i\tilde{\chi}^0_j)$ can be obtained subtracting the continuum contributions from the integrated production cross section $\sigma(\mu^+\mu^- \to \tilde{\chi}^0_i\tilde{\chi}^0_j)$. The continuum can be estimated extrapolating the production cross sections measured below and above the resonance region [25].

We can then use a measurement of the charge asymmetry and of the cross sections to determine both the ratio q_{ij} and the product of H and A couplings to the neutralinos κ_{ij}. Note that a determination of γ_{ij} from a measurement of the cross section $\sigma(\mu^+\mu^- \to \tilde{\chi}^0_i\tilde{\chi}^0_j)$ alone is not possible.

Scenarios	**SPS1a**	**N5**	**N10**	**N20**	**N5'**	**N10'**	**N5"**	**N10"**
$\tan\beta$	10	5	10	20	5	10	5	10
M_2[GeV]	192.7	280	280	280	280	280	280	280
μ[GeV]	352.4	250	250	250	250	250	250	250
$m_{\chi_3^0}$[GeV]	359	255	257	258	255	257	255	257
$m_{\chi_2^0}$[GeV]	177	209	212	214	209	212	209	212
$m_{\chi_1^0}$[GeV]	96	128	131	132	128	131	128	131
m_0[GeV]	100	100	100	100	100	100	100	100
$m_{\tilde{e}_R}$[GeV]	143	173	173	173	173	173	173	173
m_A[GeV]	393.6	450	450	450	350	350	550	550
m_H[GeV]	394.1	451.4	450.4	450.1	351.9	350.5	551.1	550.3
Γ_A[GeV]	1.38	2.29	2.11	4.33	0.43	0.82	3.63	3.34
Γ_H[GeV]	0.93	1.12	1.33	3.68	0.27	0.71	2.83	2.76

Table 3.2: Reference scenarios. GUT relations are assumed for the gaugino soft breaking symmetry mass parameters $M_1 = 5/3\tan^2\theta_W M_2$ and for the slepton mass parameters [35]. The resonance parameters are evaluated with HDECAY [32].

3.2.5 Numerical analysis

We present numerical results for the neutralino production cross sections $\sigma(\mu^+\mu^- \to \tilde{\chi}_i^0\tilde{\chi}_j^0)$, the asymmetries $\mathcal{A}_\ell^R$ and $\mathcal{A}_\tau^1$ of the lepton energy distribution and the statistical significance at center of mass energies around the resonances of the neutral Higgs bosons H and A. We study the dependence on the MSSM parameters $\tan\beta$, μ, M_2 and m_A in the mixed scenarios **N** and in the gaugino-like scenario **SPS1a** defined in Table 3.2. Further, we discuss in scenario **SPS1a** [38] the influence of beam polarization.

In order to reduce the number of parameters we assume the GUT relations for the gaugino mass parameters, $M_1 = 5/3\tan^2\theta_W M_2$, and for the slepton masses [35]. Mixing between left and right sleptons is neglected for the first two generations, $\ell = e, \mu$. For staus, on the other hand, mixing has a strong effect on the masses and couplings. Explicit expressions for the masses of the sleptons of the first two generations as well as for the mixing formalism of the staus is given in Appendix A.4. Our scenarios have been chosen such that the mass of the lightest (heaviest) stau, $\tilde{\tau}_1$ ($\tilde{\tau}_2$), is of order $m_{\tilde{\ell}_R}$ ($m_{\tilde{\ell}_L}$), $\ell = e, \mu$, and $m_{\tilde{\ell}_R} < m_{\chi_j^0} < m_{\tilde{\ell}_L}$. Therefore, neglecting the three-body decays of $\tilde{\chi}_j^0$, only $\tilde{\chi}_j^0 \to \ell\tilde{\ell}_R$, $\ell = e, \mu$ and $\tilde{\chi}_j^0 \to \tau\tilde{\tau}_1$ contribute to the energy spectrum of the leptons. We show the

Scenarios	SPS1a	N5	N10	N20
A_τ[GeV]	-254	0	0	0
BR($\tilde{\chi}^0_2 \to \ell^- \tilde{\ell}^+_R$)[%]	3.2	16.3	15.2	11.3
BR($\tilde{\chi}^0_2 \to \tau^- \tilde{\tau}^+_1$)[%]	42.5	17.3	19.6	27.4

Table 3.3: Neutralino branching ratios, $\ell = e, \mu$.

neutralino branching ratios into lepton slepton pairs in Table 3.3.

3.2.5.1 $\tilde{\chi}^0_1\tilde{\chi}^0_2$ production

We first discuss, for $\tilde{\chi}^0_1\tilde{\chi}^0_2$ production, the dependence of the asymmetries and cross sections on the beam polarization in scenario **SPS1a**, the dependence on $\tan\beta$ in scenarios **N5**, **N10** and **N20** and the dependence on m_A in scenarios **N5'**,**N5"**, **N10'** and **N10"**. All the scenarios are defined in Table 3.2

3.2.5.2 Beam polarization

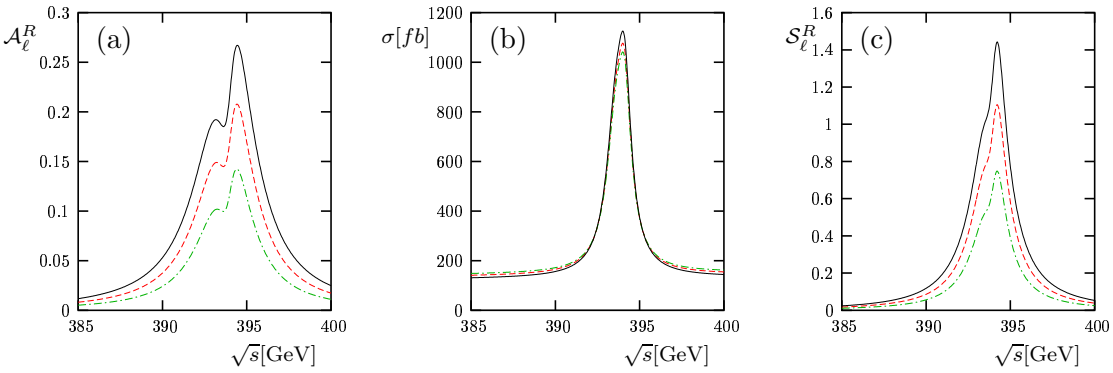

Figure 3.8: $\mu^+\mu^- \to \tilde{\chi}^0_1\tilde{\chi}^0_2$, $\tilde{\chi}^0_2 \to \ell^-\tilde{\ell}^+_R$, $\ell = e, \mu$, for scenario **SPS1a**. (a): $\mathcal{A}^R_\ell$, (b): neutralino production cross section and (c): significance with luminosity times detection efficiency $\epsilon\mathcal{L} = \mathcal{L}_{eff} = 0.5 fb^{-1}$ (for $\tilde{\chi}^0_2 \to \ell^-\tilde{\ell}^+_R$), for beam polarizations: $\mathcal{P}^L_+ = \mathcal{P}^L_- = -0.2$ (dash-dotted), -0.3 (dashed), and -0.4 (solid).

In Figs. 3.8a and 3.8b we show the asymmetry $\mathcal{A}^R_\ell$, $\ell = e, \mu$, and the cross section $\sigma(\mu^+\mu^- \to \tilde{\chi}^0_1\tilde{\chi}^0_2)$, respectively, for scenario **SPS1a** as a function of the center of mass energy around the heavy Higgs resonances. Since the resonances are completely overlapping the interference between the CP-even and CP-odd amplitudes is large, resulting in large asymmetries in the resonance region. The largest asymmetries are found at $\sqrt{s} \simeq m_H$ where the CP-even and CP-odd amplitudes are of the same order, because, due to the relative CP phase factor

$\eta_{12} \equiv \eta_1\eta_2 = 1$ of the neutralinos, the CP-even amplitudes are P-wave suppressed. The largest production cross sections are found at $\sqrt{s} \simeq m_A$.

We show the cross section, the asymmetry and the significance of scenario **SPS1a** for $\mathcal{P}_+^L = \mathcal{P}_-^L = -0.2,\ -0.3,\ -0.4$. The dependence on the longitudinal beam polarization of the resonant cross section is given by the factor $1 + \mathcal{P}_+^L\mathcal{P}_-^L$, and is rather weak for the polarization degrees expected at a muon collider. From eqs. (3.36) and (3.38) follows that the polarization dependence of the asymmetry is then roughly $\mathcal{A}_\ell^n \sim \mathcal{P}_+^L + \mathcal{P}_-^L$. For the statistical significance, defined in eq. (D.33), follows then $\mathcal{S}_\ell^n \sim \mathcal{P}_+^L + \mathcal{P}_-^L$.

3.2.5.3 Stau mixing dependence

The asymmetry for the τ energy spectrum depends strongly on the mixing in the stau sector. The τ energy asymmetry is obtained by $\mathcal{A}_\tau^1 = \eta_\tau^1\mathcal{A}_\ell^R$, eqs. (3.36) and (C.84). For the **SPS1a** scenario $\eta_\tau^1 = -0.87$. Note that the asymmetries $\mathcal{A}_\tau^1$ and $\mathcal{A}_\ell^R$ have opposite signs. The marked difference between $\mathcal{A}_\tau^1$ and $\mathcal{A}_\ell^R$ is due to stau mixing, which allows the lightest scalar tau $\tilde{\tau}_1$ to have a large left component. For the gaugino-like **SPS1a** scenario the second lightest neutralino $\tilde{\chi}_2^0$ is wino-like, and thus has large left handed couplings to lepton-slepton pairs. Therefore, $\tilde{\chi}_2^0$ decays dominantly into τ-$\tilde{\tau}_1$ pairs, see the branching ratios for **SPS1a** in Table 3.3. For $A_\tau = \mu\tan\beta$ the stau mass matrix is diagonal, eq. (A.23). Then, the branching ratios for the decays $\tilde{\chi}_2^0 \to \ell\tilde{\ell}_R$ and $\tilde{\chi}_2^0 \to \tau\tilde{\tau}_1$ are comparable in size. However, $\mathcal{A}_\tau^1$ is still smaller than $\mathcal{A}_\ell^R$, with $\eta_\tau^1 = 0.53$, due of the larger couplings to the higgsino components to the scalar taus.

In the resonance region we find, for $\mathcal{P}_+^L = \mathcal{P}_-^L = -0.3$, $\mathcal{S}_\ell^R \simeq 1.5\sqrt{\mathcal{L}_{eff}[fb^{-1}]}$, $\ell = e, \mu$, and $\mathcal{S}_\tau^1 \simeq 4.5\sqrt{\mathcal{L}_{eff}[fb^{-1}]}$. In Fig. 3.8c we show the statistical significance, defined in eq. (D.33), for $\mathcal{A}_\ell^R,\ \ell = e, \mu$ with an effective integrated luminosity $\mathcal{L}_{eff} = 0.5fb^{-1}$.

3.2.5.4 $\tan\beta$ dependence

In Fig. 3.9a we show the asymmetry $\mathcal{A}_\ell^R,\ \ell = e, \mu$, for scenarios **N5, N10** and **N20**, for $\mathcal{P}_+^L = \mathcal{P}_-^L = -0.3$. These scenarios differ only by the value of $\tan\beta$. For increasing $\tan\beta$ the mass difference $m_H - m_A$ decreases and the widths Γ_H and Γ_A increase. This results in a larger overlap of the resonances which leads to large asymmetries in the resonant region. For $\tan\beta = 5$, with only partial overlap of the resonances, the asymmetry is further suppressed by the relative larger continuum contribution to the cross section due to the smaller Higgs-muon couplings. However, it shows an interesting energy dependence due to the different complex phases of the Breit-Wigner propagators of H and A. The maximum of the asymmetry is found at $\sqrt{s} \simeq m_H$, as already discussed for scenario **SPS1a**.

In Fig. 3.9b we show the cross sections $\sigma(\mu^+\mu^- \to \tilde{\chi}_1^0\tilde{\chi}_2^0)$ for scenarios **N5, N10**

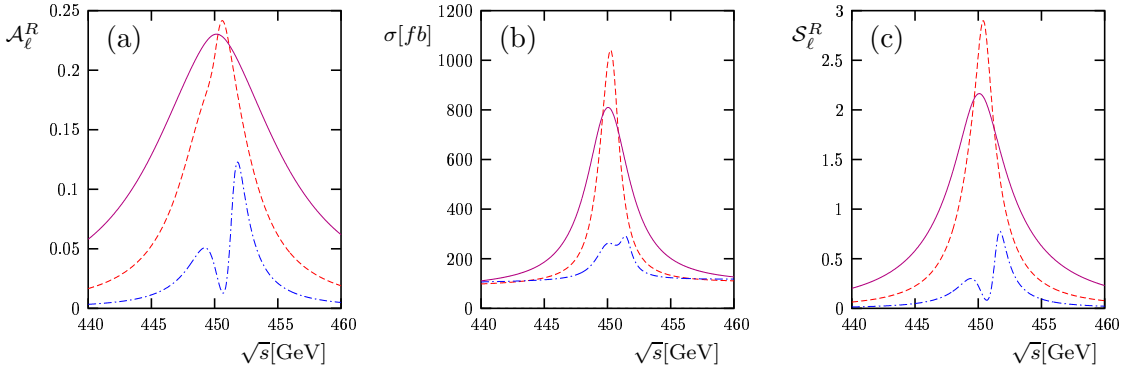

Figure 3.9: $\mu^+\mu^- \to \tilde{\chi}_1^0\tilde{\chi}_2^0$, $\tilde{\chi}_2^0 \to \ell^-\tilde{\ell}_R^+$, $\ell = e, \mu$ for scenarios **N5**, **N10** and **N20**. (a): $\mathcal{A}_\ell^R$, (b): neutralino production cross section and (c): statistical significance with luminosity times detection efficiency $\epsilon\mathcal{L} = \mathcal{L}_{eff} = 0.5fb^{-1}$ and $\mathcal{P}_+^L = \mathcal{P}_-^L = -0.3$. $\tan\beta = 5$ (dash-dotted), 10 (dashed), and 20 (solid).

and **N20**. The largest peak cross sections are found for $\tan\beta = 10$. For $\tan\beta = 5$ the resonant cross sections are suppressed by the smaller Higgs-muon couplings, while for $\tan\beta = 20$ they are suppressed by the larger resonance widths.

In the resonant region we find, for $\ell = e, \mu$, $\mathcal{S}_\ell^R \geq 3\sqrt{\mathcal{L}_{eff}[fb^{-1}]}$ for $\tan\beta = 10$ and $\tan\beta = 20$, while for $\tan\beta = 5$ the statistical significances reach $\mathcal{S}_\ell^R \simeq \sqrt{\mathcal{L}_{eff}[fb^{-1}]}$ at $\sqrt{s} \simeq m_H$. In Fig. 3.9c we show the statistical significances for an effective integrated luminosity $\mathcal{L}_{eff} = 0.5fb^{-1}$.

The effect of stau mixing on the asymmetry $\mathcal{A}_\tau^1 = \eta_\tau^1\mathcal{A}_\ell^R$, with η_τ^1 defined in eq. (C.84), increases with $\tan\beta$. It is weaker in the mixed scenarios than in the gaugino-like **SPS1a** scenario, as can also be observed comparing the neutralino branching ratios of Table 3.3. We find, for scenarios **N5, N10** and **N20**, $\eta_\tau^1 =$ 0.88, 0.49 and -0.31, respectively. The statistical significance for $\mathcal{A}_\tau^1$ is obtained from eq. (D.33), where the branching ratios of $\tilde{\chi}_2^0 \to \ell^\mp\tilde{\ell}_R^\pm$, $\ell = e, \mu$, and $\tilde{\chi}_2^0 \to \ell^\mp\tilde{\tau}_1^\pm$ are shown in Table 3.3.

For $A_\tau = \mu\tan\beta$, i.e. for a diagonal stau mass matrix with $\tilde{\tau}_1 = \tilde{\tau}_R$, we find $\eta_\tau^1 = 0.96$, 0.79 and 0.30 for scenarios **N5, N10** and **N20**, respectively.

3.2.5.5 m_A dependence

In Fig. 3.10a we compare the asymmetries $\mathcal{A}_\ell^R$, $\ell = e, \mu$, for scenarios **N5', N5** and **N5"**, with different values of m_A, as a function of $\sqrt{s} - m_A$, for $\mathcal{P}_+^L = \mathcal{P}_-^L = -0.3$. In Fig. 3.10b we show the corresponding cross section $\sigma(\mu^+\mu^- \to \tilde{\chi}_1^0\tilde{\chi}_2^0)$. For larger Higgs masses their widths increase, and thus the interference of the H and A exchange amplitudes. However, the asymmetries are reduced by the larger continuum contribution to the cross section.

For smaller Higgs masses, here for $m_A = 350$ GeV, threshold effects are stronger. Since $\eta_{12} = 1$, the asymmetries nearly vanish for $\sqrt{s} \simeq m_A$, where the largest cross sections are found, while the largest asymmetries are found at

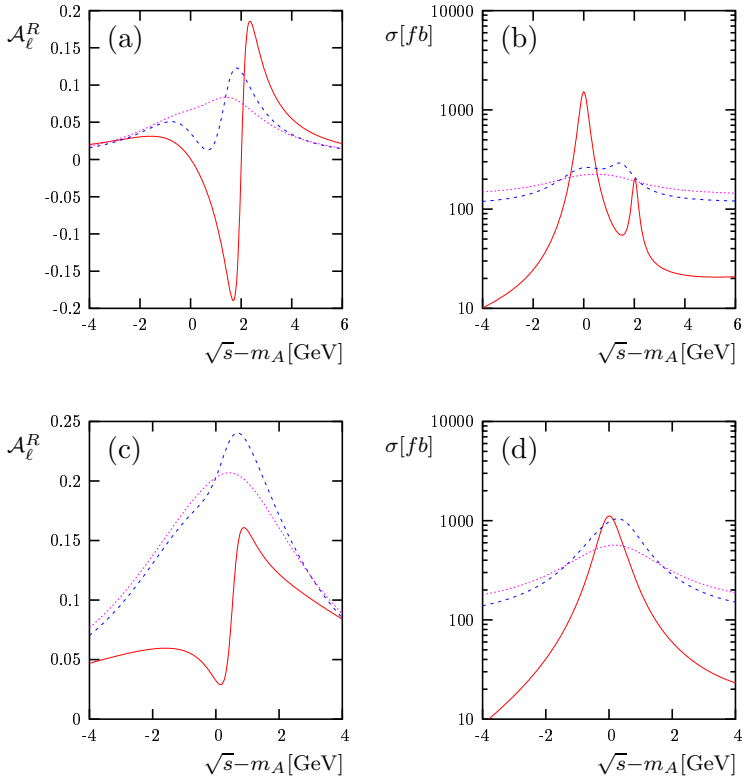

Figure 3.10: $\mu^+\mu^- \to \tilde{\chi}_1^0\tilde{\chi}_2^0$, $\tilde{\chi}_2^0 \to \ell^-\tilde{\ell}_R^+$, $\ell = e, \mu$, with $\mathcal{P}_+^L = \mathcal{P}_-^L = -0.3$, for scenarios **N5, N10** with $m_A = 450$ GeV (dashed), **N5', N10'** with $m_A = 350$ GeV (solid) and **N5", N10"** with $m_A = 550$ GeV (dotted). (a): $\mathcal{A}_\ell^R$ for $\tan\beta = 5$, (b): neutralino production cross section for $\tan\beta = 5$, (c): $\mathcal{A}_\ell^R$ for $\tan\beta = 10$, (d): neutralino production cross section for $\tan\beta = 10$.

$\sqrt{s} \approx m_H$. The asymmetries change sign between the two resonances, due to the complex phases of the propagators, and the maxima of $|\mathcal{A}_\ell^R|$ are found at center of mass energies slightly above and below m_H and not on top of the CP-even resonance. For larger values of m_A, here for $m_A = 550$ GeV, the peak cross sections are suppressed by the larger widths. To a lesser degree, they are enhanced by the larger phase space for neutralino production.

In Figs. 3.10b and 3.10d we show the analogous figures for scenarios **N10', N10** and **N10"**, with $\tan\beta = 10$. The effect of larger Higgs masses is weaker than for $\tan\beta = 5$ because the overlap of the resonances is already large for $m_A = 450$ GeV.

The statistical significances at the center of mass energies where $|\mathcal{A}_\ell^R|$ is maximal is $\mathcal{S}_\ell^R \sim 0.8\sqrt{\mathcal{L}_{eff}[fb^{-1}]}$ for scenario **N5'** and $\mathcal{S}_\ell^R \sim 1.4\sqrt{\mathcal{L}_{eff}[fb^{-1}]}$ at $\sqrt{s} \simeq m_H$ for scenario **N10'**.

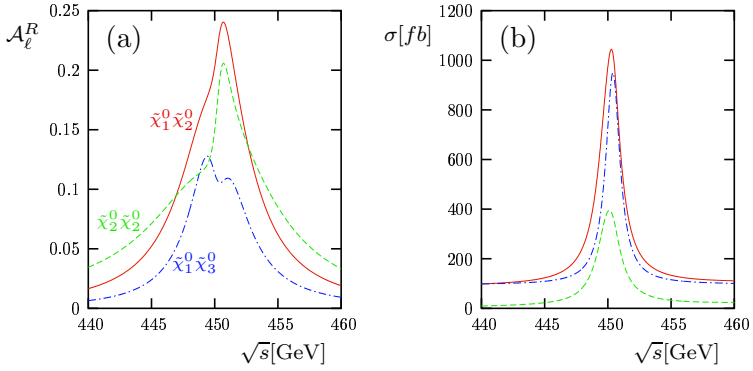

Figure 3.11: $\mu^+\mu^- \to \tilde{\chi}_i^0\tilde{\chi}_j^0$, $\tilde{\chi}_j^0 \to \ell^-\tilde{\ell}_R^+$, $\ell = e, \mu$, for scenario **N10** with $i = 1,\ j = 2$ (solid), $i = 1,\ j = 3$ (dash-dotted) and $i = 2,\ j = 2$ (dashed). (a): $\mathcal{A}_\ell^R$ and (b): neutralino production cross section, with $\mathcal{P}_+^L = \mathcal{P}_-^L = -0.3$.

3.2.5.6 $\tilde{\chi}_1^0\tilde{\chi}_2^0, \tilde{\chi}_2^0\tilde{\chi}_2^0$ and $\tilde{\chi}_1^0\tilde{\chi}_3^0$ production

In Fig. 3.11 we show, for scenario **N10**, the asymmetry $\mathcal{A}_\ell^R, \ell = e, \mu$, and the cross sections $\sigma(\mu^+\mu^- \to \tilde{\chi}_i^0\tilde{\chi}_j^0)$ for the kinematically allowed pairs $\tilde{\chi}_1^0\tilde{\chi}_2^0$, $\tilde{\chi}_1^0\tilde{\chi}_3^0$ and $\tilde{\chi}_2^0\tilde{\chi}_2^0$, for $\mathcal{P}_+^L = \mathcal{P}_-^L = -0.3$. Threshold effects are stronger in $\tilde{\chi}_2^0\tilde{\chi}_2^0$ and $\tilde{\chi}_1^0\tilde{\chi}_3^0$ production than in $\tilde{\chi}_1^0\tilde{\chi}_2^0$ production. Therefore the P-wave suppression of the CP-even (CP-odd) amplitude for $\tilde{\chi}_2^0\tilde{\chi}_2^0$, ($\tilde{\chi}_1^0\tilde{\chi}_3^0$) production is stronger, since $\eta_{22} = 1$ ($\eta_{13} = -1$). The asymmetries for $\tilde{\chi}_1^0\tilde{\chi}_2^0$ and $\tilde{\chi}_2^0\tilde{\chi}_2^0$ production, however, are comparable in size, since the continuum contribution to $\tilde{\chi}_2^0\tilde{\chi}_2^0$ production is very small. For $\tilde{\chi}_1^0\tilde{\chi}_3^0$ production, the asymmetry is smaller due to the interplay of the widths and the amplitudes, with $\Gamma_H < \Gamma_A$ and A exchange suppressed, which results in a smaller interference of the two amplitudes. Note also the different energy dependence of the asymmetry, with maxima at $\sqrt{s} < m_A$ and $\sqrt{s} > m_H$, and of the cross section, with a maximum at $\sqrt{s} \simeq m_H$.

For the asymmetry in $\tilde{\chi}_2^0\tilde{\chi}_2^0$ production the statistical significance for $\ell = e, \mu$ in the resonance region is $\mathcal{S}_\ell^R \simeq 2\sqrt{\mathcal{L}_{eff}[fb^{-1}]}$. For $\tilde{\chi}_1^0\tilde{\chi}_3^0$, the statistical significance for $\ell = e, \mu$ is significantly smaller, of order $\mathcal{S}_\ell^R \simeq 0.6\sqrt{\mathcal{L}_{eff}[fb^{-1}]}$ in the resonance region, because the branching ratios of $\tilde{\chi}_3^0$ into lepton and slepton pairs are strongly suppressed by the competing decay channels $\tilde{\chi}_3^0 \to Z\tilde{\chi}_1^0$ and $\tilde{\chi}_3^0 \to h\tilde{\chi}_1^0$, with $BR(\tilde{\chi}_3^0 \to \ell\tilde{\ell}_R) = 1\%$ for $\ell = e, \mu$, and $BR(\tilde{\chi}_3^0 \to \tau\tilde{\tau}_1) \simeq 5\%$.

3.2.5.7 $\mu - M_2$ plane

The MSSM parameters μ and M_2 affect strongly the neutralino couplings both to the Higgs bosons as to the lepton-slepton pairs. The lepton energy asymmetries for neutralino decays into leptons of the first two families, e and μ, do not depend on the couplings, while the dependence of stau mixing on the neutralino character has been briefly discussed in Section 3.2.5.4. The neutralino couplings to H and A are both enhanced in mixed scenarios since Higgs bosons couple to a higgsino-

gaugino pair. Therefore, the Higgs boson widths, and thus the interference of the resonances, are also enhanced. In figs 3.12a and 3.12b we show contours in the $\mu - M_2$ plane of constant $\gamma_{12}q_{12}$ and $\mathrm{Im}(d_{ij}^{(H)}d_{ij}^{(A)*})$, respectively, for $\tan\beta = 10$ and $m_A = 450$ GeV (see Section 3.2.4 for the notation on the couplings). Note that γ_{12} is negative in most of the experimentally allowed parameter space. Therefore the sign of the asymmetries for the first two lepton families constitutes a test of the Higgs-neutralino couplings in the MSSM.

The same qualitative dependence of $\gamma_{12}q_{12}$ and κ_{12} on μ and M_2 is found for different values of $\tan\beta$ and m_A.

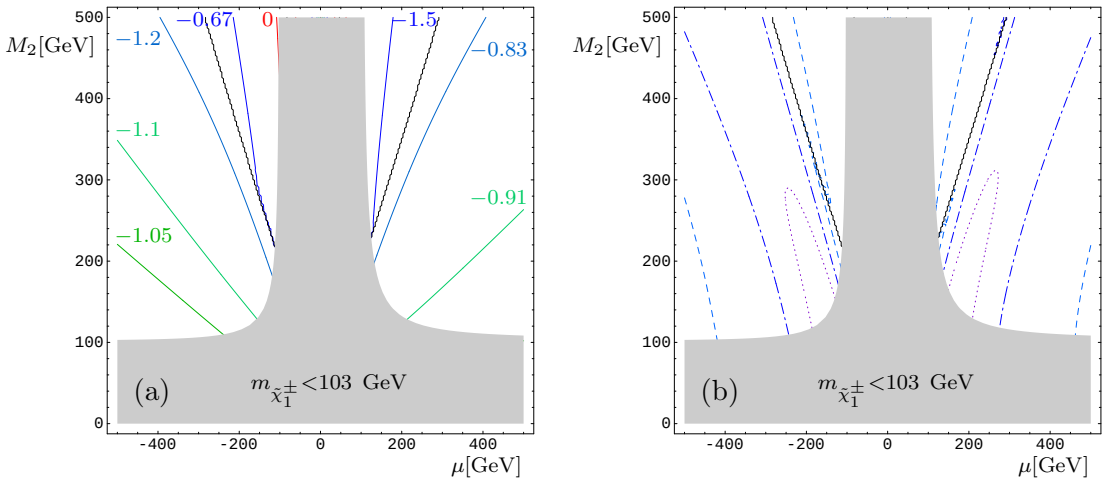

Figure 3.12: Contours of constant $\gamma_{12}q_{12}$ (a) and $\mathrm{Im}(d_{12}^{(H)}d_{12}^{(A)*})$ (b), for $\tan\beta = 10$ and $m_A = 450$ GeV. In (b) the contour lines correspond to $\mathrm{Im}(d_{12}^{(H)}d_{12}^{(A)*}) = 0.01$ (dashed), 0.03 (dash-dotted) and 0.05 (dotted). The wiggly lines in both figures indicate the level crossing of the $\tilde{\chi}_2^0$ and $\tilde{\chi}_3^0$ states, with $\eta_{12} = 1$ in the area below and $\eta_{12} = -1$ in the area above the level crossing line. The gray area is experimentally excluded by $m_{\chi_1^\pm} < 103$ GeV.

3.2.6 Summary of Section 3.2

We have discussed the interference of the CP-even and CP-odd amplitudes of the neutral Higgs boson s-channel exchange in $\mu^+\mu^- \to \tilde{\chi}_i^0\tilde{\chi}_j^0$ with longitudinally polarized beams in the CP conserving MSSM. To study this interference we use the energy distribution of the lepton from the decay $\tilde{\chi}_j^0 \to \ell^\pm\tilde{\ell}_{L,R}^\mp$, $\ell = e, \mu, \tau$. The asymmetry of the lepton energy distributions is correlated to the longitudinal neutralino polarization, averaged over the production angles. Since the average neutralino longitudinal polarization can only be non-vanishing for scalar and pseudoscalar Higgs exchange interference terms, this asymmetry can be used

to determine the product of the couplings of the H and A bosons to the neutralinos and those to the muons. In particular, the sign of the asymmetry is sensitive to the sign of the product of couplings of neutralinos and muons. For a set of scenarios we have analyzed the lepton energy asymmetries for $\tilde{\chi}^0_i\tilde{\chi}^0_j$ production with subsequent two-body decay, with emphasis on $\tilde{\chi}^0_1\tilde{\chi}^0_2$ production. We find large asymmetries for nearly degenerate heavy neutral Higgs bosons and intermediate values of $\tan\beta$ and m_A. Especially for $\tilde{\chi}^0_1\tilde{\chi}^0_2$ we find statistical significances which would allow one to measure the asymmetries at a muon collider.

3.3 Production of neutralino pairs with subsequent decay of both neutralinos

We can further probe the Higgs-neutralino interaction with the correlation of the polarizations of both neutralinos in the process $\mu^+\mu^- \to \tilde{\chi}^0_i\tilde{\chi}^0_j$. Therefore we study their subsequent two-body decays. We build asymmetries of the energy and angular distributions of the final particles and discuss their dependence on the Higgs-neutralino couplings.

In the preceding section we discussed the spin correlation between production and decay in the production process eq. (3.1). We found that two-body decays in which parity is not conserved can be used to probe the neutralino polarizations. The spin-spin correlation terms of the neutralinos are described by the last term of the spin density matrix, eq. (C.25), which we subdivide the expansion coefficients of the neutralino production density matrix into contributions from the Higgs resonances $\Sigma^{ab}_{r_j}$ and the continuum $\Sigma^{ab}_{cont_j}$, eq. (3.3), as discussed in Section 3.1. The resonant contributions are further separated into pure Higgs exchange and interference terms

$$\Sigma^{ab}_r = \sum_{\phi=H,A} \Sigma^{ab\,(\phi\phi)}_r + \Sigma^{ab\,(HA)}_r, \qquad a,b = 1,\ldots,3. \tag{3.48}$$

Due to the Majorana character of the neutralinos only absorptive term contribute to the H-A interference contributions. Evaluating the spin density matrix in the CMS and using the notation of Section 3.1, the pure Higgs exchange terms are given by

$$\begin{aligned}\Sigma^{ab\,(\phi\phi)}_r &= f^{(a,\phi)}_{ij}\delta_{ab}\,\frac{g^4}{4}(1+\mathcal{P}^L_+\mathcal{P}^L_-)|\Delta(\phi)|^2|c^{(\phi\mu)}|^2|d^{(\phi)}_{ij}|^2 \\ &\quad s[s-(m_{\chi^0_i}+\eta^\phi_{ij}m_{\chi^0_j})^2],\end{aligned} \tag{3.49}$$

$$\begin{aligned}\Sigma^{ab\,(HA)}_r &= \frac{g^4}{2}(\mathcal{P}^L_+ + \mathcal{P}^L_-)\mathrm{Im}\{\Delta(H)\Delta(A)^*\}\mathrm{Im}\{c^{(H\mu)}c^{(A\mu)^*}\} \\ &\quad \mathrm{Im}\{d^{(H)}_{ij}d^{(A)}_{ij}\}\sqrt{\lambda_{ij}}\,s\,(\delta_{a1}\delta_{b2}+\delta_{a2}\delta_{b1}),\end{aligned} \tag{3.50}$$

where $f_{ij}^{(a,\phi)}$ is defined in eq. (3.6) and

$$f_{ij}^{(1,\phi)} = -\eta_{ij}^{\phi}, \qquad f_{ij}^{(2,\phi)} = \eta_{ij}^{\phi}, \qquad f_{ij}^{(3,\phi)} = 1. \tag{3.51}$$

Comparing eq. (3.49) with the coefficient of the production spin density matrix $P_r^{(\phi\phi)}$, eq. (3.5), we obtain

$$\Sigma_r^{ab\,(\phi\phi)} \;=\; \delta_{ab} f_{ij}^{(a,\phi)} P_r^{(\phi\phi)}. \tag{3.52}$$

The relation for longitudinal neutralino polarizations, $\Sigma_r^{33\,(\phi\phi)} = P_r^{(\phi\phi)}$, follows from angular momentum conservation for a pair of fermions produced in scalar s-channel exchange, and is equivalent to the analogous relation for spin-spin correlations in chargino production, eq. (2.79).

More interesting are the transverse polarizations of the neutralinos. As discussed in Section 2.5 for the chargino spin-spin correlations, there is no preferred direction in a process that proceeds via s-channel scalar exchange and the sign between $\Sigma_r^{11\,(\phi\phi)}$ and $\Sigma_r^{22\,(\phi\phi)}$ is only due to our choice of the spin vectors, eqs. (C.18) and (C.21).

From the relation between the coefficient for unpolarized neutralino production P_r and the spin-spin terms, eq. (3.52), results

$$P_r^{(HH)} \;=\; \frac{1}{2}(P_r - \eta_{ij}^H \Sigma_r^{11}), \tag{3.53}$$

$$P_r^{(AA)} \;=\; \frac{1}{2}(P_r - \eta_{ij}^A \Sigma_r^{11}), \tag{3.54}$$

with $\eta_{ij}^H = -\eta_{ij}^A = \eta_i \eta_j$.

As in Section 2.5 for equal charginos we generalize eqs. (3.53) and (3.54) for the case of not necessarily CP conserving couplings and separate the CP-even and CP-odd contributions to the spin density matrix coefficient P_r

$$P_r^{(CP+)} \;=\; \frac{1}{2}(P_r - \eta_i \eta_j \Sigma_r^{11}), \tag{3.55}$$

$$P_r^{(CP-)} \;=\; \frac{1}{2}(P_r + \eta_i \eta_j \Sigma_r^{11}), \tag{3.56}$$

which applies both to the case of interfering resonances with different CP quantum numbers as well as to a single resonance.

In order to determine the spin-spin correlation terms we study the leptonic two-body decays of both neutralinos, eq. (3.2). In analogy to Section 2.5.2 for chargino production with subsequent decay of both charginos, we study, for the process $\mu^+\mu^- \to \tilde{\chi}_i^0 \tilde{\chi}_j^0$ with subsequent decays $\tilde{\chi}_i^0 \to \ell^\pm \tilde{\ell}^\mp$ and $\tilde{\chi}_j^0 \to \ell'^\pm \tilde{\ell}'^\mp$, the dependence of the differential cross section on the azimuth angles φ_i and φ_j of the final leptons $\ell^\pm$ and $\ell'^\pm$. The azimuth angles are defined with respect to the direction of $\tilde{\chi}_j^0$, in the reference frame R_{χ_j} given in Section C.1.4. Note that the charges of the leptons $\ell^\pm$ and $\ell'^\pm$ are not necessary equal.

As in Section 2.5.2 we express the differential cross section for $\tilde{\chi}_i^0\tilde{\chi}_j^0$ production and decay

$$\frac{d^2\sigma_{\ell,\ell'}}{d\varphi_i d\varphi_j} = \frac{\sigma_{\ell,\ell'}}{4\pi^2}[1 + K^{11}\cos(\varphi_i - \varphi_j) + K^{12}\sin(\varphi_i - \varphi_j)], \tag{3.57}$$

where $\sigma_{\ell,\ell'}$ is the cross section for neutralino production and subsequent two-body decays with ℓ and ℓ' in the final state. Further,

$$K^{11} = -\eta_{\ell\pm}\eta_{\ell'\pm}K_\ell K_{\ell'}\frac{\bar{\Sigma}_r^{11}}{\bar{P}}, \tag{3.58}$$

$$K^{12} = -\eta_{\ell\pm}\eta_{\ell'\pm}K_\ell K_{\ell'}\frac{\bar{\Sigma}_r^{12}}{\bar{P}}. \tag{3.59}$$

where the averages over the neutralino production angles $\bar{P}$ and $\bar{\Sigma}_P^{ab}$ are defined in analogy to eqs. (2.92) and (2.94), and the coefficients K_ℓ and $K_{\ell'}$ result from the integration over the polar angles of the decay particles ℓ and ℓ', respectively. Since we assume that leptons are light enough so that the relation $m_\ell < \bar{m}_\ell$, is fulfilled, with $\bar{m}_\ell = (m^2_{\chi_j^0} - m^2_\ell - m^2_{\tilde{\ell}_\ell})/2E_{\chi_j^0}$,

$$K_\ell = K_{\ell'} = \frac{\pi}{4}. \tag{3.60}$$

We define the angular distribution asymmetry in the azimuth angles φ_i and φ_j of the decay particles $\ell^\pm$ and $\ell'^\pm$ in the laboratory reference system

$$\mathcal{A}^{T\parallel} = \frac{\sigma(\cos(\varphi_i - \varphi_j) > 0) - \sigma(\cos(\varphi_i - \varphi_j) < 0)}{\sigma(\cos(\varphi_i - \varphi_j) > 0) + \sigma(\cos(\varphi_i - \varphi_j) < 0)} = -\frac{2}{\pi}\eta_{\ell\pm}\eta_{\ell'\pm}K_\ell K_{\ell'}\frac{\bar{\Sigma}^{11}}{\bar{P}}, \tag{3.61}$$

where $\eta_{\ell^\pm}$ and $\eta_{\ell^\pm}$ are the decay factors defined in eq. (3.25). Note that the asymmetry only depends on the absolute value of the difference of azimuth angles and is thus independent of the production plane, as expected from resonant scalar exchange channels. With the cosine theorem relation we obtain $\cos(\varphi_i - \varphi_j)$ from the angle $\theta_{\ell,\ell'}$ between $\ell^\pm$ and $\ell'^\pm$, and from the polar angles θ_i and θ_j, which in turn are obtained from the energies of $\ell^\pm$ and $\ell'^\pm$.

3.3.1 Summary of Section 3.3

In this section we analyzed the spin-spin correlation terms in neutralino pair production in $\mu^+\mu^-$-annihilation with longitudinally polarized beams. We have shown that the correlation of the transverse neutralino polarizations can be studied with the azimuth angular distribution of the decay leptons. We have defined the asymmetry $\mathcal{A}^{T\parallel}$ in this angular distribution which can be used to determine the CP quantum number of the Higgs boson. For overlapping resonances with opposite CP quantum numbers the asymmetry is ideal to separate their contributions. Here we have restricted the analysis to the CP conserving case.

3.4 Production and decay with transverse beam polarization

Here we briefly discuss the effect of transverse polarization on pair production and decay of neutralinos in $\mu^+\mu^-$ annihilation at the neutral Higgs resonances H and A.

The dependence of the neutralino production process on transverse polarization introduces new possibilities to probe the Higgs-neutralino interactions. Specifically, for completely polarized beams, transverse polarization would allow to create states with any CP phase. The CP-even (CP-odd) state would then be obtained for parallel (anti-parallel) μ^+ and μ^- polarizations.

The transverse polarization dependent terms for the Higgs exchange channels, on the other hand, are proportional to $|\vec{\mathcal{P}}_+^T||\vec{\mathcal{P}}_-^T|$, with the transverse polarization vectors defined by

$$\vec{\mathcal{P}}_\pm^T = (\mathcal{P}_\pm^1, \mathcal{P}_\pm^2, 0) \tag{3.62}$$

in the reference frame defined in Section C.1.3, with the x-axis on the production plane.

As expected for resonant scalar exchange channels, these contributions only depend on the relative orientation of $\vec{\mathcal{P}}_+^T$ and $\vec{\mathcal{P}}_-^T$. This implies that, rotating both $\vec{\mathcal{P}}_+^T$ and $\vec{\mathcal{P}}_-^T$ has no effect on the resonant channels.

Unlike for longitudinally polarized beams, for transverse polarization the interference of the Higgs and non-Higgs exchange channels is not suppressed by approximate chirality conservation. These interference effects are linear in $\mathcal{P}_+^a$ and $\mathcal{P}_-^a$, $a = 1, 2$, Therefore, they depend on the production plane, and may thus be either eliminated or isolated using their dependence on the azimuth angle in the laboratory reference frame φ_{Lab}, see Section D.1.1.

The non-Higgs contributions from Z boson s-channel and scalar muon t- and u-channel exchange are proportional to $|\vec{\mathcal{P}}_+^T||\vec{\mathcal{P}}_-^T|$ [39]. As for the interference term, the dependence on the production azimuth angle φ_{Lab} can be used to separate these terms.

Denoting $\rho^{P,T}$ the transverse polarization dependent part of the production spin density matrix ρ^P, we separate the resonant, continuum and interference contributions $\rho_r^{P,T}$, $\rho_{cont}^{P,T}$ and $\rho_{int}^{P,T}$, respectively. From the dependence on the

azimuth production angle we obtain

$$\rho^{P,T}_{cont}(\varphi_{Lab}) = \frac{1}{4}\sum_{n=0}^{3}(-1)^n\rho^{P,T}(\varphi_{Lab}+n\pi/2), \tag{3.63}$$

$$\rho^{P,T}_{int}(\varphi_{Lab}) = \frac{1}{2}\left[\rho^{P,T}(\varphi_{Lab})-\rho^{P,T}_{int}(\varphi_{Lab}+\pi)\right], \tag{3.64}$$

$$\rho^{P,T}_{r}(\varphi_{Lab}) = \frac{1}{4}\sum_{n=0}^{3}\rho^{P,T}(\varphi_{Lab}+n\pi/2). \tag{3.65}$$

3.4.1 Neutralino production

The neutralino polarization independent coefficient P_r of the production spin density matrix, for longitudinally *and* transversely polarized beams, is obtained from eq. (3.5) with the new dependence on the beam polarization

$$P_r^{(\phi\phi)} = (2-\delta_{ij})\frac{g^4}{8}\ell'^{(\phi\phi)}|\Delta(\phi)|^2|c^{(\phi\mu)}|^2|d^{(\phi)}_{ij}|^2 s[s-(m_{\chi^0_i}+\eta^{\phi}_{ij}m_{\chi^0_j})^2], \tag{3.66}$$

with

$$\ell'^{(\phi\phi)} = \left(1+\mathcal{P}^L_+\mathcal{P}^L_- + \eta_\phi(\vec{\mathcal{P}}^T_+\cdot\vec{\mathcal{P}}^T_-)\right), \tag{3.67}$$

where η_ϕ is the CP quantum number of the exchanged Higgs boson and η^{ϕ}_{ij} is defined in eq. (3.6). The dependence of $P_r^{(\phi\phi)}$ on the beam transverse polarization is thus similar to the polarization dependence on the final neutralinos, discussed in the preceding section. It is then possible, for parallel and anti-parallel beam polarizations, to enhance the CP-even and CP-odd amplitudes, respectively. This is a powerful tool discussed in [34]. The only drawback is that, for realistic values of beam polarizations of $\mathcal{O}(30\%)$, the quadratic dependence on $|\vec{P}^T_+||\vec{\mathcal{P}}^T_-|$ results in effects of $\mathcal{O}(10\%)$. Therefore large beam polarizations are required in order to perform a precise determination of the CP properties of the scalar resonances.

The production spin density matrix for general CP violating couplings is given in Appendix C.4.2. The polarization dependent coefficient

$$\begin{aligned}\ell'^{(\alpha\beta)} &= (1+\mathcal{P}^L_+\mathcal{P}^L_-)\cos(\xi_\alpha-\xi_\beta) + \mathcal{P}^T_+\mathcal{P}^T_-\cos(\xi_\alpha+\xi_\beta-\zeta_+-\zeta_-)\\ &+ i(\mathcal{P}^L_+ + \mathcal{P}^L_-)\sin(\xi_\alpha-\xi_\beta)\end{aligned} \tag{C.75}$$

is a function of the angles ζ_+ and ζ_+ which parametrize the direction of the transverse polarization vectors $\vec{\mathcal{P}}^T_+$ and $\vec{\mathcal{P}}^T_-$ in the laboratory reference frame and on the CP phases ξ_α and ξ_β of the muon couplings to the Higgs bosons α and β, defined in eq. (B.17).

Note that, since the function ℓ' depends on the difference $\zeta_+-\zeta_+$, it is independent of a specific choice of reference frame. From eq. (C.75) follows that

a measurement of the production cross section with longitudinal and transverse polarizations allows to measure the phases ξ_α and ξ_β, and thus the CP quantum number of a single Higgs resonance. However, in order to distinguish the interference of scalar and pseudoscalar resonances from a single resonance with CP violating couplings to the muons we need to consider the subsequent decays of the neutralinos.

3.4.2 Production with subsequent decay of one neutralino

For transversely polarized beams, the spin-correlation term of the production spin density matrix has an additional absorptive term. Therefore, the pure Higgs exchange contributions still vanish, as with longitudinal polarization only. We obtain for $\mu^+\mu^- \to \tilde{\chi}^0_i\tilde{\chi}^0_j$

$$\begin{aligned}\Sigma_{rj}^{3\,(HA)} &= \frac{g^4}{2}|d_{ij}^{(H)}||d_{ij}^{(A)}||c^{(H\mu)}||c^{(A\mu)}|s\sqrt{\lambda_{ij}}\eta_j \\ &\quad \Big[-(\mathcal{P}_+^L+\mathcal{P}_-^L)\mathrm{Re}\{\Delta(H)\Delta(A)^*\}+\hat{n}_+\cdot(\vec{\mathcal{P}}_+^T\times\vec{\mathcal{P}}_-^T)\mathrm{Im}\{\Delta(H)\Delta(A)^*\}\Big]\,,\end{aligned} \tag{3.68}$$

with $\hat{n}_+ = \vec{p}_{\mu^+}/|\vec{p}_{\mu^+}|$.

We conclude that here longitudinal polarization is more convenient to analyze the H-A interference, since its contribution is to the polarization of the neutralinos is larger.

3.4.3 Production with subsequent decay of both neutralinos

The spin-spin correlations for pure Higgs exchange are obtained from eq. (3.49) substituting the polarization term $(1+\mathcal{P}_+^L\mathcal{P}_-^L)$ with the function ℓ', eq. (3.67), as for the coefficient P_r. The coefficients P_r and Σ_r^{ab} must have the same dependence on the polarizations since they are related by eq. (3.52). It is now possible to separate the CP-even and CP-odd amplitudes either analyzing the transverse polarizations of the beams or those of the neutralinos.

For the contribution to the spin-spin correlations from H-A interference we find an additional non-absorptive term,

$$\begin{aligned}\Sigma_r^{ab\,(HA)} &= \frac{g^4}{2}|c^{(H\mu)}||c^{(A\mu)}||d_{ij}^{(H)}||d_{ij}^{(A)}|\sqrt{\lambda_{ij}}\,s\,(\delta_{a1}\delta_{b2}+\delta_{a2}\delta_{b1}) \\ &\quad \Big[\mathrm{Im}\{\Delta(H)\Delta(A)^*\}(\mathcal{P}_+^L+\mathcal{P}_-^L)+\mathrm{Re}\{\Delta(H)\Delta(A)^*\}\,\hat{n}_+\cdot(\vec{\mathcal{P}}_+^T\times\vec{\mathcal{P}}_-^T)\Big]\,.\end{aligned} \tag{3.69}$$

This term gains relevance when the resonances are completely degenerate and thus the absorptive term vanishes.

3.4.4 Summary of Section 3.4

We have analyzed the effect of transverse beam polarization on the neutralino production spin density matrix in order to identify interesting new observables. We found a strong similarity between transverse beam and neutralino polarization effects. Both tuning the transverse beam polarization in neutralino production as well as studying the angular distributions of the decays of both neutralinos we can separate the CP-even and odd contributions, and thus determine the CP properties of the resonance region. While beam polarization is a very interesting tool, at a muon collider polarization it will be difficult to achieve large degrees of polarization. Of less interest are the effects of transverse beam polarization on the polarizations of neutralinos. For the spin correlation terms between production and decay, transverse polarization adds a new absorptive contribution to the longitudinal neutralino polarization which, however, is expected to be small. For the spin-spin correlation terms, transverse beam polarization adds a new non-absorptive contribution to the H-A interference term.

Chapter 4

Summary and Conclusions

4.1 Summary

The mechanism of spontaneous symmetry breaking is essential to provide masses to the $W^{\pm}$ and Z gauge bosons and fermions of the SM. We hope to elucidate this mechanism at the next generation of colliders. While the SM has been tested with astonishing precision it is believed to be an effective theory of a more fundamental Great Unified Theory. SUSY is one of the most attractive extensions of the SM of particle physics. Therefore, the search for SUSY is a top priority at the next generation of colliders.

Once Higgs bosons are discovered, a precise determination of their properties is necessary to differentiate between different models, in particular the MSSM. A muon collider, running at center of mass energies around the neutral Higgs boson resonances, would allow precise measurements of masses and widths, as well as the couplings to their decay products. In particular their couplings to supersymmetric particles are essential to probe SUSY. Therefore, we study the decays of the heavier CP-even and CP-odd Higgs bosons into lighter chargino or neutralino pairs.

In this thesis we have analyzed the polarization effects of the beams and the charginos and neutralinos produced in $\mu^+\mu^-$ annihilation around the center of mass energies of the Higgs boson resonances H and A.

For the chargino pair production, $\mu^+\mu^- \to \tilde{\chi}_i^{\mp}\tilde{\chi}_j^{\pm}$, we can summarize as follows:

- For the production of equal charginos we have shown that the ratio of H-chargino and A-chargino couplings can be precisely determined independently of the chargino decay mechanism. This method avoids reference to other experiments and makes only a few model-dependent assumptions. In the numerical analysis we have shown that, for small $\tan\beta$, the process yields large cross sections of up to a pb. Finally we have analyzed the effect of the energy spread and of the error from the non-resonant channels,

including an irreducible standard model background contribution.

- For the production of two different charginos we have shown that the H-A interference can be analyzed using asymmetries of the $\tilde{\chi}_1^+\tilde{\chi}_2^-$ cross section and its charge conjugate. The asymmetries depend on the muon beam polarizations and vanish for unpolarized beams.

- For the chargino pair production with subsequent two-body decay of one of the charginos, $\tilde{\chi}_j^\pm \to \ell^\pm\tilde{\nu}$, for $\ell = e, \mu, \tau$, and $\tilde{\chi}_j^\pm \to W^\pm\tilde{\chi}_k^0$, we have shown that charge and polarization asymmetries in the energy distributions of the decay particles are sensitive to the interference of scalar exchange channels with different CP quantum numbers. These asymmetries depend on the longitudinal beam polarizations. In the numerical analysis we have shown that the asymmetries can be measured with enough statistical significance. The effect is larger for regions of parameter space with intermediate values of $\tan\beta$ and light sleptons or LSP. This process provides unique information on the interference of overlapping Higgs boson resonances.

- For the chargino pair production with subsequent two-body decays of both charginos we have defined energy distribution and angular asymmetries in the final particles, in order to analyze the spin-spin correlations of the charginos. The transverse polarizations of the charginos are sensitive to the CP quantum number of the exchanged Higgs bosons and can thus be used to separate overlapping resonances, as well as to determine the CP quantum number of a single resonance. For equal charginos, these asymmetries are not sensitive to the interference of CP-even and CP-odd Higgs exchange channels. It is here not possible to distinguish between two overlapping CP conserving scalar resonances with different CP quantum numbers and a single CP violating one.

For the neutralino pair production, $\mu^+\mu^- \to \tilde{\chi}_i^0\tilde{\chi}_j^0$, we can summarize as follows:

- Line shape measurements of neutralino pair production allow to precisely determine the ratio of H-neutralino and A-neutralino couplings independently of the decay mechanism of the neutralinos, in analogy to the analysis of the production of equal charginos. In the numerical analysis we briefly analyze the dependence on the production cross sections for neutralino pairs on the MSSM parameter space.

- For neutralino pair production with subsequent two-body decay of one of the neutralinos, $\tilde{\chi}_j^0 \to \ell^\pm\tilde{\ell}_{R,L}^\mp$, for $\ell = e, \mu, \tau$, we have shown that the asymmetry in the energy distribution of the decay lepton is sensitive to the interference of H and A when they are nearly degenerate. In the numerical

analysis we have shown that the asymmetries are large and can be measured with enough statistical significance for a set of representative scenarios with intermediate $\tan\beta$.

- For neutralino pair production with subsequent two-body decays of both neutralinos we analyze the energy and angular distributions of the decay particles. This dependence of the neutralino spin-spin correlations on the Higgs-neutralino interaction is similar to that of charginos, with the difference that the intrinsic relative CP quantum number of the neutralinos which depends on the scenario and on the neutralino pair.

- Finally we analyzed the effect of transverse beam polarization on neutralino production. Similarly as for the spin-spin correlations, we can separate the CP even and odd Higgs exchange contributions using their dependence on the correlations of transverse beam polarizations. We also analyze the effects on the neutralino polarizations and on the spin-spin correlations.

4.2 Conclusions

We have shown that the interaction of the Higgs bosons to the gaugino-higgsino sector can be probed at a muon collider in chargino and neutralino pair production. When the resonance contributions can be separated in the production line shape the ratio of couplings of H and A to the charginos and neutralinos can be determined with precisions of down to the $\mathcal{O}(\%)$. Especially interesting are here scenarios with $\tan\beta \approx 5$, for which the H and A may decay mainly into charginos and neutralinos and their production cross sections are up to a pb.

Alternatively, beam polarization correlations provide a very elegant tool to separate the resonances. However, large polarizations are needed, obtained at a cost of luminosity, since this effects are proportional to the product of beam polarizations. The correlations of the transverse polarizations of the charginos or neutralinos can be analyzed when both subsequent two-body decays are observed. For charginos and neutralinos, the leptonic decays, if kinematically allowed, are optimal probes of their polarization.

We find large correlations between the beam and the chargino or neutralino polarizations, shown to be sensitive to the interference of H and A. Assuming longitudinal polarizations of 30% we obtain charge and polarization asymmetries larger than 20% when the overlap of the resonances is large. Here, scenarios with $\tan\beta \approx 10$, with nearly degenerate heavier Higgs bosons and large branching ratios into charginos and neutralinos, are the best case scenario. For these scenarios we obtain statistical significances in the range $1 - 5$ for integrated luminosities $\mathcal{L} = 1$ fb^{-1}.

Chapter 5

Zusammenfassung und Schlussfolgerungen

Der Mechanismus der spontanen Symmetriebrechung ist notwendig, um den W- und Z-Eichbosonen sowie den Fermionen des Standardmodels Masse geben zu können. Wir hoffen, diesen Mechanismus in der nächsten Generation von Teilchenbeschleunigern nachweisen zu können. Obwohl die Vorhersagen des Standardmodels (SM) bisher mit sehr großer Präzision bestätigt werden konnten, glaubt man, dass es sich um einen effektiven Niederenergielimes einer fundamentaleren Großvereinheitlichten Theorie handelt. Supersymmetrie (SUSY) ist eine der attraktivsten Erweiterungen des Standardmodels der Teilchenphysik. Deswegen ist die Suche nach SUSY eine der Prioritäten der nächsten Generation von Beschleunigern.

Werden Higgs-Bosonen entdeckt, ist eine präzise Bestimmung ihrer Eigenschaften nötig. Ein Myonenbeschleuniger mit einer Schwerpunktsenergie in der Nähe der Resonanzen der neutralen Higgs-Bosonen würde eine ideale ,,Higgs-Fabrik" darstellen, die genaue Messungen der Massen und Breiten sowie der Kopplungen und Zerfallsprodukte der Higgsbosonen erlauben würde. Insbesondere deren Kopplungen an SUSY-Teilchen ist wichtig, um das in der Natur realisierte SUSY-Szenario zu ermitteln. Deswegen haben wir die Zerfälle der schwereren CP-geraden und CP-ungeraden Higgs-Bosonen in leichtere Chargino- oder Neutralino-Paare studiert.

In dieser Arbeit wurden der Einfluss der Strahlpolarisation der Myonen sowie die Polarisation der erzeugten Charginos und Neutralinos untersucht.

Für die Produktion $\mu^+\mu^- \to \tilde{\chi}_i^\mp \tilde{\chi}_j^\pm$ können wir folgendermaßen zusammenfassen:

- Für die Produktion gleicher Charginos wurde gezeigt, dass das Verhältnis der H-Chargino-und der A-Chargino Kopplungen unabhängig vom Chargino Zerfallsmechanismus mit hoher Präzision bestimmt werden kann. Diese Methode vermeidet Anleihen bei anderen Experimenten und macht nur wenige modelabhängige Annahmen. In der numerischen Auswertung haben wir gezeigt, dass für kleine Werte von $\tan\beta$ der Prozess große Wirkungsquerschnitte von bis zu einem pb erzielt. Zuletzt haben wir den Effekt der Energieverteilung der Myonenstrahlen und des Fehlers aus den nichtresonanten Kanäle, mit Berücksichtigung des irreduziblen Standardmodel-Hintergrundbeitrags, untersucht.

- Für die Produktion von zwei unterschiedlichen Charginos wurde gezeigt, dass die H-A-Interferenz mit der Asymmetrie der Wirkungsquerschnitte für $\mu^+\mu^- \to \tilde{\chi}_1^+ \tilde{\chi}_2^-$ und dessen ladungskonjugierten Prozess analysiert werden kann.

- Für Chargino-Paarproduktion mit anschließendem Zweikörperzerfall eines der Charginos, $\tilde{\chi}_j^\pm \to \ell^\pm \tilde{\nu}$, für $\ell = e, \mu, \tau$, und $\tilde{\chi}_j^\pm \to W^\pm \tilde{\chi}_k^0$, haben wir gezeigt, dass die Ladungs-und Polarisationsasymmetrien den Energieverteilungen der Zerfallsprodukte auf die Interferenz der skalaren Austausch-Kanäle mit unterschiedlichen CP-Quantenzahlen sensitiv sind. Diese Asymmetrien sind von der Longitudinalenpolarisation abhängig. In einer numerischen Analyse haben wir gezeigt, dass die Asymmetrien mit ausreichender statistischer Signifikanz gemessen werden können. Der Effekt ist für Regionen des Parameterraums mit mittleren Werten von $\tan\beta$ und für leichte Sleptonen oder LSPs $\tilde{\chi}_1^0$ größer. Dieser Prozess liefert eindeutige Informationen über die Interferenz überlappender Higgsboson-Austausch-Resonanzen.

- Für Chargino-Paarproduktion mit anschließendem Zweikörperzerfall beider Charginos wurden Energie- und Winkelverteilungen der Zerfallsprodukte definiert, um damit die Chargino-Spin-Spin-Korrelationen analysieren zu können. Die transversalen Polarisationen der Charginos sind auf die CP-Quantenzahl des ausgetauschten Higgs-Bosons sensitiv. Dadurch kann man überlappende Resonanzen trennen, sowie auch die CP-Quantenzahl einer einzelnen Resonanz bestimmen. Für gleiche Charginos sind diese Asymmetrien auf die Interferenz CP-gerader und CP-ungerader Higgs-Kanäle nicht sensitiv. Es ist deswegen nicht möglich, mit ihrer Hilfe zwischen zwei überlappenden skalaren Resonanzen mit unterschiedlichen CP-Quantenzahlen und einer CP-verletzenden einzelnen Resonanz zu unterscheiden.

Für die Produktion $\mu^+\mu^- \to \tilde{\chi}_i^0\tilde{\chi}_j^0$ können wir folgendermaßen zusammenfassen:

- Line-Shape-Messungen der Neutralino-Paarproduktion erlauben eine präzise Bestimmung des Verhältnisses der H-Neutralino- und A-Neutralino-Kopplungen, unabhängig vom Zerfallsmechanismus der Neutralinos, analog der Chargino-Paarproduktion. In der numerischen Analyse untersuchten wir die Abhängigkeit der Produktionswirkungsquerschnitte verschiedener Neutralino-Paare vom MSSM Parameterraum.

- Für Neutralino Paarproduktion mit anschließendem Zweikörperzerfall eines der Neutralinos, $\tilde{\chi}_j^0 \to \ell^\pm\tilde{\ell}_{R,L}^\mp$, für $\ell = e, \mu, \tau$, haben wir gezeigt, dass die Energieverteilungsasymmetrie des Zerfallsleptons sensitiv auf Interferenz von H und A ist, wenn letztere teilweise entartet sind. In der numerischen Analyse zeigten wir für repräsentative Szenarien mit mittleren Werten von $\tan\beta$, dass die Asymmetrien groß sind und mit ausreichender statistischer Signifikanz gemessen werden können.

- Für Neutralino-Paarproduktion mit anschließendem Zweikörperzerfall beider Neutralinos analysierten wir die Energie- und Winkelverteilungen der Zerfallsprodukte. Die Abhängigkeit der Neutralino-Spin-Spin-Korrelationen von der Higgs-Neutralino-Wechselwirkung ist ähnlich der der Charginos, mit dem Unterschied, dass die intrinsische CP-Quantenzahl des erzeugten Neutralinopaares vom Szenario abhängt.

- Zuletzt untersuchten wir den Effekt der Transversalpolarisation der Strahlen auf die Neutralino-Produktionsobservablen. Analog wie bei den Spin-Spin-Korrelationen können wir die CP-geraden und CP-ungeraden Higgsaustausch-Beiträge anhand deren Abhängigkeit von der Strahlpolarisation trennen.

5.1 Schlussfolgerungen

Wir haben gezeigt, dass die Kopplungen der Higgsbosonen an den Gaugino-Higgsino-Sektor an einem Myonbeschleuniger getestet werden können. Wenn die Beiträge der Resonanzen mit Hilfe der Linienform getrennt werden können ist es möglich, das Verhältnis der H-und A-Kopplungen an die Charginos oder Neutralinos mit hoher Präzision zu bestimmen. Besonders interessant sind hier Szenarien mit $\tan\beta \approx 5$, in denen H und A hauptsächlich in Charginos und Neutralinos zerfallen, sodaß deren Produktionswirkungsquerschnitte im pb-Bereich liegen können.

Die Strahlenpolarisation liefert ein sehr elegantes Mittel um die Resonanzen zu trennen. Dies setzt allerdings, da die Effekte proportional zum Polarisationsgrad sind, hohe Polarisationsgrade voraus, welche an einem Myonbeschleuniger schwer zu erreichen sind. Im Falle von Zweikörperzerfällen können die Spinkorellationen der Charginos oder Neutralinos bei transversaler Polarisation untersucht werden. Die leptonischen Zerfälle, wenn kinematisch erlaubt, sind optimale Proben der Polarisation.

Wir finden große Korrelationen zwischen Strahl-und Chargino-Polarisationen, die auf die Interferenz von H und A sensitiv sind. Für eine longitudinale Strahlpolarisation von 30% bekommen wir Ladungs- und Polarisationsasymmetrien die größer als 20% sind wenn der Überlapp der Resonanzen groß ist. Die höchsten Asymmetrien findet man hier in Szenarien mit $\tan\beta \approx 10$, in denen die schweren Higgsbosonen fast entartet sind und gleichzeitig große Verzweigungsverhältnisse in Charginos und Neutralinso aufweisen. In diesen Fällen finden wir statistische Signifikanzen im Bereich zwischen 1 und 5 bei einer integrierten Luminosität von $\mathcal{L} = 1\ \mathrm{fb}^{-1}$.

Appendix A

Minimal Supersymmetric Standard Model

A.1 Introduction

The MSSM is defined by the four basic assumptions [33, 41]:

- Minimal gauge group: $SU(3)_C \times SU(2)_L \times U(1)_Y$, i.e. SM gauge symmetry.
- Minimal particle content: 3 generations of leptons and quarks as in the SM, 12 gauge bosons, 2 Higgs doublets, and their superpartners, see Table A.1.
- Minimal Yukawa interactions and R-parity conservation: To enforce lepton and baryon number conservation the symmetry $R = (-1)^{2s+3B+L}$ is postulated, where L and B are lepton and barion numbers and s is the spin quantum number. Ordinary particles have thus $R = +1$ while their superpartners have $R = -1$.
- Minimal set of soft SUSY-breaking terms.

A.2 Chargino sector

A.2.1 Chargino mixing

The mass eigenvalues of the charginos, $m_{\chi^{\pm}_{1,2}}$, are determined diagonalizing the chargino mass matrix, given in the $\{-i\tilde{W}^-, \tilde{H}^-\}$ basis [33] by

$$\mathcal{M}_C = \begin{pmatrix} M_2 & \sqrt{2} m_W \sin\beta \\ \sqrt{2} m_W \cos\beta & \mu \end{pmatrix}, \tag{A.1}$$

SM particles	SUSY-partners weak eigenstates		SUSY-partners mass eigenstates	
$q_u = u, c, t$ $q_d = d, s, b$	$\tilde{q}_L, \tilde{q}_R$	squarks	$\tilde{q}_1, \tilde{q}_2$	squarks
$\ell = e, \mu, \tau$	$\tilde{\ell}_L, \tilde{\ell}_R$	sleptons	$\tilde{\ell}_1, \tilde{\ell}_2$	sleptons
$\nu = \nu_e, \nu_\mu, \nu_\tau$	$\tilde{\nu}_\ell$	sneutrinos	$\tilde{\nu}_\ell$	sneutrinos
g	$\tilde{g}$	gluino	$\tilde{g}$	gluino
$W^\pm$	$\tilde{W}^\pm$	wino		
(H_1^+, H_2^-)	$\tilde{H}_1^+, \tilde{H}_2^-$	higgsinos	$\tilde{\chi}_{1,2}^\pm$	charginos
γ	$\tilde{\gamma}$	photino		
Z	$\tilde{Z}$	zino	$\tilde{\chi}_{1,\ldots,4}^0$	neutralinos
$H_1^0, (H_2^0)$	$\tilde{H}_1^0, \tilde{H}_2^0$	higgsinos		

Table A.1: Particle spectrum of the MSSM

which depends on the $SU(2)$ gaugino mass parameter M_2, the Higgs mass parameter μ, and the ratio of vacuum expectation values of the neutral Higgs fields $\tan\beta = v_1/v_2$. The gaugino mass parameter can be chosen real, absorbing the phases into the electroweak eigenstates. The Higgs mass parameter μ is in general complex while in the CP conserving MSSM it is either positive or negative.

Since the chargino mass matrix is not hermitian we need two different matrices, U and V, to diagonalize it, acting on the left- and right-chiral $\{-i\tilde{W}_L^-, \tilde{H}_L^-\}$ and $\{-i\tilde{W}_R^-, \tilde{H}_R^-\}$, respectively [33],

$$\mathcal{M}_C^{diag} = U^* \mathcal{M}_C V^T. \tag{A.2}$$

The choice of the diagonalization matrices U and V fixes the phases of the eigenvalues of $\mathcal{M}_C$. The matrices U and V can be chosen unitary. In this case the eigenvalues of $\mathcal{M}_C$ are not always positive. In the CP conserving chargino sector the relative phase of the eigenvalues is given by

$$\eta_\chi = \mathrm{sgn}(\det \mathcal{M}_C) = \mathrm{sgn}(M_2\mu - m_W^2 \sin 2\beta). \tag{A.3}$$

The chargino masses, given by the absolute values of the eigenvalues of $\mathcal{M}_C$, are

$$m_{\chi_{1,2}^\pm} = \frac{1}{2}\left\{M_2^2 + \mu^2 + 2m_W^2 \mp \Lambda^2\right\}^{\frac{1}{2}}, \tag{A.4}$$

$$\Lambda^2 = \sqrt{(M_2^2 + \mu^2 + 2m_W^2)^2 - 4(M_2\mu - m_W^2 \sin 2\beta)^2}. \tag{A.5}$$

Alternatively, in order to obtain positive mass eigenvalues we can parametrize the matrices U and V by

$$U = \begin{pmatrix} \cos\phi_L & \sin\phi_L \\ \sin\phi_L & \cos\phi_L \end{pmatrix}, \tag{A.6}$$

$$V = \begin{pmatrix} \cos\phi_R & \sin\phi_R \\ \eta_\chi \sin\phi_R & \eta_\chi \cos\phi_R \end{pmatrix}, \tag{A.7}$$

with the angles ϕ_L and ϕ_R obtained from

$$\sin\phi_L = -\frac{2\sqrt{2}m_W(M_2\cos\beta + \mu\sin\beta)}{\Lambda^2}, \tag{A.8}$$

$$\cos\phi_L = -\frac{(M_2^2 + \mu^2 - 2m_W^2\cos 2\beta)}{\Lambda^2}, \tag{A.9}$$

$$\sin\phi_R = -\frac{2\sqrt{2}m_W(M_2\sin\beta + \mu\cos\beta)}{\Lambda^2}, \tag{A.10}$$

$$\cos\phi_R = -\frac{(M_2^2 + \mu^2 + 2m_W^2\cos 2\beta)}{\Lambda^2}, \tag{A.11}$$

with Λ^2 given in (A.5).

The left- and right-handed chiral components of the eigenstates $\tilde{\chi}^+_{1,2}$ are related to the wino and higgsino components by

$$\tilde{\chi}^-_{kL} = U_{k1}\tilde{W}^-_L + U_{k2}\tilde{H}^-_L, \tag{A.12}$$

$$\tilde{\chi}^-_{kR} = V_{k1}\tilde{W}^-_R + V_{k2}\tilde{H}^-_R. \tag{A.13}$$

A.2.1.1 Approximate solution to chargino mixing

For $\tan\beta \gg 1$ the chargino mixing matrix can be approximated by a triangular matrix,

$$\mathcal{M}_C \approx \begin{pmatrix} M_2 & \sqrt{2}m_W \\ 0 & \mu \end{pmatrix}, \tag{A.14}$$

leading to chargino masses and relative phase

$$m_{\tilde{\chi}^\pm_1} \approx \min(M_2, |\mu|), \quad m_{\tilde{\chi}^\pm_2} \approx \max(M_2, |\mu|), \quad \eta_\chi \approx \mathrm{sgn}(\mu). \tag{A.15}$$

A.3 Neutralino sector

A.3.1 Neutralino mixing

The neutralino mass matrix is built up by the $U(1)$ and $SU(2)$ gaugino mass parameters M_1 and M_2, respectively, the higgsino mass parameter μ, and the ratio $\tan\beta = v_2/v_1$ of the vacuum expectation values of the two neutral Higgs fields.

In the $\{\tilde{\gamma}, \tilde{Z}, \tilde{H}_1^0, \tilde{H}_2^0\}$ basis [33] the neutralino mass matrix $\mathcal{M}_N$ is given by

$$\mathcal{M}_N = \begin{pmatrix} M_1 c_W^2 + M_2 s_W^2 & (M_2 - M_1) c_W s_W & 0 & 0 \\ (M_2 - M_1) c_W s_W & M_2 c_W^2 + M_1 s_W^2 & m_Z c_\beta & -m_Z s_\beta \\ 0 & m_Z c_\beta & 0 & -\mu \\ 0 & -m_Z s_\beta & -\mu & 0 \end{pmatrix}, \quad \text{(A.16)}$$

with the short-hand notation $s_\beta = \sin\beta,\ c_\beta = \cos\beta,\ s_W = \sin\theta_W,\ c_W = \cos\theta_W$.

The neutralino mass eigenvalues are obtained diagonalizing the neutralino mass matrix. If CP is conserved in the neutralino sector the matrix $\mathcal{M}_N$ is real and symmetric and can be diagonalized with a 4×4 unitary matrix N:

$$\mathcal{M}_N^{diag} = N^* \mathcal{M}_N N^\dagger, \quad \text{(A.17)}$$

with $(\mathcal{M}_N^{diag})_{ik} = \delta_{ik} \eta_k m_{\chi_k^0}$, where the masses $m_{\chi_k^0},\ k = 1, ..., 4$ are positive and η_k is a phase which depends on the choice of diagonalization matrix N. Since it is possible to redefine one phase $\eta_{\chi_k^0}$ through a phase reparametrization of the fields, only the relative phases are physical and we define

$$\eta_{ij} = \eta_i \eta_j. \quad \text{(A.18)}$$

The relative phases η_{ij} are related to the relative CP intrinsic phase of $\tilde{\chi}_i^0 \tilde{\chi}_j^0$.

A.4 Sfermion sector

The left and right sfermions are the scalar supersymmetric partners of the left handed and right fermions, respectively. Their couplings to the gauge sector are thus fixed by the gauge structure. Mixing between the left and right sfermions is proportional to the mass of the associated fermion, see Section A.4.1.1. Therefore, for the first two fermion families we neglect mixing. We also neglect mixing between sfermion families.

If gauge unification is assumed and left and right sfermions do not mix then the sfermion masses can be evaluated from their common mass m_0 at the unification energy scale (GUT-scale) via the Hall-Polchiski renormalization group relations (RGE) [35]

$$m_{\tilde{f}_{L,R}}^2 = m_f^2 + m_0^2 + C_{f_{LR}} M_2^2 + m_Z^2 \cos 2\beta (T_{3f} - e_f \sin^2\theta_W), \quad \text{(A.19)}$$

where m_f is the mass of the fermion partner, T_{3f} is the third component of the weak isospin of the fermion f, e_f is its electric charge and $C_{f_{L,R}}$ is a coefficient

evaluated with the RGE. At the electroweak breaking scale $C_{f_{L,R}}$ has the approximate values

$$C_{\ell_L} \approx 0.79, \qquad C_{\ell_R} \approx 0.23,$$
$$C_{q_L} \approx 10.8, \qquad C_{q_R} \approx 10.1.$$

Note that for the squarks $C_{q_{L,R}} \gg 1$. This implies that squarks are expected to be considerably heavier than sleptons. When GUT relations are assumed squarks are heavier than the lighter chargino and, for a large region of parameter space, heavier than the heavier chargino. If the scalar mass m_0 is of the order of the electroweak energy scale squarks are also considerably heavier than sleptons.

A.4.1 Scalar lepton sector

Explicitly for leptons, eq. (A.19) reads

$$m^2_{\tilde{\ell}_L} = m_0^2 + m_\ell^2 + 0.79M_2^2 - m_Z^2 \cos 2\beta(\frac{1}{2} - \sin^2\theta_W), \tag{A.20}$$
$$m^2_{\tilde{\ell}_R} = m_0^2 + m_\ell^2 + 0.23M_2^2 - m_Z^2 \cos 2\beta \sin^2\theta_W, \tag{A.21}$$
$$m^2_{\tilde{\nu}_\ell} = m_0^2 + 0.79M_2^2 + \frac{1}{2}m_Z^2 \cos 2\beta. \tag{A.22}$$

A.4.1.1 Mixing in the third generation

The mass eigenvalues of the staus, $m_{\tilde{\tau}_{1,2}}$, are determined diagonalizing the stau mass matrix, given in the $\tilde{\tau}_L - \tilde{\tau}_R$ basis by

$$\mathcal{L}_M^{\tilde{\tau}} = -(\tilde{\tau}_R^*,\, \tilde{\tau}_L^*) \begin{pmatrix} m^2_{\tilde{\tau}_R} & -m_\tau \Lambda_\tau \\ -m_\tau \Lambda_\tau & m^2_{\tilde{\tau}_L} \end{pmatrix} \begin{pmatrix} \tilde{\tau}_R \\ \tilde{\tau}_L \end{pmatrix}, \tag{A.23}$$

with $m^2_{\tilde{\tau}_R}$ and $m^2_{\tilde{\tau}_L}$ given by eqs. (A.21) and (A.20) replacing m_ℓ^2 by m_τ^2, and

$$\Lambda_\tau = A_\tau - \mu \tan\beta, \tag{A.24}$$

where A_τ is the trilinear scalar coupling parameter. The $\tilde{\tau}$ mass eigenstates are $(\tilde{\tau}_1, \tilde{\tau}_2) = (\tilde{\tau}_R, \tilde{\tau}_L)\mathcal{R}^{\tilde{\tau}T}$ with the stau mixing matrix

$$\mathcal{R}^{\tilde{\tau}} = \begin{pmatrix} \cos\theta_{\tilde{\tau}} & \sin\theta_{\tilde{\tau}} \\ -\sin\theta_{\tilde{\tau}} & \cos\theta_{\tilde{\tau}} \end{pmatrix}, \tag{A.25}$$

and

$$\cos\theta_{\tilde{\tau}} = \frac{m^2_{\tilde{\tau}_L} - m^2_{\tilde{\tau}_1}}{\sqrt{m_\tau^2\Lambda_\tau^2 + (m^2_{\tilde{\tau}_1} - m^2_{\tilde{\tau}_L})^2}}., \quad \sin\theta_{\tilde{\tau}} = \frac{m_\tau \Lambda_\tau}{\sqrt{m_\tau^2\Lambda_\tau^2 + (m^2_{\tilde{\tau}_1} - m^2_{\tilde{\tau}_L})^2}} \tag{A.26}$$

The mass eigenvalues are

$$m^2_{\tilde{\tau}_{1,2}} = \frac{1}{2}\left((m^2_{\tilde{\tau}_L} + m^2_{\tilde{\tau}_R}) \mp \sqrt{(m^2_{\tilde{\tau}_L} - m^2_{\tilde{\tau}_R})^2 + 4m_\tau^2\Lambda_\tau^2}\right). \tag{A.27}$$

Appendix B

Lagrange densities and couplings

B.1 Chargino production

The MSSM interaction Lagrangians for chargino production in $\mu^+\mu^-$-annihilation eq. (2.1) via Higgs exchange are

$$\mathcal{L}_{\mu^+\mu^-\phi} = g\,\bar{\mu}\,(c^{(\phi\mu)\,*}P_L + c^{(\phi\mu)}P_R)\,\mu\,\phi, \tag{B.1}$$

$$\mathcal{L}_{\tilde{\chi}^+\tilde{\chi}^+\phi} = g\,\bar{\tilde{\chi}}_i^+(c_{L\,ij}^{(\phi)}P_L + c_{R\,ij}^{(\phi)}P_R)\tilde{\chi}_j^+\,\phi, \tag{B.2}$$

where $P_{R,L} = \frac{1}{2}(1 \pm \gamma^5)$, g is the weak coupling constant and $\phi = H, A, h$. The muon couplings to H and A are [40]:

$$c^{(H\mu)} = -\frac{m_\mu}{2m_W}\frac{\cos\alpha}{\cos\beta}, \tag{B.3}$$

$$c^{(A\mu)} = i\frac{m_\mu}{2m_W}\tan\beta, \tag{B.4}$$

where α is the Higgs mixing angle, $\tan\beta = v_2/v_1$ is the ratio of the vacuum expectation values of the two neutral Higgs fields. The chargino couplings to H and A are [40]:

$$c_{L\,ij}^{(H)} = -Q_{ij}^*\cos\alpha - S_{ij}^*\sin\alpha, \tag{B.5}$$

$$c_{L\,ij}^{(A)} = i(Q_{ij}^*\sin\beta + S_{ij}^*\cos\beta), \tag{B.6}$$

$$c_{R\,ij}^{(\phi)} = c_{L\,ji}^{(\phi)*}, \quad \phi = H, A, \tag{B.7}$$

$$Q_{ij} = \frac{1}{\sqrt{2}}U_{i2}V_{j1}, \tag{B.8}$$

$$S_{ij} = \frac{1}{\sqrt{2}}U_{i1}V_{j2}, \tag{B.9}$$

where U and V are the 2×2 diagonalization unitary matrices U and V given in eqs. (A.6) and (A.7), respectively.

The muon and chargino couplings to the lighter Higgs boson h are obtained substituting α by $\alpha + \pi/2$ in (B.3) and (B.5), respectively.

B.2 Neutralino production

The MSSM muon-Higgs interaction Lagrangian (B.1) has been given in the preceding section. The interaction Lagrangian for neutralino production in $\mu^+\mu^-$-annihilation via Higgs exchange, eq. (3.1), is

$$\mathcal{L}_{\tilde{\chi}^0\tilde{\chi}^0\phi} = \frac{1}{2} g\, \bar{\tilde{\chi}}^0_i (d^{(\phi)*}_{ij} P_L + d^{(\phi)}_{ij} P_R) \tilde{\chi}^0_j\, \phi, \tag{B.10}$$

where $P_{R,L} = \frac{1}{2}(1 \pm \gamma^5)$, g is the weak coupling constant and $\phi = H, A, h$.

In the neutralino basis $\{\tilde{\gamma}, \tilde{Z}, \tilde{H}^0_1, \tilde{H}^0_2\}$ [33, 42] the neutralino couplings to H and A are [40]:

$$d^{(H)}_{ij} = -Q''_{ij} \cos\alpha + S''_{ij} \sin\alpha, \tag{B.11}$$

$$d^{(A)}_{ij} = -i(Q''_{ij} \sin\beta - S''_{ij} \cos\beta), \tag{B.12}$$

$$Q''_{ij} = \frac{1}{2\cos\theta_W}[N_{i3}N_{j2} + (i \leftrightarrow j)], \tag{B.13}$$

$$S''_{ij} = \frac{1}{2\cos\theta_W}[N_{i4}N_{j2} + (i \leftrightarrow j)], \tag{B.14}$$

where α is the Higgs mixing angle, $\tan\beta = v_2/v_1$ is the ratio of the vacuum expectation values of the two neutral Higgs fields, θ_W is the weak mixing angle and N is the unitary 4×4 matrix which diagonalizes the neutralino mass matrix $\mathcal{M}_N$ If CP is conserved $\mathcal{M}_N$ is real and the matrix N can be chosen real and orthogonal: $N_{i\alpha}\mathcal{M}_{N\,\alpha\beta}N^T_{\beta k} = \eta_i m_{\chi_i}\delta_{ik}$, where $m_{\chi_i}, i = 1, \ldots, 4$ are the masses of the neutralinos and $\eta_i = \pm 1$ is related to the CP eigenvalue of the neutralino $\tilde{\chi}^0_i$.

The neutralino couplings to the lighter Higgs boson h are obtained substituting α with $\alpha + \pi/2$ in (B.11).

B.3 CP conserving and CP violating couplings

When CP is conserved in the chargino sector the chargino mass matrix $\mathcal{M}_C$, eq. (A.1), is real and the diagonalization matrices U and V can be chosen real. In analogous way for the CP conserving neutralino sector the neutralino mass matrix $\mathcal{M}_N$ is real and symmetric and the diagonalization matrix N can be chosen real and orthogonal. Therefore, with this choice of diagonalization prescription, the chargino and neutralino couplings to the CP-even Higgs boson, (B.5) and (B.11), are real those to the CP odd Higgs boson, (B.6) and (B.12), are pure imaginary.

In the general case of non CP conserving chargino or neutralino sectors the coefficients Q_{ij} and S_{ij} as well as Q''_{ij} and S''_{ij} are complex. We define the phases of the couplings of the Higgs bosons to charginos and neutralinos $\gamma_{\phi ij}$ and $\delta_{\phi ij}$,

respectively, in the relations

$$c_{ij}^{(\phi)} = \bar{c}_{ij}^{(\phi)} e^{i\gamma_{\phi ij}}, \tag{B.15}$$

$$d_{ij}^{(\phi)} = \bar{d}_{ij}^{(\phi)} e^{i\delta_{\phi ij}}. \tag{B.16}$$

where $\phi = H, A$. These phases may be defined in the interval $[0, \pi)$, which implies $\gamma_{Hij} = \delta_{Hij} = 0$ and $\gamma_{Aij} = \delta_{Aij} = \pi/2$ in the CP conserving limit.

At tree level, the MSSM Higgs sector is CP conserving. However, CP violating phases arise through loop corrections. These phases can be absorbed in the couplings to the charginos and neutralinos, (B.15) and (B.15), respectively, as well as in those to the muons, with

$$c^{(\phi\mu)} = \bar{c}^{(\phi\mu)} e^{i\xi_\phi}. \tag{B.17}$$

with $\bar{c}^{(\phi\mu)}$ real. Defining the muon-Higgs couplings in the interval $[0, \pi)$ leads to $\xi_H = 0$ and $\xi_A = \pi/2$ for the CP conserving Higgs sector.

B.4 Chargino decay

The Lagrangians for chargino decay into a charged lepton ℓ and a sneutrino, $\tilde{\chi}_j^\pm \to \ell^\pm \, \tilde{\nu}_\ell^{(*)}$, with $\ell = e, \mu, \tau$, are

$$\mathcal{L}_{\ell\tilde{\nu}_\ell\tilde{\chi}^+} = -gV_{j1}\bar{\ell}P_R\tilde{\chi}_j^{+C}\tilde{\nu}_\ell + \text{h.c.}, \qquad \ell = e, \mu, \tag{B.18}$$

$$\mathcal{L}_{\tau\tilde{\nu}_\tau\tilde{\chi}^+} = -g\bar{\tau}(V_{j1}P_R - Y_\tau U_{j2}^* P_L)\tilde{\chi}_j^{+C}\tilde{\nu}_\tau + \text{h.c.}, \tag{B.19}$$

with the τ-Yukawa coupling $Y_\tau = m_\tau/(\sqrt{2}m_W \cos\beta)$.

The Lagrangian for chargino decay into a W boson and a neutralino, $\tilde{\chi}_j^\pm \to W^\pm \tilde{\chi}_k^0$, is

$$\mathcal{L}_{W^-\tilde{\chi}^+\tilde{\chi}^0} = gW_\mu^- \bar{\tilde{\chi}}_k^0 \gamma^\mu [O_{kj}^L P_L + O_{kj}^R P_R]\tilde{\chi}_j^+ + \text{h.c.}, \tag{B.20}$$

with the couplings [33]

$$O_{kj}^L = -\frac{1}{\sqrt{2}} N_{k4} V_{j2}^* + (\sin\theta_W N_{k1} + \cos\theta_W N_{k2}) V_{j1}^*, \tag{B.21}$$

$$O_{kj}^R = +\frac{1}{\sqrt{2}} N_{k3}^* U_{j2} + (\sin\theta_W N_{k1}^* + \cos\theta_W N_{k2}^*) U_{j1}. \tag{B.22}$$

The 4×4 unitary matrix N diagonalizes the neutralino mass matrix $\mathcal{M}_N$ in the basis $\{\tilde{\gamma}, \tilde{Z}, \tilde{H}_1^0, \tilde{H}_2^0\}$ [33, 42] with $N_{il}^* \mathcal{M}_{N\,lm} N_{mj}^\dagger = \delta_{ij}\eta_j m_{\chi_j^0}$.

Alternatively, diagonalizing the matrix $\mathcal{M}_N$ in the basis $\{\tilde{\gamma}, \tilde{Z}, \tilde{H}_a, \tilde{H}_b\}$ [42] with the the 4×4 unitary matrix N', with $N_{il}'^* \mathcal{M}_{N\,lm} N_{mj}'^\dagger = \delta_{ij}\eta_j m_{\chi_j^0}$, eqs. (B.21)

and (B.21) read [33]

$$\begin{aligned} O^L_{kj} &= -\frac{1}{\sqrt{2}}(\cos\beta N'_{k4} - \sin\beta N'_{k3})V^*_{j2} \\ &\quad +(\sin\theta_W N'_{k1} + \cos\theta_W N'_{k2})V^*_{j1}, \qquad \text{(B.23)} \\ O^R_{kj} &= +\frac{1}{\sqrt{2}}(\sin\beta N'^*_{k4} + \cos\beta N'^*_{k3})U_{j2} \\ &\quad +(\sin\theta_W N'^*_{k1} + \cos\theta_W N'^*_{k2})U_{j1}. \qquad \text{(B.24)} \end{aligned}$$

The Lagrangian for heavier chargino decay into a Z boson and a lighter chargino, $\tilde{\chi}^\pm_2 \to \tilde{\chi}^\pm_1 Z$ is

$$\mathcal{L}_{Z\tilde{\chi}^+\tilde{\chi}^+} = \frac{g}{\cos\theta_W} Z_\mu \bar{\tilde{\chi}}^+_i \gamma^\mu [O'^L_{ij} P_L + O'^R_{ij} P_R] \tilde{\chi}^+_j, \qquad \text{(B.25)}$$

with the couplings [33]

$$\begin{aligned} O'^L_{ij} &= -V_{i1}V^*_{j1} - \frac{1}{2}V_{i2}V^*_{j2} + \delta_{ij}\sin^2\theta_W, \qquad \text{(B.26)} \\ O'^R_{ij} &= -U^*_{i1}U_{j1} - \frac{1}{2}U^*_{i2}U_{j2} + \delta_{ij}\sin^2\theta_W. \qquad \text{(B.27)} \end{aligned}$$

The Lagrangian for the decay $\tilde{\chi}^\pm_2 \to \tilde{\chi}^\pm_1 h$ is given by the Lagrangian for production, eq. (B.2), where the couplings $c^{(h)}_{L\,ij}$ and $c^{(h)}_{R\,ij}$ are obtained from eqs. (B.5) and (B.7) substituting α by $\alpha + \pi/2$.

B.5 Neutralino decay

The interaction Lagrangian for neutralino decay into a lepton and a slepton of the first two generations is [33]

$$\mathcal{L}_{\ell\tilde{\ell}\tilde{\chi}^0_j} = g f^L_{\ell_j} \bar{\ell} P_R \tilde{\chi}^0_j \tilde{\ell}_L + g f^R_{\ell_j} \bar{\ell} P_L \tilde{\chi}^0_j \tilde{\ell}_R + \text{h.c.}, \quad \ell = e, \mu, \qquad \text{(B.28)}$$

with couplings

$$\begin{aligned} f^L_{\ell j} &= -\sqrt{2}\left[\frac{1}{\cos\theta_W}(T_{3\ell} - e_\ell \sin^2\theta_W)N_{j2} + e_\ell \sin\theta_W N_{j1}\right], \qquad \text{(B.29)} \\ f^R_{\ell j} &= -\sqrt{2} e_\ell \sin\theta_W \left[\tan\theta_W N^*_{j2} - N^*_{j1}\right], \qquad \text{(B.30)} \end{aligned}$$

where e_ℓ and $T_{3\ell}$ denote the electric charge and third component of the weak isospin of the lepton ℓ.

For the neutralino decay into staus $\tilde{\chi}^0_i \to \tilde{\tau}^\pm_n \tau^\mp$, stau mixing has to be taken into account. The interaction Lagrangian is [43]

$$\mathcal{L}_{\tau\tilde{\tau}\chi_i} = g\tilde{\tau}_n \bar{\tau}(a^{\tilde{\tau}}_{nj} P_R + b^{\tilde{\tau}}_{nj} P_L)\tilde{\chi}^0_i + \text{h.c.}\,, \quad n = 1, 2;\ j = 1, \ldots, 4, \qquad \text{(B.31)}$$

with couplings

$$a^{\tilde{\tau}}_{nj} = (\mathcal{R}^{\tilde{\tau}}_{nm})^* \mathcal{A}^{\tau}_{jm}, \qquad b^{\tilde{\tau}}_{nj} = (\mathcal{R}^{\tilde{\tau}}_{nm})^* \mathcal{B}^{\tau}_{jm}, \qquad m = L, R \tag{B.32}$$

with $\mathcal{R}^{\tilde{\tau}}_{nm}$ the stau mixing matrix defined in eq. (A.25) and

$$\mathcal{A}^{\tau}_{j} = \begin{pmatrix} f^{L}_{\tau j} \\ h^{R}_{\tau j} \end{pmatrix}, \qquad \mathcal{B}^{\tau}_{j} = \begin{pmatrix} h^{L}_{\tau j} \\ f^{R}_{\tau j} \end{pmatrix}. \tag{B.33}$$

In eq. (B.33), $f^{L}_{\tau j}$ and $f^{R}_{\tau j}$ are defined by eqs. (B.29) and (B.30), respectively, and

$$h^{L}_{\tau j} = (h^{R}_{\tau j})^* = m_\tau/(\sqrt{2} m_W \cos\beta) N^*_{j3}, \tag{B.34}$$

with m_W the mass of the W boson, m_τ the mass of the τ-lepton and N the neutralino mixing matrix in the $\tilde{\gamma}, \tilde{Z}, \tilde{H}^0_1, \tilde{H}^0_2$ basis.

The Lagrangian for the decay $\tilde{\chi}^0_k \to \tilde{\chi}^{\pm}_i W^{\mp}$ is given in eq. (B.20).

The Lagrangian for the decay $\tilde{\chi}^0_k \to \tilde{\chi}^0 h$ is given by (B.10), where the coupling $d^{(h)}_{ij}$ is obtained substituting α by $\alpha + \pi/2$ in from eq. (B.11).

The Lagrangian for heavier neutralino decay into a Z boson and a lighter neutralino, $\tilde{\chi}^0_k \to \tilde{\chi}^0_i Z$, $k = 2, 3, 4$ and $i = 1, 2, 3$ is

$$\mathcal{L}_{Z\tilde{\chi}^0\tilde{\chi}^0} = \frac{1}{2}\frac{g}{\cos\theta_W} Z_\mu \bar{\tilde{\chi}}^0_k \gamma^\mu [O''^L_{ki} P_L + O''^R_{ki} P_R] \tilde{\chi}^0_i, \tag{B.35}$$

with the couplings [33]

$$O''^L_{ki} = -\frac{1}{2}(N_{k3} N^*_{i3} - N_{k4} N^*_{i4}), \tag{B.36}$$

$$O''^R_{ki} = -O''^{L*}_{ki}, \tag{B.37}$$

in the $\tilde{\gamma}, \tilde{Z}, \tilde{H}^0_1, \tilde{H}^0_2$ basis.

Appendix C

Chargino and neutralino spin density matrices

Here we present the spin formalism used to evaluate the spin-correlations between production and decay, as well as the spin-spin correlations, for chargino and neutralino production in
$mu^+\mu^-$-annihilation.

C.1 Spin density matrix formalism

In this section we present the spin density matrix formalism, see, e.g. [28], for chargino and neutralino production and decay in $\mu^+\mu^-$-annihilation with polarized beams. We denote here with χ_i and χ_j the produced charginos or neutralinos, where i and j label the chargino or neutralino mass eigenstates. The helicities of χ_i and χ_j are denoted by λ_i, λ_i' and λ_j, λ_j', respectively. The helicities of μ^+ and μ^- are denoted by λ_+, λ_+' and λ_-, λ_-', respectively.

C.1.1 Helicity spinor formalism for spin-$\frac{1}{2}$ particles

For the calculation of the cross sections for production and decay we use the spin density formalism [28].

The helicity spinor $u(p, \lambda)$ is the solution of the Dirac equation of a particle with four-momentum p, mass m and helicity λ

$$(\not{p} - m)u(p, \lambda) = 0 \tag{C.1}$$

and are eigenvectors of γ^5

$$\gamma^5 u(p, \lambda) = 2\lambda u(p, \lambda). \tag{C.2}$$

The spinor for its antiparticle is obtained through charge conjugation

$$v(p, \lambda) = C\bar{u}^T(p, \lambda), \tag{C.3}$$

where C is the charge conjugation operator. The spinor for the antiparticle is a solution of the Dirac equation

$$(\not{p} + m)v(p,\lambda) = 0 \tag{C.4}$$

and

$$\gamma^5 v(p,\lambda) = 2\lambda v(p,\lambda). \tag{C.5}$$

Here the spinors are normed such that

$$\bar{u}(p,\lambda)u(p,\lambda) = 2m, \tag{C.6}$$
$$\bar{v}(p,\lambda)v(p,\lambda) = -2m, \tag{C.7}$$

The gamma matrices in the Weyl representation are given in Appendix E.

C.1.2 Bouchiat-Michel formalism for spin-$\frac{1}{2}$ particles

Using a set of spin-basis vectors $s^{a,\mu}$, $a = 1,2,3$, for an initial or final fermion the amplitudes squared are expanded in terms of Pauli matrices σ^a and the Kronecker delta in helicity-space. The spin vectors and the four-momentum p form an orthogonal set

$$p^\mu s^a_\mu = 0, \tag{C.8}$$
$$s^{a,\mu} s^b_\mu = -\delta^{ab}, \tag{C.9}$$
$$s^a_\nu s^a_\nu = -g_{\mu\mu} + \frac{p_\mu p_\nu}{m^2}. \tag{C.10}$$

The Bouchiat-Michel formulae for massive spin 1/2 particles are then [28]

$$u(p,\lambda')\bar{u}(p,\lambda) = \frac{1}{2}[\delta_{\lambda\lambda'} + \gamma^5 \not{s}^a \sigma^a_{\lambda\lambda'}](\not{p} + m), \tag{C.11}$$
$$v(p,\lambda')\bar{v}(p,\lambda) = \frac{1}{2}[\delta_{\lambda'\lambda} + \gamma^5 \not{s}^a \sigma^a_{\lambda'\lambda}](\not{p} - m). \tag{C.12}$$

C.1.3 Muon spin density matrix

The spin density matrix ρ of a particle with spin s and with eigenvalue of the z-component of the spin operator m_s is given by [44, 45]

$$\rho = \sum_{m_s, m'_s} |sm'_s\rangle \rho_{m_s,m'_s} \langle sm_s|. \tag{C.13}$$

The density matrix for the incoming spin-$\frac{1}{2}$ μ^+ and μ^-, with spin vectors $\mathcal{P}^m_+$ and $\mathcal{P}^m_-$, respectively, can then be expressed as

$$\rho^{(\mu^\pm)}_{\lambda_\pm\lambda'_\pm} = \frac{1}{2}(I + \mathcal{P}^m_\pm \sigma^m)_{\lambda_\pm\lambda'_\pm} \tag{C.14}$$

where $\sigma^m,\ m = 1, \ldots, 3$ are the Pauli matrices and I is the 2×2 identity matrix.

We define the spin vectors in the μ^+ and μ^- reference frames, Section D.1.3, where the z-axis is chosen, respectively, in the direction of the μ^+ and μ^- beams. Then $\mathcal{P}^3_\pm$ denotes the longitudinal polarizations of the beams. The x axis lies on the production plane and the y axis is perpendicular to the production plane, for both reference frames. Thus $\mathcal{P}^1_\pm$ and $\mathcal{P}^2_\pm$ are the transverse polarizations on the production plane and perpendicular to it. The transverse parts of the spin vectors can be described by $\mathcal{P}^T_\pm = \sqrt{{\mathcal{P}^1_\pm}^2 + {\mathcal{P}^2_\pm}^2}$ and the unit vectors $\vec{t}_\pm = (\mathcal{P}^1_\pm, \mathcal{P}^2_\pm, 0)/\mathcal{P}^T_\pm$.

C.1.4 Chargino and neutralino spin vectors

We define the spin vectors of the charginos $\tilde{\chi}^\mp_i$ and $\tilde{\chi}^\pm_j$ (neutralinos $\tilde{\chi}^0_i$ and $\tilde{\chi}^0_j$), in the reference frame in the center of mass system (CMS) R_{χ_j}. In R_{χ_j} the four-momentum of the chargino $\tilde{\chi}^\pm_j$ (neutralino $\tilde{\chi}^0_j$), denoted here with χ_j, is given by

$$p^\nu_{\chi_j} = (E_{\chi_j}; 0, 0, |\vec{p}_{\chi_j}|), \tag{C.15}$$

with

$$E_{\chi_j} = \frac{s + m^2_{\chi_j} - m^2_{\chi_i}}{2\sqrt{s}}, \quad |\vec{p}_{\chi_j}| = \frac{\lambda^{\frac{1}{2}}(s, m^2_{\chi_i}, m^2_{\chi_j})}{2\sqrt{s}}. \tag{C.16}$$

The four-momentum of the incoming μ^- is given by

$$p^\nu_{\mu^-} = \frac{\sqrt{s}}{2}(1; \beta \sin\theta, 0, \beta \cos\theta), \tag{C.17}$$

with $\beta = \sqrt{1 - 4m^2_{\mu^\pm}/s}$.

The spin vectors of the chargino (neutralino) in the CMS are chosen such that $\vec{s}^1_{\chi_j}$ and $\vec{s}^2_{\chi_j}$ are perpendicular to the momentum of the chargino (neutralino) $\vec{p}_{\chi_j}$ and $\vec{s}^3_{\chi_j}$ is parallel to $\vec{p}_{\chi_j}$. They are defined by

$$s^{1,\nu}_{\chi_j} = (0; 1, 0, 0), \qquad s^{2,\nu}_{\chi_j} = (0; 0, 1, 0), \qquad s^{3,\nu}_{\chi_j} = \frac{1}{m_{\chi_j}}(|\vec{p}_{\chi_j}|; 0, 0, E_{\chi_j}). \tag{C.18}$$

The production plane is defined by

$$\frac{\vec{p}_{\mu^-} \times \vec{p}_{\chi_j}}{|\vec{p}_{\mu^-} \times \vec{p}_{\chi_j}|} = (0, 1, 0), \tag{C.19}$$

Then $s^{1,\nu}_{\chi_j}$ and $s^{2,\nu}_{\chi_j}$ lie parallel and perpendicular to the production plane, respectively.

The four-momentum of the chargino $\tilde{\chi}_i^{\mp}$ (neutralino $\tilde{\chi}_i^0$), denoted here with χ_i, is then

$$p^{\nu}_{\chi_i} = (E_{\chi_i}; 0, 0, -|\vec{p}_{\chi_i}|), \tag{C.20}$$

with E_{χ_i} and $\vec{p}_{\chi_i}$ defined in analogy to eq. (C.16).

The spin vectors of χ_i are defined by

$$s^{1,\nu}_{\chi_i} = (0; -1, 0, 0), \qquad s^{2,\nu}_{\chi_i} = (0; 0, 1, 0), \qquad s^{3,\nu}_{\chi_i} = \frac{1}{m_{\chi_i}}(|\vec{p}_{\chi_i}|; 0, 0, -E_{\chi_i}). \tag{C.21}$$

Note that in our convention $s^{2,\nu}_{\chi_i} = s^{2,\nu}_{\chi_j}$ while $s^{1,\nu}_{\chi_i} = -s^{1,\nu}_{\chi_j}$.

C.1.5 Production and decay spin density matrices

For the calculation of the cross section for the combined process of chargino production eq. (2.1) and decay, we use the spin density matrix formalism of [28], as e.g. used for chargino production in e^+e^--annihilation in [21, 22]. The unnormalized spin matrix ρ^P of $\tilde{\chi}_i^{\mp}\tilde{\chi}_j^{\pm}$ production is given by

$$\tilde{\rho}^P_{\lambda_+\lambda'_+\lambda_-\lambda'_-,\lambda_i\lambda'_i\lambda_j\lambda'_j} = T^P_{\lambda_+\lambda_-,\lambda_i\lambda_j} T^{P*}_{\lambda'_+\lambda'_-,\lambda'_i\lambda'_j}, \tag{C.22}$$

where $T^P_{\lambda_+\lambda_-,\lambda_i\lambda_j}$ is the helicity amplitude for production, λ_+, λ_- are the helicities indices of μ^+ and μ^-, respectively, and λ_i, λ_j those of the charginos. To obtain the beam polarization dependent production density matrix we contract eq. (C.22) with the muon spin density matrices, eq. (C.14),

$$\rho^P_{\lambda_i\lambda'_i\lambda_j\lambda'_j} = \sum_{\lambda_+,\lambda'_+} \sum_{\lambda_-,\lambda'_-} \rho^{(\mu^+)}_{\lambda_+\lambda'_+} \rho^{(\mu^-)}_{\lambda_-\lambda'_-} \tilde{\rho}^P_{\lambda_+\lambda'_+\lambda_-\lambda'_-,\lambda_i\lambda'_i\lambda_j\lambda'_j}. \tag{C.23}$$

The spin density matrix is then a function of the μ^+ and μ^- polarization degrees $\mathcal{P}^m_+$ and $\mathcal{P}^m_-$, respectively, with $m = 1, 2, 3$.

Similarly, the unnormalized spin matrix ρ^D of $\tilde{\chi}_j^{\pm}$ decay is given by

$$\rho^D_{\lambda'_j\lambda_j} = T^{D*}_{\lambda'_j} T^D_{\lambda_j}, \tag{C.24}$$

where $T^D_{\lambda_j}$ are the helicity amplitudes for decay. The unnormalized spin density matrix ρ^D of $\tilde{\chi}_i^{\mp}$ decay is obtained from eq. (C.24) replacing λ_j and λ'_j with λ_i and λ'_i, respectively, in the helicity amplitudes for the chargino with opposite charge.

Introducing the set of chargino spin vectors $s^a_{\chi_i}$ and $s^b_{\chi_j}$, given in Appendix C.1.4, the spin density matrices (C.22) and (C.24) can be expanded in terms of the Pauli

matrices τ^a and the Kronecker δ,

$$\begin{aligned}\rho^P_{\lambda_j\lambda'_j} &= \delta_{\lambda_i\lambda'_i}\delta_{\lambda_j\lambda'_j}P \\ &+ \sum_{a=1}^{3}\delta_{\lambda_j\lambda'_j}\tau^a_{\lambda_i\lambda'_i}\Sigma^a_{P_i} + \sum_{b=1}^{3}\delta_{\lambda_i\lambda'_i}\tau^b_{\lambda_j\lambda'_j}\Sigma^b_{P_j} \\ &+ \sum_{a,b=1}^{3}\tau^a_{\lambda_i\lambda'_i}\tau^b_{\lambda_j\lambda'_j}\Sigma^{ab}_{P_{ij}}, \qquad \text{(C.25)}\end{aligned}$$

$$\rho^D_{\lambda'_k\lambda_k} = \delta_{\lambda'_k\lambda_k}D_k + \sum_{c=1}^{3}\tau^c_{\lambda'_k\lambda_k}\Sigma^c_{D_k}. \qquad \text{(C.26)}$$

With our choice of the spin vectors, $\Sigma^3_{P_j}/P$ is the longitudinal polarization of $\tilde{\chi}^{\pm}_j$, $\Sigma^1_{P_j}/P$ is its transverse polarization in the production plane and $\Sigma^2_{P_j}/P$ is its polarization perpendicular to the production plane. The spin tensor $\Sigma^{ab}_{P_{ij}}/P$ gives the probability of $\tilde{\chi}^{\mp}_i$ and $\tilde{\chi}^{\pm}_j$ having polarizations in the a and b directions, respectively. Note that the chargino polarizations are defined in two different reference systems, each with the third component pointing in the direction of motion of the corresponding chargino. For instance, $\Sigma^{33}_{P_{ij}}/P = 1(-1)$ implies that the helicities of both charginos are equal (opposite), independent of the polarization degree of the charginos.

C.1.6 Amplitudes squared

The amplitude squared for chargino production is obtained contracting the chargino spins of the production spin density matrix,

$$|T^P|^2 = \sum_{\lambda_i\lambda_j\lambda'_i\lambda'_j}\rho^P_{\lambda_i\lambda'_i\lambda_j\lambda'_j}\delta_{\lambda_i\lambda'_i}\delta_{\lambda_j\lambda'_j}. \qquad \text{(C.27)}$$

Here we summed over the helicity indices λ_i and λ'_i of $\tilde{\chi}^{\mp}_i$ and λ_j and λ'_j of $\tilde{\chi}^{\pm}_j$ whose decays are not observed. Expressing the production spin density matrix as in eq. (C.25) we obtain

$$|T^P|^2 = 4P. \qquad \text{(C.28)}$$

The amplitude squared for production and decay of one of the charginos, here $\tilde{\chi}^{\pm}_j$, is obtained contracting the spin indices of the decaying chargino with those of the decay matrix,

$$|T^{PD}_j|^2 = |\Delta(\tilde{\chi}^{\pm}_j)|^2\sum_{\lambda_i\lambda_j\lambda'_i\lambda'_j}\rho^P_{\lambda_i\lambda'_i\lambda_j\lambda'_j}\rho^D_{\lambda'_j\lambda_j}\delta_{\lambda_i\lambda'_i}, \qquad \text{(C.29)}$$

with the propagator $\Delta(\tilde{\chi}^{\pm}_j) = i/[p^2_{\chi^{\pm}_j} - m^2_{\chi^{\pm}_j} + im_{\chi^{\pm}_j}\Gamma_{\chi^{\pm}_j}]$, where $p_{\chi^{\pm}_j}$, $m_{\chi^{\pm}_j}$ and $\Gamma_{\chi^{\pm}_j}$ denote the four-momentum, mass and width of the chargino, respectively.

Expressing the production spin density matrix as in eqs. (C.25) and (C.26) we obtain

$$|T_j^{PD}|^2 = 4|\Delta(\tilde{\chi}_j^{\pm})|^2 \left(PD_j + \sum_{b=1}^{3} \Sigma_{P_j}^b \Sigma_{D_j}^b \right). \tag{C.30}$$

where we sum over the helicity indices λ_i and λ_i' of $\tilde{\chi}_i^{\mp}$ whose decay is not observed.

The amplitude squared for production and decay of both charginos is obtained contracting the spin indices of both charginos with those of the decay matrices,

$$|T_{ij}^{PD}|^2 = |\Delta(\tilde{\chi}_i^{\mp})|^2 |\Delta(\tilde{\chi}_j^{\pm})|^2 \sum_{\lambda_i \lambda_j \lambda_i' \lambda_j'} \rho^P_{\lambda_i \lambda_i' \lambda_j \lambda_j'} \rho^D_{\lambda_i' \lambda_i} \rho^D_{\lambda_j' \lambda_j}. \tag{C.31}$$

From eqs. (C.25) and (C.26) we obtain

$$\begin{aligned} |T_{ij}^{PD}|^2 &= 4|\Delta(\tilde{\chi}_i^{\mp})|^2 |\Delta(\tilde{\chi}_j^{\pm})|^2 \\ &\times \left(PD_iD_j + D_j \sum_{a=1}^{3} \Sigma_{P_i}^a \Sigma_{D_i}^a + D_i \sum_{b=1}^{3} \Sigma_{P_j}^b \Sigma_{D_j}^b + \sum_{a,b=1}^{3} \Sigma_{P_{ij}}^{ab} \Sigma_{D_i}^a \Sigma_{D_j}^b \right). \end{aligned} \tag{C.32}$$

As expected from eq. (C.23), the terms proportional to P in eqs. (C.30) and (C.32), (as well as the amplitude squared for total production, eq. (C.28)) are independent of the chargino polarization. The terms proportional to $\Sigma_{P_i}^a$ or $\Sigma_{P_j}^b$ in eqs. (C.30) and (C.32) describe the spin correlations between production and decay while the third term in eq. (C.32), proportional to $\Sigma_{P_{ij}}^{ab}$, describes the spin correlation between the two charginos.

C.1.7 Differential cross sections

The differential cross section for chargino pair production is given by

$$d\sigma^P = \frac{1}{2s} |T^P|^2 d\mathrm{Lips}(p; p_{\chi_i}, p_{\chi_j}), \tag{C.33}$$

where the Lorentz invariant phase space element is given in eq. (D.21).

For chargino production and decay analogous expressions follow, replacing the the amplitude squared and the phase space element.

For neutralino production the differential cross section is obtained as eq. (C.33), taking into account of the statistical factor $\frac{1}{2}$ necessary for equal neutralinos,

$$d\sigma^P = (2 - \delta_{ij}) \frac{1}{4s} |T^P|^2 d\mathrm{Lips}(p; p_{\chi_i}, p_{\chi_j}). \tag{C.34}$$

Analogous expressions are derived for neutralino production with subsequent decay

C.1.8 Contributions to the spin density matrix

It is useful to express the production density matrix as a sum of the contributions from the different production channels α, β,

$$\rho^P = \sum_{\alpha\leq\beta} \rho^P(\alpha\beta) \tag{C.35}$$

where the channels have been ordered in some arbitrary way. The amplitudes are

$$T^P_\lambda = \sum_\alpha T^P_\lambda(\alpha), \tag{C.36}$$

where λ denotes all the helicity indices. Then

$$\rho^P_{\lambda\lambda'}(\alpha\beta) = T^P_\lambda(\alpha) T^{P*}_{\lambda'}(\beta) + T^P_\lambda(\beta) T^{P*}_{\lambda'}(\alpha) \tag{C.37}$$

for $\alpha \neq \beta$, and

$$\rho^P_{\lambda\lambda'}(\alpha\alpha) = T^P_\lambda(\alpha) T^{P*}_{\lambda'}(\alpha). \tag{C.38}$$

From eqs. (C.37) and (C.38) follows that $\rho^P(\alpha\beta)$ is hermitian in the spin indices and thus the coefficients $P(\alpha\beta)$, $\Sigma^a_{P_i}(\alpha\beta)$, $\Sigma^b_{P_j}(\alpha\beta)$ and $\Sigma^{ab}_P(\alpha\beta)$, are real.

C.2 Spin density matrix for chargino production

C.2.1 Higgs exchange channels

The contribution to the spin density matrix for $\mu^+\mu^- \to \tilde{\chi}^\mp_i \tilde{\chi}^\pm_j$ from the resonant Higgs boson exchange channels, denoted here α and β, can be expressed in the general form

$$\begin{aligned} P_r(\alpha\beta) &= N^{(\alpha\beta)} g^4 \,\mathrm{Re}\{\Delta(\alpha)\Delta(\beta)^*\, \ell^{(\alpha\beta)}(\vec{\mathcal{P}}_+, \vec{\mathcal{P}}_-) \\ &\quad [a^{\alpha\beta}_+ (p_i p_j) - b^{\alpha\beta}_+ m_i m_j]\}(p_1 p_2), \end{aligned} \tag{C.39}$$

$$\begin{aligned} \Sigma^a_{r\,i}(\alpha\beta) &= -N^{(\alpha\beta)} g^4 \,\mathrm{Re}\{\Delta(\alpha)\Delta(\beta)^*\, \ell^{(\alpha\beta)}(\vec{\mathcal{P}}_+, \vec{\mathcal{P}}_-) \\ &\quad a^{\alpha\beta}_- m_i \,(s^a_i p_j)(p_1 p_2)\,\}, \end{aligned} \tag{C.40}$$

$$\begin{aligned} \Sigma^b_{r\,j}(\alpha\beta) &= -N^{(\alpha\beta)} g^4 \,\mathrm{Re}\{\Delta(\alpha)\Delta(\beta)^*\, \ell^{(\alpha\beta)}(\vec{\mathcal{P}}_+, \vec{\mathcal{P}}_-) \\ &\quad a^{\alpha\beta}_- m_j \,(s^b_j p_i)(p_1 p_2)\,\}, \end{aligned} \tag{C.41}$$

$$\begin{aligned} \Sigma^{ab}_r(\alpha\beta) &= N^{(\alpha\beta)} g^4 \,\mathrm{Re}\{\Delta(\alpha)\Delta(\beta)^*\, \ell^{(\alpha\beta)}(\vec{\mathcal{P}}_+, \vec{\mathcal{P}}_-) \\ &\quad \{\, a^{\alpha\beta}_+ \, m_i m_j \,(s^a_i s^b_j) \\ &\quad + b^{\alpha\beta}_+ \,\left[\, (s^a_i p_j)(s^b_j p_i) - (s^a_i s^b_j)(p_i p_j) \,\right] \\ &\quad + i b^{\alpha\beta}_- \,[s^a_i, p_i, s^b_j, p_j]\,\}(p_1 p_2)\}, \end{aligned} \tag{C.42}$$

where $\Delta(H)$ and $\Delta(A)$ are the Breit-Wigner propagators, eq. (2.8). We used the short hand notation for momenta and masses

$$p_1 = p_{\mu^+}, \quad p_2 = p_{\mu^-}, \quad p_i = p_{\chi_i^\mp}, \quad p_j = p_{\chi_j^\pm}, \quad m_k = m_{\chi_k^\pm},\ k = i, j, \tag{C.43}$$

and for the spin vectors

$$s_i^a = s^a_{\chi_i^\mp}, \quad s_j^b = s^b_{\chi_j^\pm}. \tag{C.44}$$

In eq. (C.42) we used the function

$$[a, b, c, d] = -\frac{i}{4}\mathrm{Tr}\{\not{a}\not{b}\not{c}\not{d}\gamma^5\} = \epsilon_{\alpha\beta\gamma\delta}a^\alpha b^\beta c^\gamma d^\delta. \tag{C.45}$$

The coefficients $\ell^{(\alpha\beta)}$ are functions of the muon-Higgs couplings,

$$\ell^{(\alpha\beta)} = \ell_1^{(\alpha\beta)} + \ell_2^{(\alpha\beta)} + i\ell_3^{(\alpha\beta)}, \tag{C.46}$$

$$\begin{aligned}\ell_1^{(\alpha\beta)} &= \mathrm{Re}(c^{(\alpha\mu)}c^{(\beta\mu)^*})(1 + \mathcal{P}_+^L\mathcal{P}_-^L),\\ &\quad +\mathrm{Re}(c^{(\alpha\mu)}c^{(\beta\mu)})(\vec{\mathcal{P}}_+^T \cdot \vec{\mathcal{P}}_-^T),\end{aligned} \tag{C.47}$$

$$\ell_2^{(\alpha\beta)} = \mathrm{Im}(c^{(\alpha\mu)}c^{(\beta\mu)})\,(\vec{\mathcal{P}}_+^T \times \vec{\mathcal{P}}_-^T) \cdot \vec{n}_+, \tag{C.48}$$

$$\ell_3^{(\alpha\beta)} = \mathrm{Im}(c^{(\alpha\mu)}c^{(\beta\mu)^*})(\mathcal{P}_+^L + \mathcal{P}_-^L), \tag{C.49}$$

and $a_\pm^{(\alpha\beta)}, b_\pm^{(\alpha\beta)}$ are functions of the the chargino-Higgs couplings,

$$a_\pm^{\alpha\beta} = \frac{1}{2}\left(c_{R\,ij}^{(\alpha)}c_{R\,ij}^{(\beta)*} \pm c_{L\,ij}^{(\alpha)}c_{L\,ij}^{(\beta)*}\right), \tag{C.50}$$

$$b_\pm^{\alpha\beta} = \frac{1}{2}\left(c_{R\,ij}^{(\alpha)}c_{L\,ij}^{(\beta)*} \pm c_{L\,ij}^{(\alpha)}c_{R\,ij}^{(\beta)*}\right). \tag{C.51}$$

The coefficient $N^{(\alpha\beta)} = 2 - \delta_{\alpha\beta}$ takes into account the sum of eq. (C.37) for $\alpha \neq \beta$.

Note that for pure Higgs exchange, with $\alpha = \beta$, the functions $a_\pm^{(\alpha\alpha)}$, $b_\pm^{(\alpha\alpha)}$ and $\ell^{(\alpha\alpha)}$ are real, which implies that the linear dependence on the sum of beam polarizations $\mathcal{P}_+^L + \mathcal{P}_-^L$ vanishes, both for CP conserving as for CP violating couplings. Thus, it is possible to build observables using this dependence on the beam polarizations to study the interference of overlapping scalar exchange channels.

C.2.2 Non-Higgs exchange channels

The contributions to the spin density matrix for chargino pair production from γ, Z s-channel and $\tilde{\nu}_\mu$ t-channel exchange can be found in Appendix C of [22] for $e^+e^- \to \tilde{\chi}_i^\mp\tilde{\chi}_j^\pm$ and can be used for $\mu^+\mu^-$-annihilation. An important difference with respect to the Higgs exchange channels is the dependence on the longitudinal beam polarizations. In Higgs exchange the beam polarization dependence is

described by the functions $\ell^{(\alpha\beta)}$, eq. (C.46). These contributions depend on the combinations of beam polarizations $1+\mathcal{P}_+^L\mathcal{P}_+^L$ and $\mathcal{P}_+^L+\mathcal{P}_+^L$, which are maximal for $\mathcal{P}_+^L=\mathcal{P}_+^L=\pm1$ and vanish for $\mathcal{P}_+^L=-\mathcal{P}_+^L=\pm1$. The non-Higgs contributions, on the other hand, depend on the combinations of beam polarizations $1-\mathcal{P}_+^L\mathcal{P}_+^L$ and $\mathcal{P}_+^L-\mathcal{P}_+^L$, whose behavior is exactly opposite.

C.3 Spin density matrix for chargino decay

C.3.1 Two-body decays

The expansion coefficients of the chargino decay matrix, eq. (C.26), for $\tilde{\chi}_j^+ \to \ell^+\ \tilde{\nu}_\ell$, with $\ell = e, \mu$, are

$$D = \frac{g^2}{2}|V_{j1}|^2(m^2_{\chi_j^\pm} - m^2_{\tilde{\nu}_\ell}), \tag{C.52}$$

$$\Sigma_D^a = -g^2|V_{j1}|^2 m_{\chi_j^\pm}(s^a_{\chi_j^\pm}\cdot p_\ell). \tag{C.53}$$

Here $s^a_{\chi_j^\pm}$ are the neutralino spin-vectors defined in Section C.1.4, and p_ℓ is the four-momentum of the lepton ℓ. The coefficient Σ_D^a for the charge conjugated process, $\tilde{\chi}_j^- \to \ell^-\ \tilde{\nu}_\ell^*$, is obtained by inverting the sign of (C.53).

The expansion coefficients of the chargino decay matrix, eq. (C.26), for $\tilde{\chi}_j^+ \to \tau^+\ \tilde{\nu}_\tau$ are

$$D = \frac{g^2}{2}(|V_{j1}|^2 + Y_\tau^2|U_{j2}|^2)(m^2_{\chi_j^\pm} - m^2_{\tilde{\nu}_\tau}), \tag{C.54}$$

$$\Sigma_D^a = -g^2(|V_{j1}|^2 - Y_\tau^2|U_{j2}|^2) m_{\chi_j^\pm}(s^a_{\chi_j^\pm}\cdot p_\tau). \tag{C.55}$$

The expansion coefficients for the decay $\tilde{\chi}_j^+ \to W^+\tilde{\chi}_k^0$ are

$$\begin{aligned} D = {} & \frac{g^2}{2}(|O^L_{kj}|^2 + |O^R_{kj}|^2)\left(m^2_{\chi_j^\pm} + m^2_{\chi_k^0} - 2m_W^2 + \frac{(m^2_{\chi_j^\pm} - m^2_{\chi_k^0})^2}{m_W^2}\right) \\ & -6g^2\mathrm{Re}\{O^L_{kj}O^{R*}_{kj}\} m_{\chi_j^\pm} m_{\chi_k^0}, \end{aligned} \tag{C.56}$$

$$\Sigma_D^a = g^2(|O^L_{kj}|^2 - |O^R_{kj}|^2)\,\frac{(m^2_{\chi_j^\pm} - m^2_{\chi_k^0} - 2m_W^2)}{m_W^2}\, m_{\chi_j^\pm}(s^a_{\chi_j^\pm}\cdot p_W). \tag{C.57}$$

With these definitions we can rewrite the factor Σ_D^3, eqs. (C.53), (C.55) and (C.57), in the CMS for $\lambda = e, \mu, \tau, W$, respectively,

$$\Sigma_D^3 = \eta_{\lambda\pm}\frac{D}{\Delta_\lambda}(E_\lambda - \bar{E}_\lambda), \tag{C.58}$$

where E_λ is the energy of λ, $\bar{E}_\lambda$ is defined in Section D.2.1 and given explicitly for $\lambda = e, \mu, \tau, W$, and we have used the relation

$$m_{\chi_j^\pm}(s^3_{\chi_j^\pm} \cdot p_\lambda) = -\frac{m^2_{\chi_j^\pm}}{|\vec{p}_{\chi_j^\pm}|}(E_\lambda - \bar{E}_\lambda). \tag{C.59}$$

The factor $\eta_{\lambda^\pm}$ is a measure of parity violation, which is maximal $\eta_{\ell^\pm} = \pm 1$ for the decay $\tilde{\chi}_j^\pm \to \ell^\pm \, \tilde{\nu}_\ell^{(*)}$, for $\ell = e, \mu$, since the sneutrino couples purely left handed.

The factor $\eta_{\lambda^\pm}$ (C.58) for the decay $\tilde{\chi}_j^\pm \to \tau^\pm \, \tilde{\nu}_\tau^{(*)}$ is given by

$$\eta_{\tau^\pm} = \pm\frac{|V_{j1}|^2 - Y_\tau^2|U_{j2}|^2}{|V_{j1}|^2 + Y_\tau^2|U_{j2}|^2}. \tag{C.60}$$

For the decay $\tilde{\chi}_j^\pm \to W^\pm \, \tilde{\chi}_k^0$ (C.56) and (C.57) lead to

$$\eta_{W^\pm} \;=\; \pm\frac{(|O^L_{kj}|^2 - |O^R_{kj}|^2)f_1}{(|O^L_{kj}|^2 + |O^R_{kj}|^2)f_2 + \mathrm{Re}\{O^L_{kj}O^{R*}_{kj}\}f_3}, \tag{C.61}$$

with

$$\begin{aligned} f_1 &= (m^2_{\chi_j^\pm} - m^2_{\chi_k^0} - 2m_W^2)\sqrt{\lambda(m^2_{\chi_j^\pm}, m_W^2, m^2_{\chi_k^0})}, \\ f_2 &= (m^2_{\chi_j^\pm} + m^2_{\chi_k^0} - 2m_W^2)\; m_W^2 + (m^2_{\chi_j^\pm} - m^2_{\chi_k^0})^2, \\ f_3 &= -12\; m_{\chi_j^\pm}\; m_{\chi_k^0}\; m_W^2. \end{aligned}$$

The factors Σ_D^1 and Σ_D^2, eqs. (C.53), (C.55) and (C.57), are

$$\Sigma_D^1 = \eta_{\lambda\pm} D \sin\theta_j \cos\varphi_j, \tag{C.62}$$

$$\Sigma_D^2 = \eta_{\lambda\pm} D \sin\theta_j \sin\varphi_j, \tag{C.63}$$

Here the polar and azimuth angles of $\lambda^\pm$ with respect to the the momentum of $\tilde{\chi}_j^\pm$ are defined in Section D.2.

C.4 Spin density matrix for neutralino production

C.4.1 Higgs exchange channels

The contributions to the density matrix from Z boson and slepton exchange can be found in [21] for neutralino production in e^+e^--annihilation. Therefore, in the t and u channels, the exchanged selectron needs to be substituted by a smuon. In addition, for $\alpha \neq \beta$, a factor two needs multiplied, due to a different definition of the spin density matrix contributions.

The contribution to the production spin density matrix from the Higgs boson exchange channels are

$$\begin{aligned} P_r(\alpha\beta) &= N^{(\alpha\beta)} g^4 \,\mathrm{Re}\{\Delta(\alpha)\Delta(\beta)^*\, \ell^{(\alpha\beta)}(\vec{\mathcal{P}}_+, \vec{\mathcal{P}}_-)\} \\ &\quad \Big[\mathrm{Re}(d_{ij}^{(\alpha)} d_{ij}^{(\beta)*})\,(p_i p_j) - \mathrm{Re}(d_{ij}^{(\alpha)} d_{ij}^{(\beta)})\,\eta_i\eta_j m_i m_j\Big]\,(p_1 p_2), \quad \text{(C.64)} \\ \Sigma^a_{r\,i}(\alpha\beta) &= N^{(\alpha\beta)} g^4 \,\mathrm{Im}\{\Delta(\alpha)\Delta(\beta)^*\, \ell^{(\alpha\beta)}(\vec{\mathcal{P}}_+, \vec{\mathcal{P}}_-)\} \\ &\quad \mathrm{Im}(\, d_{ij}^{(\alpha)} d_{ij}^{(\beta)*})\,\eta_i m_i\,(s_i^a p_j)(p_1 p_2), \quad \text{(C.65)} \\ \Sigma^b_{r\,j}(\alpha\beta) &= N^{(\alpha\beta)} g^4 \,\mathrm{Im}\{\Delta(\alpha)\Delta(\beta)^*\, \ell^{(\alpha\beta)}(\vec{\mathcal{P}}_+, \vec{\mathcal{P}}_-)\} \\ &\quad \mathrm{Im}(\, d_{ij}^{(\alpha)} d_{ij}^{(\beta)*})\,\eta_j m_j\,(s_j^b p_i)(p_1 p_2), \quad \text{(C.66)} \\ \Sigma_r^{ab}(\alpha\beta) &= N^{(\alpha\beta)} g^4 \,\mathrm{Re}\{\Delta(\alpha)\Delta(\beta)^*\, \ell^{(\alpha\beta)}(\vec{\mathcal{P}}_+, \vec{\mathcal{P}}_-)\} \\ &\quad \{\,\mathrm{Re}(\, d_{ij}^{(\alpha)} d_{ij}^{(\beta)*})\eta_i\eta_j m_i m_j\,(s_i^a s_j^b) \\ &\quad +\mathrm{Re}(\, d_{ij}^{(\alpha)} d_{ij}^{(\beta)})\,\left[\,(s_i^a p_j)(s_j^b p_i) - (s_i^a s_j^b)(p_i p_j)\,\right] \\ &\quad +\mathrm{Im}(\, d_{ij}^{(\alpha)} d_{ij}^{(\beta)})\,[s_i^a p_i s_j^b p_j]\,\}(p_1 p_2), \quad \text{(C.67)} \end{aligned}$$

where $N^{(\alpha\beta)} = 2 - \delta_{\alpha\beta}$ has been introduced in Section C.2.1, $\Delta(H)$ and $\Delta(A)$ are Breit-Wigner propagators, eq. (2.8). We used the short hand notation for momenta and masses

$$p_1 = p_{\mu^+}, \quad p_2 = p_{\mu^-}, \quad p_k = p_{\chi_k^0}, \quad m_k = m_{\chi_k^0}, \quad k = i, j, \qquad \text{(C.68)}$$

and for the spin vectors

$$s_i^a = s^a_{\chi_i^0}, \quad s_j^b = s^b_{\chi_j^0}. \qquad \text{(C.69)}$$

The function $[a\,b\,c\,d]$ has been defined in eq. (E.10). Further, the functions $\ell^{(\alpha\beta)}$ of the polarizations of the μ^+ and μ^- are given in Section C.2.1, eqs. (C.46-C.49),

C.4.2 General CP violating couplings

For CP non-conserving muon-Higgs and neutralino-Higgs couplings, given in eqs. (B.16) and (B.17), the spin density matrix coefficients, eqs. (C.64-C.67),

read

$$\begin{aligned} P_r(\alpha\beta) &= K_{ij}^{(\alpha\beta)}\,\mathrm{Re}\{\Delta(\alpha)\Delta(\beta)^*\,\ell'^{(\alpha\beta)}(\vec{\mathcal{P}}_+,\vec{\mathcal{P}}_-)\} \\ &\quad [\cos(\delta_{\alpha ij}-\delta_{\beta ij})\,(p_ip_j)-\cos(\delta_{\alpha ij}+\delta_{\beta ij})\,\eta_i\eta_j m_i m_j]\,(p_1p_2), \quad \text{(C.70)} \\ \Sigma^a_{r\,i}(\alpha\beta) &= K_{ij}^{(\alpha\beta)}\,\mathrm{Im}\{\Delta(\alpha)\Delta(\beta)^*\,\ell'^{(\alpha\beta)}(\vec{\mathcal{P}}_+,\vec{\mathcal{P}}_-)\} \\ &\quad \sin(\delta_{\alpha ij}-\delta_{\beta ij})\,\eta_i m_i\,(s_i^a p_j)(p_1p_2), \quad \text{(C.71)} \\ \Sigma^b_{r\,j}(\alpha\beta) &= K_{ij}^{(\alpha\beta)}\,\mathrm{Im}\{\Delta(\alpha)\Delta(\beta)^*\,\ell'^{(\alpha\beta)}(\vec{\mathcal{P}}_+,\vec{\mathcal{P}}_-)\} \\ &\quad \sin(\delta_{\alpha ij}-\delta_{\beta ij})\,\eta_j m_j\,(s_j^b p_i)(p_1p_2), \quad \text{(C.72)} \\ \Sigma^{ab}_{r}(\alpha\beta) &= K_{ij}^{(\alpha\beta)}\,\mathrm{Re}\{\Delta(\alpha)\Delta(\beta)^*\,\ell'^{(\alpha\beta)}(\vec{\mathcal{P}}_+,\vec{\mathcal{P}}_-)\} \\ &\quad \{\cos(\delta_{\alpha ij}-\delta_{\beta ij})\eta_i\eta_j m_i m_j\,(s_i^a s_j^b) \\ &\quad +\cos(\delta_{\alpha ij}+\delta_{\beta ij})\,\left[\,(s_i^a p_j)(s_j^b p_i)-(s_i^a s_j^b)(p_ip_j)\,\right] \\ &\quad +\sin(\delta_{\alpha ij}+\delta_{\beta ij})\,[s_i^a p_i s_j^b p_j]\,\}(p_1p_2), \quad \text{(C.73)} \end{aligned}$$

with

$$K_{ij}^{(\alpha\beta)} = N^{(\alpha\beta)} g^4 \bar{c}^{(\alpha\mu)}\bar{c}^{(\beta\mu)}\bar{d}_{ij}^{(\alpha)}\bar{d}_{ij}^{(\beta)}, \quad \text{(C.74)}$$

and

$$\begin{aligned} \ell'^{(\alpha\beta)} &= (1+\mathcal{P}_+^L\mathcal{P}_-^L)\,\cos(\xi_\alpha-\xi_\beta)\;+\;\mathcal{P}_+^T\mathcal{P}_-^T\,\cos(\xi_\alpha+\xi_\beta-\zeta_++\zeta_-) \\ &+\; i(\mathcal{P}_+^L+\mathcal{P}_-^L)\,\sin(\xi_\alpha-\xi_\beta). \quad \text{(C.75)} \end{aligned}$$

Here we used the short hand notation $\mathcal{P}_\pm^T \equiv |\vec{\mathcal{P}}_\pm^T|$. The coefficient $N^{(\alpha\beta)}$ has been defined in Section C.4.1. The laboratory angles ζ_+ and ζ_+ of $\vec{\mathcal{P}}_+^T$ and $\vec{\mathcal{P}}_-^T$, respectively, are defined Appendix Laboratory.reference.frame

C.5 Spin density matrix for neutralino decay

C.5.1 Two-body decays

The interaction Lagrangians are given in eqs. (B.28) and (B.31). The neutralino decay density matrix, eq. (C.26), is

$$\rho_D^{\lambda'_j\lambda_j} = \delta_{\lambda'_j\lambda_j}D + \sum_a \sigma^a_{\lambda'_j\lambda_j}\Sigma^a_D.$$

The expansion coefficients D and Σ^a_D for the two-body decay into a positive charged lepton of the first two generations and a right or left slepton are [46]:

$$\begin{aligned} D &= \frac{g^2}{2}|f^n_{\ell j}|^2(m^2_{\chi^0_j}-m^2_{\tilde{\ell}}), \quad \text{(C.76)} \\ \Sigma^a_D &= -\eta^n_{\ell^+}g^2|f^n_{\ell j}|^2 m_{\chi^0_j}(s^a_{\chi^0_j}\cdot p_\ell)\eta_j, \quad n=R,L, \quad \text{(C.77)} \end{aligned}$$

respectively, with $s^a_{\chi^0_j}$ the neutralino spin-vector defined in Section C.1.4, p_ℓ the lepton four-momentum, and $\eta^R_{\ell^+} = -1$ and $\eta^L_{\ell^+} = 1$. The couplings $f^n_{\ell j}$ are defined in eqs. (B.29) and (B.30).

In the CMS

$$\Sigma^3_D = \eta^n_{\ell^+} g^2 |f^n_{\ell j}|^2 \frac{m^2_{\chi^0_j}}{|\vec{p}_{\chi^0_j}|}(E_\ell - \bar{E}_\ell), \tag{C.78}$$

$$\bar{E}_\ell = \frac{m^2_{\chi^0_j} - m^2_{\tilde{\ell}}}{2m^2_{\chi^0_j}} E_{\chi^0_j}. \tag{C.79}$$

For the decay $\tilde{\chi}^0_j \to \tau^+ \tilde{\tau}^-_n,\ n = 1, 2$ the coefficients are

$$D = \frac{g^2}{2}(|a^{\tilde{\tau}}_{nj}|^2 + |b^{\tilde{\tau}}_{nj}|^2)(m^2_{\chi^0_j} - m^2_{\tilde{\tau}}), \tag{C.80}$$

$$\Sigma^a_D = g^2(|a^{\tilde{\tau}}_{nj}|^2 - |b^{\tilde{\tau}}_{nj}|^2) m_{\chi^0_j}(s^a_{\chi^0_j} \cdot p_\ell)\eta_j. \tag{C.81}$$

The couplings $a^{\tilde{\tau}}_{nj}, n = 1, 2$ are defined in eq. (B.32).

In the CMS

$$\Sigma^3_D = -\eta^n_{\tau^+} g^2(|a^{\tilde{\tau}}_{nj}|^+ |b^{\tilde{\tau}}_{nj}|^2) \frac{m^2_{\chi^0_j}}{|\vec{p}_{\chi^0_j}|}(E_\tau - \bar{E}_\tau)\eta_j, \quad n = 1, 2, \tag{C.82}$$

$$\bar{E}_\tau = \frac{m^2_{\chi^0_j} - m^2_{\tilde{\tau}}}{2m^2_{\chi^0_j}} E_{\chi^0_j}, \tag{C.83}$$

with the stau decay factor is given by

$$\eta^n_{\tau^\pm} = \pm \frac{|a^{\tilde{\tau}}_{nj}|^2 - |b^{\tilde{\tau}}_{nj}|^2}{|a^{\tilde{\tau}}_{nj}|^2 + |b^{\tilde{\tau}}_{nj}|^2}, \tag{C.84}$$

The decay density matrix coefficients for the charge conjugated processes, $\tilde{\chi}^0_j \to \ell^- \tilde{\ell}^+_n, n = R, L$ and $\tilde{\chi}^0_j \to \tau^- \tilde{\tau}^+_n, n = 1, 2$ are obtained exchanging $\eta^n_{\lambda^+}$, $\lambda = e, \mu, \tau$, with $\eta^n_{\lambda^-} = -\eta^n_{\lambda^+}$ in eqs. (C.77), (C.78), (C.81) and (C.83), which corresponds to inverting the sign of Σ^a_D.

Appendix D

Kinematics and phase space

D.1 Reference frames

In this section we define the laboratory reference frame R_{Lab} and give the momenta of the muons, charginos or neutralinos. Then we define the momenta of the two-body decays of the charginos or neutralinos and give the kinematical limits as a function of the energy of the decay particles.

D.1.1 Laboratory reference frame

The laboratory reference frame R_{Lab}, with basis vectors $\{\hat{x}_{Lab}, \hat{y}_{Lab}, \hat{z}_{Lab}\}$, is defined here with respect to the the momentum of μ^-. Denoting with $\hat{e}_r$ the unit vector pointing from the center of the muon storage ring outward the basis vectors are given by

$$\hat{z}_{Lab} = \vec{p}_{\mu^-}/|\vec{p}_{\mu^-}|, \qquad \hat{x}_{Lab} = -\hat{e}_r, \qquad \hat{y}_{Lab} = \hat{z}_{Lab} \times \hat{x}_{Lab}. \tag{D.1}$$

This reference frame is independent of the production process and thus useful to study transverse beam and chargino polarization effects.

The momentum of the charginos $\tilde{\chi}_i^{\mp}$ and $\tilde{\chi}_j^{\pm}$ (neutralinos $\tilde{\chi}_i^0$ and $\tilde{\chi}_j^0$), denoted with χ_i and χ_j, respectively, have been defined in the chargino (neutralino) reference frame R_{χ_j}, see Section C.1.4. In R_{Lab} these four-momenta are given by

$$p^{\nu}_{\chi_j} = (E_{\chi_j}; \vec{p}_{\chi_j}), \qquad p^{\nu}_{\chi_i} = (E_{\chi_i}; -\vec{p}_{\chi_j}), \tag{D.2}$$

with

$$\vec{p}_{\chi_j} = |\vec{p}_{\chi_j}|(\sin\theta_{Lab}\cos\varphi_{Lab}, \sin\theta_{Lab}\sin\varphi_{Lab}, \cos\theta_{Lab}), \tag{D.3}$$

which define the production polar and azimuth angles $\theta_{Lab} \equiv \theta_p$ and $\varphi_{Lab} \equiv \varphi_p$.

Analogously, the momentum of the muon is given in R_{χ_j} by

$$\vec{p}_{\mu^-} = |\vec{p}_{\mu^-}|(-\sin\theta, 0, \cos\theta)_{\chi_j}. \tag{D.4}$$

D.1.2 Reference frame $R^{Lab}_{\chi_j}$

We define the reference frame $R^{Lab}_{\chi_j}$ obtained from R_{χ_j} rotating the $x-y$ plane with the production azimuth angle φ_p so that the $\hat{y} = \hat{y}_{Lab}$. The momentum of the muon is then

$$\vec{p}_{\mu^-} = |\vec{p}_{\mu^-}|(-\sin\theta\cos\varphi, -\sin\theta\sin\varphi, \cos\theta)_{\chi_j^{Lab}}. \tag{D.5}$$

D.1.3 Muon reference frames

We define the μ^+ and μ^--reference frames $\{\hat{x}_\pm, \hat{y}_\pm, \hat{z}_\pm\}$ for the production process $\mu^+\mu^- \to \chi_i\chi_j$, where χ_i and χ_j denote either charginos or neutralinos. The z-axis is given by the direction of the corresponding muon, i.e.

$$\hat{z}_\pm = \frac{\vec{p}_{\mu^\pm}}{|\vec{p}_{\mu^\pm}|} \equiv \vec{n}_\pm, \tag{D.6}$$

and the x and y axes lie, respectively, on the production plane and perpendicular to it. We choose

$$\hat{y}_+ = \hat{y}_- = \frac{(\vec{p}_{\mu^-} \times \vec{p}_{\chi_j})}{|\vec{p}_{\mu^-} \times \vec{p}_{\chi_j}|}. \tag{D.7}$$

Then

$$\hat{x}_+ = -\hat{x}_- = \hat{y}_+ \times \hat{z}_+. \tag{D.8}$$

D.2 Two-body decays of charginos and neutralinos

In this section we define the momenta for the two-body decays of the chargino (2.2) and (2.3) and of the neutralino (3.2), denoted here $\tilde{\chi}^\pm_k \to \lambda^\pm_k \tilde{N}$ and $\tilde{\chi}^0_k \to \lambda^\pm_k \tilde{\Lambda}^\mp$, respectively, where $\tilde{N}$ and $\tilde{\Lambda}$ are the supersymmetric decay particles and $k = i, j$.

We express the momenta of the standard model decay particles λ_i and λ_j as a function of the polar and azimuth angles θ_i, φ_i and θ_j, φ_j, respectively, defined with respect to the momentum of the chargino or neutralino χ_j

$$\vec{p}_{\lambda_j} = |\vec{p}_{\lambda_j}|(\sin\theta_j\cos\varphi_j, \sin\theta_j\sin\varphi_j, \cos\theta_j)_{\chi_j}, \tag{D.9}$$

$$\vec{p}_{\lambda_i} = |\vec{p}_{\lambda_i}|(\sin\theta_i\cos\varphi_i, \sin\theta_i\sin\varphi_i, \cos\theta_i)_{\chi_j}. \tag{D.10}$$

This corresponds to the reference frame R_{χ_j}, Section C.1.4, In the reference frame $R^{Lab}_{\chi_j}$, Section D.1.2, the momenta of λ_i and λ_j are obtained from eqs. (D.9) and (D.10) substituting φ_k with $\varphi_k - \varphi_p$, $k = i, j$.

D.2.1 Kinematical limits for charginos and neutralinos

In the center of mass system of the two produced charginos (CMS), the kinematical limits of the energy of the decay particle $\lambda = e, \mu, \tau, W$ from the chargino decays (2.2) and (2.3) are

$$E_\lambda^{max(min)} = \bar{E}_\lambda \pm \Delta_\lambda, \tag{D.11}$$

which read for the leptonic ($\lambda = \ell$) chargino decays

$$\bar{E}_\ell = \frac{E_\ell^{max} + E_\ell^{min}}{2} = \frac{m^2_{\chi_j^\pm} - m^2_{\tilde{\nu}_\ell}}{2m^2_{\chi_j^\pm}} E_{\chi_j^\pm}, \tag{D.12}$$

$$\Delta_\ell = \frac{E_\ell^{max} - E_\ell^{min}}{2} = \frac{m^2_{\chi_j^\pm} - m^2_{\tilde{\nu}_\ell}}{2m^2_{\chi_j^\pm}} |\vec{p}_{\chi_j^\pm}|, \qquad \ell = e, \mu, \tau. \tag{D.13}$$

For the decays into a W-boson and a neutralino, eq. (D.11) reads

$$\bar{E}_W = \frac{E_W^{max} + E_W^{min}}{2} = \frac{m^2_{\chi_j^\pm} + m^2_W - m^2_{\chi_k^0}}{2m^2_{\chi_j^\pm}} E_{\chi_j^\pm}, \tag{D.14}$$

$$\Delta_W = \frac{E_W^{max} - E_W^{min}}{2} = \frac{\sqrt{\lambda(m^2_{\chi_j^\pm}, m^2_W, m^2_{\chi_k^0})}}{2m^2_{\chi_j^\pm}} |\vec{p}_{\chi_j^\pm}|, \tag{D.15}$$

with $\lambda(x, y, z) = x^2 + y^2 + z^2 - 2xy - 2xz - 2yz$.

The kinematical limits of the two-body decays of neutralinos in the CMS, $\tilde{\chi}_j^0 \to \lambda^\pm \tilde{N}^\mp$, with $\lambda = e, \mu, \tau, Z$ are parametrized by $\bar{E}_\lambda$ and Δ_λ, as in eq. (D.11). For the leptonic decays of the neutralino ($\lambda = \ell$) the kinematical limits are given by

$$\bar{E}_\ell = \frac{E_\ell^{max} + E_\ell^{min}}{2} = \frac{m^2_{\chi_j^0} - m^2_{\tilde{\ell}_X}}{2m^2_{\chi_j^0}} E_{\chi_j^0}, \tag{D.16}$$

$$\Delta_\ell = \frac{E_\ell^{max} - E_\ell^{min}}{2} = \frac{m^2_{\chi_j^0} - m^2_{\tilde{\ell}_X}}{2m^2_{\chi_j^0}} |\vec{p}_{\chi_j^0}|, \tag{D.17}$$

with $\tilde{\ell}_X^\pm = \tilde{\ell}_{L,R}^\pm$ for $\ell = e, \mu$ and $\tilde{\ell}_X^\pm = \tilde{\tau}_{1,2}^\pm$ for $\ell = \tau$.

For the decays of a neutralino into a Z-boson and another neutralino, eq. (D.11) reads

$$\bar{E}_Z = \frac{E_Z^{max} + E_Z^{min}}{2} = \frac{m^2_{\chi_j^0} + m^2_Z - m^2_{\chi_k^0}}{2m^2_{\chi_j^0}} E_{\chi_j^0}, \tag{D.18}$$

$$\Delta_Z = \frac{E_Z^{max} - E_Z^{min}}{2} = \frac{\sqrt{\lambda(m^2_{\chi_j^0}, m^2_Z, m^2_{\chi_k^0})}}{2m^2_{\chi_j^0}} |\vec{p}_{\chi_j^0}|, \tag{D.19}$$

D.3 Phase space

The Lorentz invariant phase space for the production of n particles is given by

$$d\text{Lips}(p; p_1, \ldots, p_n) = (2\pi)^4 \delta^{(4)}(p - \sum_k p_k) \prod_k \frac{1}{(2\pi)^3} d^3 p_k, \tag{D.20}$$

where p is the total momenta of the system, in the CMS $p = (\sqrt{s}, \vec{0})$ and p_k is the momentum of k-th final particle.

D.3.1 Chargino and neutralino production

For chargino (neutralino) pair production in $\mu^+\mu^-$ annihilation, eq (D.20) reads in the CMS, after integration over the momentum of the chargino (neutralino) χ_i and the energy of χ_j

$$d\text{Lips}(p; p_{\chi_i}, p_{\chi_j}) = \frac{q}{16\pi^2\sqrt{s}} d\Omega_{\chi_j}, \tag{D.21}$$

where $q = |\vec{p}_{\chi_i}| = |\vec{p}_{\chi_j}|$, $p = p_{\mu^+} + p_{\mu^-} = (\sqrt{s}, \vec{0})$, and Ω_{χ_j} is the solid angle of χ_j, with $d\Omega_{\chi_j} = \sin\theta_j d\theta_j d\varphi_j$, with θ_j and φ_j its polar and azimuth angles in some reference system in the CMS. If the amplitude squared is independent of the azimuth angle, we integrate over φ_j in eq. (D.21) and obtain

$$d\text{Lips}(p; p_{\chi_i}, p_{\chi_j}) = \frac{q}{8\pi\sqrt{s}} \sin\theta_j d\theta_j. \tag{D.22}$$

D.3.2 Pair production with subsequent two-body decays

The Lorentz invariant phase space for the decay of a chargino (neutralino) with momentum p_{χ_j} is obtained from eq. (D.20) with $p = p_{\chi_j}$ and $p_1, \ldots, p_n$ the momenta of the final particles. In general the decaying chargino (neutralino) is not on shell and its momentum p_{χ_j} is a free parameter. However, since charginos and neutralinos decay weakly their decay widths Γ_{χ_j} are small compared to their masses. When two-body decays are allowed $\Gamma_{\chi_j} \sim \mathcal{O}(\text{GeV})$, while for three-body decays $\Gamma_{\chi_j} \ll 1\text{GeV}$. Therefore the chargino (neutralino) will be nearly on shell, with $p^2_{\chi_j} \simeq m^2_{\chi_j}$.

The Lorentz invariant phase space for the production of a pair of charginos (neutralinos) with the subsequent two-body decay of one of the charginos (neutralinos) is obtained multiplying the phase space for chargino (neutralino) pair production times the phase space for chargino (neutralino) decay times the chargino (neutralino) propagator,

$$d\text{Lips} = \int_{p_{\chi_j}} d\text{Lips}(p_{\mu^+} + p_{\mu^-}; p_{\chi_i}, p_{\chi_j}) |\Delta(\chi_j)|^2 d\text{Lips}(p_{\chi_j}; p_{j1}, p_{j2}). \tag{D.23}$$

Since the decaying chargino (neutralino) is nearly on shell we use the narrow width approximation, see f.i. [22], and replace

$$|\Delta(\chi_j)|^2 \to \frac{\pi}{m_{\chi_j}\Gamma_{\chi_j}}\delta(s_{\chi_j} - m^2_{\chi_j}), \tag{D.24}$$

where m_{χ_j} is the mass of the chargino or neutralino χ_j, Γ_{χ_j} its width, and $s_{\chi_j} = p^2_{\chi_j}$.

For the subsequent decay of both charginos or neutralinos it follows,

$$\begin{aligned} d\text{Lips} &= \int_{p_{\chi_i}p_{\chi_j}} d\text{Lips}(p_{\mu^+} + p_{\mu^-}; p_{\chi_i}, p_{\chi_j})|\Delta(\chi_j)|^2|\Delta(\chi_i)|^2 \\ &\quad d\text{Lips}(p_{\chi_j}; p_{i1}, p_{i2})d\text{Lips}(p_{\chi_j}; p_{j1}, p_{j2}), \end{aligned} \tag{D.25}$$

and the corresoponding substitutions for $|\Delta(\chi_i)|^2$ and $|\Delta(\chi_j)|^2$.

D.4 Statistical significances

In this section we define statistical significances for the asymmetries for $\tilde{\chi}_1^{\pm}\tilde{\chi}_2^{\mp}$ production, chargino pair production with subsequent decay of one of the charginos and for neutralino pair production and subsequent decay, given in Chapters 2 and 3.1.

The statistical significance for the measurement of an asymmetry $\mathcal{A}$ obtained in a process with cross section σ and luminosity $\mathcal{L}$ can be defined by

$$\mathcal{S} = |\mathcal{A}|\sqrt{\sigma \times \mathcal{L}.} \tag{D.26}$$

Eq. D.26 assumes that $\mathcal{A} \ll 1$ and will be used here. A more exact definition would be

$$\mathcal{S}' = \frac{1}{\sqrt{1-A^2}}|\mathcal{A}|\sqrt{\sigma \times \mathcal{L}}, \tag{D.27}$$

which takes into account the fact that the absolute value of the asymmetry is bounded.

D.4.1 Chargino production and decay

• $\mu^+\mu^- \to \tilde{\chi}_1^{\pm}\tilde{\chi}_2^{\mp}$

For the asymmetries for $\tilde{\chi}_1^{\pm}\tilde{\chi}_2^{\mp}$ production discussed in Chapter 2 we define statistical significances for an effective integrated luminosity for chargino production $\mathcal{L}_{eff}^{prod}$. For the charge asymmetry $\mathcal{A}^C_{prod}$, eq. (2.28), we define statistical significance

$$\mathcal{S}^C_{prod} = |\mathcal{A}^C_{prod}|\sqrt{[\sigma(\tilde{\chi}_1^+\tilde{\chi}_2^-) + \sigma(\tilde{\chi}_2^+\tilde{\chi}_1^-)]\mathcal{L}_{eff}^{prod}}. \tag{D.28}$$

Here we assume that the cross sections $\sigma(\tilde{\chi}_1^+\tilde{\chi}_2^-)$ and $\sigma(\tilde{\chi}_2^+\tilde{\chi}_1^-)$ are both obtained with the same effective luminosity.

For the polarization asymmetry $\mathcal{A}^{pol}_{prod}$, eq. (2.29), we define statistical significance

$$\mathcal{S}^{pol}_{prod} = |\mathcal{A}^{pol}_{prod}|\sqrt{[\sigma(\tilde{\chi}_1^+\tilde{\chi}_2^-)(\mathcal{P}) + \sigma(\tilde{\chi}_1^+\tilde{\chi}_2^-)(-\mathcal{P})]\mathcal{L}^{prod}_{eff}}. \tag{D.29}$$

Here we assume that the cross sections $\sigma(\tilde{\chi}_1^+\tilde{\chi}_2^-)(\mathcal{P})$ and $\sigma(\tilde{\chi}_1^+\tilde{\chi}_2^-)(-\mathcal{P})$ are both obtained with the same luminosity.

• $\mu^+\mu^- \to \tilde{\chi}_i^\mp\tilde{\chi}_j^\pm$, $\tilde{\chi}_j^\pm \to \lambda^\pm\tilde{N}_\lambda$

For the asymmetry $\mathcal{A}_{\lambda^\pm}$, eq. (2.42), for chargino pair production with subsequent two-body decay of one of the charginos we define statistical significance

$$\mathcal{S}_{\lambda^\pm} = |\mathcal{A}_{\lambda^\pm}|\sqrt{\sigma(\mu^+\mu^- \to \tilde{\chi}_i^\mp\tilde{\chi}_j^\pm)\mathrm{BR}(\tilde{\chi}_j^\pm \to \lambda^\pm\tilde{N}_\lambda)\mathcal{L}_{eff}}, \tag{D.30}$$

with $\lambda = \ell$ or W and $\tilde{N}_\lambda$ the associated sneutrino or neutralino, respectively.

Further the effective integrated luminosity $\mathcal{L}_{eff} = \epsilon_\lambda\mathcal{L}$ depends on the detection efficiency ϵ_λ of leptons or W bosons in the processes $\tilde{\chi}_j^\pm \to \ell^\pm\,\tilde{\nu}_\ell^{(*)}$ or $\tilde{\chi}_j^\pm \to W^\pm\,\tilde{\chi}_k^0$, respectively.

The statistical significance for the charge asymmetry $\mathcal{A}^C_\lambda$, eq. (2.50), is given by

$$\mathcal{S}^C_\lambda = |\mathcal{A}^C_\lambda|\sqrt{2\,\sigma(\mu^+\mu^- \to \tilde{\chi}_i^-\tilde{\chi}_j^+)\mathrm{BR}(\tilde{\chi}_j^+ \to \lambda^+\tilde{N}_\lambda)\mathcal{L}_{eff}}. \tag{D.31}$$

Assuming that $\mathcal{A}_{\lambda^\pm}(\mathcal{P})$ and $\mathcal{A}_{\lambda^\pm}(-\mathcal{P})$ are both obtained with the same integrated luminosity $\mathcal{L}$, we define the statistical significance for the polarization asymmetry $\mathcal{A}^{pol}_{\lambda^\pm}$, eq. (2.52), by

$$\mathcal{S}^{pol}_{\lambda^\pm} = |\mathcal{A}^{pol}_{\lambda^\pm}|\sqrt{2\,\sigma(\mu^+\mu^- \to \tilde{\chi}_i^\mp\tilde{\chi}_j^\pm)\mathrm{BR}(\tilde{\chi}_j^\pm \to \lambda^\pm\tilde{N}_\lambda)\mathcal{L}_{eff}}. \tag{D.32}$$

D.4.2 Neutralino production and decay

• $\mu^+\mu^- \to \tilde{\chi}_i^0\tilde{\chi}_j^0$, $\tilde{\chi}_j^0 \to \lambda^\pm\tilde{N}_\lambda^\mp$

For the (charge) asymmetry $\mathcal{A}^n_\ell$ of neutralino pair production with subsequent two-body decay of one of the neutralinos, eq. (3.34), we define the statistical significance

$$\mathcal{S}^n_\ell = |\mathcal{A}^n_\ell|\sqrt{2\sigma(\mu^+\mu^- \to \tilde{\chi}_i^0\tilde{\chi}_j^0)BR(\tilde{\chi}_j^0 \to \ell^-\tilde{\ell}_n^+)\mathcal{L}_{eff}}, \tag{D.33}$$

where $\mathcal{L}_{eff} = \epsilon^n_\ell\mathcal{L}$ denotes the effective integrated luminosity, with ϵ^n_ℓ the detection efficiency of the leptons in the processes $\tilde{\chi}_j^0 \to \ell^\mp\tilde{\ell}_n^\pm$ and $\mathcal{L}$ the integrated luminosity.

Appendix E

Definitions and conventions

We use the metric tensor

$$g^{\mu\nu} = g_{\mu\nu} := \begin{pmatrix} 1 & 0 & 0 & 0 \\ 0 & -1 & 0 & 0 \\ 0 & 0 & -1 & 0 \\ 0 & 0 & 0 & -1 \end{pmatrix} \tag{E.1}$$

Covariant and contravariant four-vectors are defined by, respectively

$$a^{\mu} := (a^0, a^1, a^2, a^2, a^3), \quad a_{\mu} := g_{\mu\nu} a^{\mu} = (a_0, a_1, a_2, a_2, a_3), \tag{E.2}$$

with the scalar product

$$g_{\mu\nu} a^{\mu} b^{\nu} = a^{\mu} b_{\mu}. \tag{E.3}$$

The Dirac matrices in the Weyl representation are

$$\gamma^0 = \begin{pmatrix} 0 & \mathrm{I} \\ \mathrm{I} & 0 \end{pmatrix}, \quad \gamma^i = \begin{pmatrix} 0 & \sigma^j \\ -\sigma^j & 0 \end{pmatrix}, \quad j = 1, 2, 3, \tag{E.4}$$

$$\gamma^5 = i\gamma^0\gamma^1\gamma^2\gamma^3 = \begin{pmatrix} \mathrm{I} & 0 \\ 0 & -\mathrm{I} \end{pmatrix}, \tag{E.5}$$

where I denotes the 2×2 unity matrix. and the Pauli matrices are ,

$$\sigma^1 = \begin{pmatrix} 0 & 1 \\ 1 & 0 \end{pmatrix}, \quad \sigma^2 = \begin{pmatrix} 0 & -i \\ i & 0 \end{pmatrix}, \quad \sigma^3 = \begin{pmatrix} 1 & 0 \\ 0 & -1 \end{pmatrix}, \tag{E.6}$$

The Dirac matrices obey the Clifford algebra relations

$$\{\gamma^{\mu}, \gamma^{\nu}\} = 2g^{\mu\nu}. \tag{E.7}$$

The left and right chirality projectors are

$$P_{L,R} = \frac{1}{2}(1 \mp \gamma^5). \tag{E.8}$$

The total antisymmetric ϵ-tensor in four dimensions is defined as

$$\epsilon_{\mu\nu\alpha\beta} = -\epsilon^{\mu\nu\alpha\beta} = \begin{cases} +1 & \text{odd permutation of } \mu,\nu,\alpha,\beta = 0,1,2,3, \\ -1 & \text{even permutation of } \mu,\nu,\alpha,\beta = 0,1,2,3, \\ 0 & \text{any two indices are equal.} \end{cases} \tag{E.9}$$

The total antisymmetric function of four-momenta is defined by

$$[a,b,c,d] = \frac{i}{4}\mathrm{Tr}\{\not{a}\not{b}\not{c}\not{d}\gamma^5\} = \epsilon_{\alpha\beta\gamma\delta}a^\alpha b^\beta c^\gamma d^\delta. \tag{E.10}$$

Triangle function

$$\lambda(x,y,z) = x^2 + y^2 + z^2 - 2(xy + xz + yz). \tag{E.11}$$

The function $\lambda(s, m_i^2, m_j^2)$ can also be expressed as

$$\lambda(s, m_i^2, m_j^2) \;=\; s^2 - 2s(m_i^2 + m_j^2) + (m_i^2 - m_j^2)^2, \tag{E.12}$$

which for $m_i = m_j \equiv m$ simplifies (reduces) to $\lambda = s(s - 4m^2)$.

In the center of mass system (CMS) the absolute value of the momenta of the particles i and j, $|\vec{p}_i| = |\vec{p}_j| \equiv |\vec{p}|$ is

$$\lambda(s, m_i^2, m_j^2) \;=\; 4s|\vec{p}|^2. \tag{E.13}$$

Physical constants

For numerical calculations we have used the values

$$\begin{array}{rcll} \alpha & = & 1/128 & \mathrm{fine-structure\ constant\ at\ 500\ GeV} \\ \sin^2\theta_W & = & 0.2315 & \mathrm{weak\ mixing\ angle} \\ m_W & = & 80.41\ \mathrm{GeV} & W\ \mathrm{boson\ mass} \\ \Gamma_W & = & 2.12\ \mathrm{GeV} & W\ \mathrm{boson\ width} \\ m_Z & = & 91.187\ \mathrm{GeV} & Z\ \mathrm{boson\ mass} \\ \Gamma_Z & = & 2.49\ \mathrm{GeV} & Z\ \mathrm{boson\ width} \end{array} \tag{E.14}$$

Bibliography

[1] S. L. Glashow, Nucl. Phys. **22** (1961) 579;
S. Weinberg, Phys. Rev. Lett. **19** (1967) 1264;
A. Salam, in "Elementary Particle Theory", ed. N. Svartholm, Almqvist and Wiskells, Stockolm (1969), p. 367.

[2] M. Gell-Mann, Phys. Lett. **8** (1964) 214; G. Zweig, CERN-Report 8182/TH401 (1964); H. Fritzsch, M. Gell-Mann and H. Leutwyler, Phys. Lett. B **47** (1973) 365; D. Gross and F. Wilczek, Phys. Rev. Lett. **30** (1973) 1343; H.D. Politzer, Phys. Rev. Lett. **30** (1973) 1346; G. 't Hooft, Marseille Conference on Yang–Mills fields (1972).

[3] P.W. Higgs, Phys. Rev. Lett. **13** (1964) 508; *ibid.* Phys. Rev. **145** (1966) 1156; F. Englert and R. Brout, Phys. Rev. Lett. **13** (1964) 321; G.S. Guralnik, C.R. Hagen and T. Kibble, Phys. Rev. Lett. **13** (1965) 585; T. Kibble, Phys. Rev. **155** (1967) 1554.

[4] J. Wess and B. Zumino, Nucl. Phys. B **70** (1974) 39;
R. Haag, J. T. Lopuszanski and M. Sohnius, Nucl. Phys. B **88** (1975) 257;
J. Wess and V. D. Bager, *Supersymmetry and Supergravity*, Princeton Series in Physics, New Jersey, 1992.

[5] J. Ellis, S. Kelley and D.V. Nanopoulos, Phys. Lett. **B260** (1991) 131; U. Amaldi, W. de Boer and H. Fürstenau, Phys. Lett. B **260** (1991) 447; P. Langacker and M. Luo, Phys. Rev. D **44** (1991) 817; C. Giunti, C.W. Kim and U.W. Lee, Mod. Phys. Lett. A **6** (1991) 1745.

[6] G.R. Farrar and P. Fayet, Phys. Lett. B **76** (1978) 575.

[7] E. Witten, Nucl. Phys. B **188** (1981) 513; *ibid* Nucl. Phys. B**202** (1982) 253; N. Sakai, Z. Phys. C **11** (1981) 153; S. Dimopoulos and H. Georgi, Nucl. Phys. B **193** (1981) 150; R.K. Kaul and P. Majumdar, Nucl. Phys. B **199** (1982) 36.

[8] P. Fayet, Nucl. Phys. B **90** (1975) 104; *ibid.* Phys. Lett. B **64** (1976) 159; *ibid.* Phys. Lett. B **69** (1977) 489; *ibid.* Phys. Lett. B **84** (1979) 416.

[9] TESLA Technical Design Report, DESY 2001-011 *Part III: Physics at an e+e- Linear Collider*, hep-ph/0106315;
ACFA Linear Collider Working Group, KEK Report 2001-11, hep-ph/0109166;
T. Abe et al., *Linear collider physics resource book for Snowmass 2001. 2: Higgs and supersymmetry studies*, in *Proc. of the APS/DPF/DPB Summer Study on the Future of Particle Physics (Snowmass 2001)* ed. R. Davidson and C. Quigg, hep-ex/0106056.

[10] B. Badelek *et al.*, *The Photon Collider at TESLA*, hep-ph/0108012; A. de Roeck, hep-ph/0311138; E. Boos *et al.*, Nucl. Instrum. Meth. A **472** (2001) 100;
M.M. Velasco *et al.*, *Photon–Photon and Electron-Photon Colliders with energies below a TeV*, Snowmass 2001 Study, hep-ex/0111055; D. Asner, J. Gronberg and J. F. Gunion, Phys. Rev. D67 (2003) 035009.

[11] M. M. Mühlleitner, M. Krämer, M. Spira, P. M. Zerwas, Phys. Lett. B **508** (2001) 311.

[12] V. Barger, M. S. Berger, J. F. Gunion and T. Han, Phys. Rept. **286** (1997) 1; *ibid.* in *Proc. of the APS/DPF/DPB 2001 Snowmass Study*, hep-ph/0110340;
J. F. Gunion, hep-ph/9707379 and hep-ph/9802258;
B. Autin, A. Blondel and J. Ellis (conv.) *et al.*, *Prospective Study of Muon Storage Rings at CERN*, CERN Report 99–02 (1999);
A. Blondel *et al.*, "ECFA/CERN studies of a European neutrino factory complex," CERN-2004-002.

[13] C. Blöchinger *et al.*, *Physics Opportunities at $\mu^+\mu^-$ Higgs Factories,* hep-ph/0202199.

[14] V. D. Barger, M. S. Berger, K. Fujii, J. F. Gunion, T. Han, C. Heusch, W. Hong, S. K. Oh, Z. Parsa, S. Rajpoot, R. Thun and B. Willis: *Physics Goals of a $\mu^+\mu^-$ Collider*, hep-ph/9503258;
V. D. Barger et al.: *Physics goals of a $\mu^+\mu^-$ collider*, *AIP Conf. Proc.*, 352:55–69, 1996;
J. F. Gunion: *Higgs Physics at a Muon Collider*, hep-ph/9703203;
J. F. Gunion: *Muon Colliders: The Machine and The Physics*, hep-ph/9707379v2;
V. D. Barger, M. S. Berger, J. F. Gunion and T. Han: *Higgs Boson Physics in the s-channel at $\mu^+\mu^-$ colliders*, Phys. Rep. **286**, (1997);
M. Demarteau and T. Han: *Higgs Boson and Z Physics at the First Muon Collider*, hep-ph/9801407;
V. D. Barger: *Overview of Physics at a Muon Collider*, hep-ph/9803480.

[15] *Higgs Bosons at a Muon Collider*, Snowmass 2001, P1 Group, 2001. hep-ph/0110390;
The Physics of Higgs Factories, Snowmass 2001, E1 Group, 2001. hep-ph/0110340.

[16] R. Casalbuoni et al., JHEP **9908** (1999) 011;
V. D. Barger, M.S. Berger, J. F. Gunion, T. Han, in *Proc. of the APS/DPF/DPB Summer Study on The Future of Particle Physics (Snowmass 2001)*, ed. R. Davidson and C. Quigg, [arXiv:hep-ph/0110340];
V. D. Barger, M.S. Berger, J. F. Gunion, T. Han, Nucl. Phys. Proc. Suppl. **51A** (1996) 13.

[17] J. L. Kneur, G. Moultaka, Phys. Rev. D **59** (1999) 015005;
S.Y. Choi, A. Djouadi, M. Guchait, J. Kalinowski, H.S. Song, P.M. Zerwas, Eur. Phys. J. C **14** (2000) 535;
G. Moortgat-Pick, H. Fraas, A. Bartl, W. Majerotto, Eur. Phys. J. C **18** (2000) 379.

[18] S. Heinemeyer, W. Hollik and G. Weiglein, Phys. Lett. B **455** (1999) 179 [arXiv:hep-ph/9903404];
G. Degrassi, S. Heinemeyer, W. Hollik, P. Slavich and G. Weiglein, Eur. Phys. J. C **28** (2003) 133 [arXiv:hep-ph/0212020];
S. Heinemeyer, W. Hollik, H. Rzehak and G. Weiglein, Eur. Phys. J. C **39** (2005) 465 [arXiv:hep-ph/0411114].

[19] The LEP Collaborations (ALEPH, DELPHI, L3 and OPAL), the LEP Electroweak Working Group and the SLD Heavy Flavour Group, *A combination of preliminary Electroweak measurements and constraints on the Standard Model*, hep-ex/0412015; `http://lepewwg.web.cern.ch/LEPEWWG`.

[20] G. Moortgat-Pick, H. Fraas, A. Bartl and W. Majerotto, Eur. Phys. J. C **7** (1999) 113 [arXiv:hep-ph/9804306].

[21] G. Moortgat-Pick, H. Fraas, A. Bartl and W. Majerotto, Eur. Phys. J. C **9** (1999) 521 [Erratum-ibid. C **9** (1999) 549] [arXiv:hep-ph/9903220].

[22] G. Moortgat-Pick, "Spin effects in chargino / neutralino production and decay, " Doktoral thesis, Würzburg 1999.

[23] E. Asakawa, A. Sugamoto and I. Watanabe, Eur. Phys. J. C **17** (2000) 279 [arXiv:hep-ph/0004005];
E. Asakawa, S. Y. Choi and J. S. Lee, at muon colliders," Phys. Rev. D **63**, 015012 (2001) [arXiv:hep-ph/0005118].

[24] O. Kittel and F. von der Pahlen, arXiv:hep-ph/0508267.

[25] H. Fraas, F. Franke, G. Moortgat-Pick, F. von der Pahlen and A. Wagner, Eur. J. Phys. C **29**, 587

[26] A. Djouadi, arXiv:hep-ph/0503173.

[27] H. Fraas, C. Sachse and F. von der Pahlen: *Interference of Higgs boson resonances in* $\mu^+\mu^- \to \tilde{\chi}_i^0\tilde{\chi}_j^0$ *with longitudinal beam polarization* Eur. J. Phys. C **37**, 295

[28] H. E. Haber, *Proceedings of the 21st SLAC Summer Institute on Particle Physics: Spin Structure in High Energy Processes*, SLAC, Stanford, CA 1993. [arXiv:hep-ph/9405376].

[29] T. Tsukamoto, K. Fujii, H. Murayama, M. Yamaguchi and Y. Okada, Phys. Rev. D **51**, 3153 (1995); A. S. Belyaev and A. V. Gladyshev, arXiv:hep-ph/9703251.

[30] A. Dobado, M.J. Herrero and S. Penaranda, Eur. Phys. J. C **17** (2000) 487;
J.F. Gunion and H.E. Haber, Phys. Rev. D **67** (2003) 075019;
H.E. Haber and Y. Nir, Phys. Lett. B **306** (1993) 327;
H.E. Haber, CERN-TH/95-109 and hep-ph/9505240.

[31] V. D. Barger, M.S. Berger, T. Han, Phys. Rev. D **59** (1999) 071701.

[32] A. Djouadi, J. Kalinowski, M. Spira, Comput. Phys. Commun. **108** (1998) 56.

[33] H. Haber, K. Kane, Phys. Rep. **117** (1985) 75.

[34] D. Atwood and A. Soni, Phys. Rev. D **52** (1995) 6271 [arXiv:hep-ph/9505233];
B. Grzadkowski and J. F. Gunion, Phys. Lett. B **350** (1995) 218 [arXiv:hep-ph/9501339];
J. F. Gunion, B. Grzadkowski and X. G. He, Phys. Rev. Lett. **77** (1996) 5172 [arXiv:hep-ph/9605326];
J. F. Gunion and J. Pliszka, Phys. Lett. B **444** (1998) 136 [arXiv:hep-ph/9809306];
B. Grzadkowski and J. Pliszka, Phys. Rev. D **60** (1999) 115018 [arXiv:hep-ph/9907206].

[35] L. J. Hall and J. Polchinski, Phys. Lett. B **152**, 335 (1985).

[36] G. Moortgat-Pick and H. Fraas, Eur. Phys. J. C **25** (2002) 189 [arXiv:hep-ph/0204333].

[37] M. M. Nojiri, Phys. Rev. D **51** (1995) 6281 [arXiv:hep-ph/9412374];
M. M. Nojiri, K. Fujii and T. Tsukamoto, Phys. Rev. D **54** (1996) 6756 [arXiv:hep-ph/9606370].
E. Boos, H. U. Martyn, G. Moortgat-Pick, M. Sachwitz, A. Sherstnev and P. M. Zerwas, Eur. Phys. J. C **30** (2003) 395 [arXiv:hep-ph/0303110];
H. U. Martyn, [arXiv:hep-ph/0406123].

[38] B. C. Allanach *et al.*, in *Proc. of the APS/DPF/DPB Summer Study on the Future of Particle Physics (Snowmass 2001)* ed. N. Graf, Eur. Phys. J. C **25** (2002) 113 [eConf **C010630** (2001) P125] [arXiv:hep-ph/0202233].

[39] S. Y. Choi, J. Kalinowski, G. Moortgat-Pick and P. M. Zerwas, Eur. Phys. J. C **22** (2001) 563 [Addendum-ibid. C **23** (2002) 769] [arXiv:hep-ph/0108117].

[40] J. F. Gunion, H. Haber, Nucl. Phys. B **272** (1986) 1.

[41] M. F. Sohnius, Phys. Rept. **128** (1985) 39.

[42] A. Bartl, H. Fraas and W. Majerotto, Nucl. Phys. B **278** (1986) 1.

[43] A. Bartl, K. Hidaka, T. Kernreiter and W. Porod, Phys. Rev. D **66**, 115009 (2002) [arXiv:hep-ph/0207186].

[44] W. Hollik, Diploma thesis, Würzburg 1976.

[45] J. Werle, Relativistic Theory of Reactions, Willey, New York, 1966.

[46] A. Bartl, H. Fraas, O. Kittel and W. Majerotto, Phys. Rev. D **69**, 035007 (2004) [arXiv:hep-ph/0308141].

List of own publications

1. Higgs boson interference in $\mu^+\mu^- \to \tilde{\chi}_i^+\tilde{\chi}_j^-$ with longitudinally polarized beams
   O. Kittel, **F. von der Pahlen**;
   Phys. Rev. D72 (2005), 095004.

2. Interference of Higgs boson resonances in $\mu^+\mu^- \to \tilde{\chi}_i^0\tilde{\chi}_j^0$ with longitudinal beam polarization
   H. Fraas, **F. von der Pahlen** and C. Sachse;
   Eur.Phys.J. C37 (2004), 495-505.

3. Precise measurements of Higgs-chargino couplings at a Muon Collider
   H. Fraas, F. Franke, G. Moortgat-Pick, **F. von der Pahlen** and A. Wagner;
   Eur.Phys.J. C29 (2003), 587-595.

4. Precise determination of the Higgs-chargino couplings in chargino pair production
   C. Blöchinger, H. Fraas, F. Franke, G. Moortgat-Pick und **F. von der Pahlen**;
   in: *„CERN-2001 Muon storage rings Report"*, Eds. A.Blondel et al. (2001).

5. Chargino production and decay
   C. Blöchinger, H. Fraas, F. Franke, G. Moortgat-Pick und **F. von der Pahlen**;
   in: *„Prospective study of muon storage rings at CERN"*, Eds. B. Autin, Alain Blondel and John Ellis, CERN 99-02, ECFA 99–197 (1999).

Danksagung

An dieser Stelle möchte ich all jenen danken, die zum Gelingen dieser Arbeit beigetragen haben.

Mein Dank gilt zuerst meinem "Doktorvater" Herrn Prof. Dr. Hans Fraas für die ausgezeichnete Betreuung meiner Dissertation. Zahlreiche Diskussionen, hilfreiche Anregungen sowie seine stetige Unterstützung haben diese Arbeit ermöglicht.

Bei Gudrit Moortgat-Pick möchte ich mich besonders bedanken, da ich durch ihre Anregung erst nach Würzburg gekommen bin, um mich hier der Supersymmetrie zu widmen.

Olaf Kittel möchte ich für zahlreiche Diskusionen sowie für viele hilfreiche Anmerkungen zum Manuskript dieser Arbeit besonders danken.

Aufrichtiger Dank gilt den jetzigen und ehemaligen Mitarbeitern und Mitarbeiterinnen unserer Arbeitsgruppe, insbesondere Claus Blöchinger, Sigrun Csallner, Fabian Franke, Stefan Hesselbach, Gudrid Moortgat-Pick, Heinrich Päs, Christoph Sachse, Reimer Selle und Alexander Wagner für viele wertvolle Diskussionen und Gespräche. Des Weiteren danke ich Brigitte Wehner für die hervorrangenden Leistungen bei ihren stets professionellen und gewissenhaften Einsatz. Auch allen Systembetreuern, insbesondere Alexander Wagner und Andreas Vetter, sei gedankt für die Aufrechterhaltung eines optimal funktionierenden Rechnerbetriebs an unserem Institut.

Curriculum Vitae

Federico von der Pahlen

Address for Correspondence

Mail:	Institut für Theoretische Physik und Astrophysik Universität Würzburg Am Hubland D-97074 Würzburg, Germany
Phone:	+49-931-888-5859
Fax:	+49-931-888-4604
E-mail:	pahlen@physik.uni-wuerzburg.de

Personal Data

Date/Place of Birth:	June 9, 1967 / Buenos Aires, Argentina
Nationality:	argentine
Marital Status:	unmarried

Positions

- **August 1999 - August 2001**: Research Assistant at the Institute for Theoretical Physics and Astrophysics, University of Würzburg; Supervisor: Prof. Dr. H. Fraas

Education

- **Diploma in Physics**
  University of Rome ,,La Sapienza", Italy, November 1993
  Theoretical Physics
  Diploma Thesis: *Radiative corrections to inclusive semileptonic decays of mesons with charm*
  Advisor: Prof. M. Lusignoli, University of Rome ,,La Sapienza", Italy

- **Bachillerato** (School leaving certificate, no grades)
  Colegio San Jose, Pergamino, Argentinien, Dezember 1984

Research Fellowships

1. Fellowship of the Graduiertenkolleg, Institut for Theoretical Physics, University of Karlsruhe, April - September 1995

Teaching Activities

1. Tutor for undergraduate students in Mechanics and Electrodynamics
   University of Karlsruhe, 1995 - 1998,

2. Tutor for graduate students in Mathematics, Quantum Mechanics, Theoretical Mechanics, Electrodynamics
   University of Würzburg, 1998 - 2005

Scientific Talks

1. Constraining chargino-Higgs and neutralino-Higgs couplings at a muon collider;
   Würzburg, February 2004

2. Precise determination of the Higgs-chargino and Higgs-neutralino couplings in chargino and neutralino production at $\mu^+\mu^-$ annihilation;
   64. Physikertagung der DPG; Bonn, March 2001

3. Chargino production and decay at a Muon Collider;
   63. Physikertagung der DPG; Dresden, March 2000

4. Chargino-Produktion und Zerfall an einem Muon Collider;
   ,,31. Herbstschule für Hochenergiephysik Maria Laach" Maria Laach, September 1999

5. Chargino Produktion und Zerfall an einem Muon Collider;
   62. Physikertagung der DPG; Heidelberg, March 1999

6. Chargino production and decay at the Muon Collider;
   University of Würzburg, January 1999

7. Massive neutrinos;
   University of Karlsruhe, November 1996

8. Radiative corrections to inclusive semileptonic decays of mesons with charm;
   University of La Plata, Argentina, May 1994